the BST appears to facilitate heterosexual affiliation. Finally, future studies will examine the role of the BST in regulating male/male and heterosexual aggression. Reduced aggression is the other side of increasing prosocial behavior, and there are a number of studies that suggest that the BST may play an important role in regulating aggression [38–40].

Acknowledgments

We wish to thank N. Cushing for her comments and suggestions on this manuscript and the animal care staff at the University of Memphis.

Author Contributions

Conceived and designed the experiments: BC. Performed the experiments: KL. Analyzed the data: KL KK. Contributed reagents/materials/analysis tools: SM SO. Wrote the paper: KL BC KK.

References

1. Wersinger SR, Sannen K, Villalba C, Lubahn DB, Rissman EF, et al. (1997) Masculine sexual behavior is disrupted in male and female mice lacking a functional estrogen receptor α gene. Horm Behav 32: 176–183.
2. Ogawa S, Washburn TF, Lubahn DB, Korach KS, Pfaff DW (1998) Modifications of testosterone-dependent behaviors by estrogen receptor-α gene disruption in male mice. Endocrinology 139: 5058–5069.
3. Rissman EF, Wersinger SR, Fugger HN, Foster TC (1999) Sex with knockout models: behavioral studies of estrogen receptor alpha. Brain Res 835: 80–90.
4. Cooke BM, Breedlove SM, Jordan C (2003) Both estrogen receptors and androgen receptors contribute to testosterone-induced changes in the morphology of the medial amygdala and sexual arousal in male rats. Horm Behav 43: 335–346.
5. Patisaul HB, Bateman HL (2008) Neonatal exposure to endocrine active compounds or an ER agonist increases adult anxiety and aggression in gonadally intact male rats. Physiol Behav 53: 580–588.
6. Patisaul HB, Adewale HB, Mickens JA (2009) Neonatal agonism of ER alpha masculinizes serotonergic (5-HT) projections to the female rat ventromedial nucleus of the hypothalamus (VMN) but does not impair lordosis. Behav Brain Res 196: 317–322.
7. Hnatczuk OC, Lisciotto CA, DonCarlos LL, Carter CS, Morrell JI (1994) Estrogen receptor immunoreactivity in specific brain areas of the prairie vole (*Microtus ochrogaster*) is altered by sexual receptivity and genetic sex. J Neuroendocrinol 6: 81–100.
8. Cushing BS, Razzoli M, Murphy AZ, Epperson PD, Le WW, et al. (2004) Intraspecific variation in estrogen receptor alpha and the expression of male sociosexual behavior in two population of prairie voles. Brain Res 1016: 247–254.
9. Cushing BS, Wynne-Edwards KE (2006) Estrogen receptor-a distribution in male rodents is associated with social organization. J Comp Neurol 494: 595–605.
10. Lonstein JS, Rood BD, De Vries GJ (2002) Parental responsiveness is feminized after neonatal castration in virgin male prairie voles, but is not masculinized by perinatal testosterone in virgin females. Horm Behav 41: 80–87.
11. Cushing BS, Okorie U, Young LJ (2003) The effects neonatal castration on the subsequent behavioural response to centrally administered arginine vasopressin and the expression of V_{1a} receptors in adult male prairie voles. J Neuroendocrinol 15: 1021–1026.
12. Cushing BS, Kramer KM (2005) Mechanisms underlying epigenetic effects of early social experience: the role of neuropeptides and steroids. Neurosci Biobehav Rev 29: 1089–1105.
13. Cushing BS, Perry A, Musatov S, Ogawa S, Papademetriou E (2008) Estrogen receptors in the medial amygdala inhibit the expression of male prosocial behavior. J Neurosci 28: 10386–10403.
14. DeVries AC, DeVries MB, Taymans SE, Carter CS (1996) The effects of stress on social preferences are sexually dimorphic in prairie voles. Proc Natl Acad Sci U S A 93: 11980–11984.
15. Newman SW (1999) The medial extended amygdala in male reproductive behavior a node in the mammalian social behavior network. Ann N Y Acad Sci 877: 242–257.
16. Kirkpatrick B, Kim JW, Insel TR (1994a) Limbic system fos expression associated with paternal behavior. Brain Res 658: 112–118.
17. Pfaus JG, Heeb MM (1997) Implications of immediate-early gene induction in the brain following sexual stimulation of male and female rodents. Brain Res Bull 44: 397–407.
18. Curtis JT, Wang ZX (2003) Forebrain c-fos expression under conditions conducive to pair bonding in female prairie voles (*Microtus ochrogaster*). Physiol Behav 80: 95–101.
19. Cushing BS, Mogekwu N, Le WW, Hoffman GE, Carter CS (2003) Cohabitation induced Fos immunoreactivity in the monogamous prairie vole. Brain Res 965: 203–211.
20. Rasia-Filho AA, Londero RG, Achaval M (2000) Functional activities of the amygdala: an overview. J Psych Neurosci 25: 14–23.
21. Ferguson JN, Aldag JM, Insel TR, Young LJ (2001) Oxytocin in the medial amygdala is essential for social recognition in the mouse. J Neurosci 21: 8278–8285.
22. Yahr P, Finn PD, Hoffman NW, Sayag N (1994) Sexually dimorphic cell groups in the medial preoptic area that are essential for male sex behavior and the neural pathways needed for their effects. Psychoneuroendocrinol 19: 463–470.
23. Wang ZX, DeVries GJ (1993) Testosterone effects on paternal behavior and vasopressin immunoreactive projections in prairie voles (*Microtus ochrogaster*). Brain Res 631: 156–160.
24. De Vries GJ, Villalba C (1997) Brain sexual dimorphism and sex differences in parental and other social behaviors. Ann N Y Acad Sci 807: 273–286.
25. Wang Z, Hulihan TJ, Insel TR (1997) Sexual and social experience is associated with different patterns of behavior and neural activation in male prairie voles. Brain Res 767: 321–332.
26. Trezza V, Campolongo P (2009) Toward understanding the neurobiology of social attachment: role of estrogen receptors in the medial amygdala. J Neurosci 29: 1–2.
27. Musatov S, Chen W, Pfaff DW, Kaplitt MG, Ogawa S (2006) RNAi-mediated silencing of estrogen receptor a in the ventromedial nucleus of the hypothalamus abolishes female sexual behaviors. Proc Natl Acad Sci USA 103: 10456–10460.
28. Schultz KN, von Esenwein SA, Hu M, Bennett AL, Kennedy RT, et al. (2009) Viral vector-mediated overexpression of estrogen receptor a in striatum enhances the estradiol-induced motor activity in female rats and estradiol-modulated GABA release. J Neurosci 29: 1897–1903.
29. Liu Y, Curtis JT, Wang ZX (2001) Vasopressin in the lateral septum regulates pair bond formation in male prairie voles (*Microtus ochrogaster*) Behav Neurosci 115: 910–919.
30. Cho MM, DeVries AC, Williams JR, Carter CS (1999) The effects of oxytocin and vasopressin on partner preferences in male and female prairie voles (*Microtus ochrogaster*). Behav Neurosci 113: 1071–1079.
31. Carter CS, DeVries AC, Getz LL (1995) Physiological substrates of mammalian monogamy-the prairie vole model. Neurosci Biobehav Rev 19: 303–314.
32. Roberts RL, Williams JR, Wang AK, Carter CS (1998) Cooperative breeding and monogamy in prairie voles: influence of the sire and geographical variation. Anim Behav 55: 1131–1140.
33. Keverne EB, Curley JP (2004) Vasopressin, oxytocin and social behaviour. Curr Opin Neurobiol 14: 777–783.
34. Young LJ, Wang ZX (2004) The neurobiology of pair bonding. Nat Neurosci 7: 1048–1054.
35. Ehert G, Jurgens A, Koch M (1993) Estrogen-receptor occurrence in the male-mouse brain - modulation by paternal experience. Neuroreport 11: 1247–1250.
36. Kirkpatrick B, Carter CS, Newman SW, Insel TR (1994b) Axon-sparing lesions of the medial nucleus of the amygdala decrease affiliative behaviors in the prairie vole (*Microtus-ochrogaster*) - behavioral and anatomical specificity. Behav Neurosci 108: 501–513.
37. Frazier CRM, Trainor BC, Cravens CJ, Whitney TK, Marler CA (2006) Paternal behavior influences development of aggression and vasopressin expression in male California mouse offspring. Horm Behav 50: 699–707.
38. Bester-Meredith JK, Young LJ, Marler CA (1999) Species differences in paternal behavior and aggression in Peromyscus and their associations with vasopressin immunoreactivity and receptors. Horm Behav 36: 25–38.
39. Bester-Meredith JK, Marler CA (2001) Vasopressin and aggression in crossfostered California mice (*Peromyscus californicus*) and white-footed mice (*Peromyscus leucopus*). Horm Behav 40: 51–64.
40. Gobrogge KL, Liu Y, Jia XX, Wang ZX (2007) Anterior hypothalamic neural activation and neurochemical associations with aggression in pair-bonded male prairie voles. J Comp Neurol 502: 1109–1122.

Neuro
endocrinology

Neuroendocrinology 2010;91:41–47
DOI: 10.1159/000257408

Received: May 21, 2009
Accepted after revision: May 30, 2009
Published online: November 7, 2009

Food Availability Affects Orexin A/Hypocretin-1-Induced Inhibition of Pulsatile Luteinizing Hormone Secretion in Female Rats

Miyako Furuta[a, d] Dai Mitsushima[a] Kazuyuki Shinohara[b] Fukuko Kimura[a, c] Toshiya Funabashi[a]

[a]Department of Physiology, Yokohama City University Graduate School of Medicine, Yokohama, [b]Department of Neurobiology and Behavior, Nagasaki University Graduate School of Biomedical Sciences, Nagasaki, [c]International University of Health and Welfare, Tokyo, and [d]Department of Physiology, St. Marianna University School of Medicine, Kawasaki, Japan

Key Words

Orexin A/hypocretin-1 · Luteinizing hormone pulse · Glucose · Lactic acid · Stress · Fasting

Abstract

Orexin A/hypocretin-1 inhibits pulsatile luteinizing hormone (LH) secretion in female rats. In this study, we investigated whether this inhibition was tied to the fasting state, as suggested by our previous study. We first examined whether orexin A inhibited pulsatile LH secretion when food was available ad libitum during blood sampling. Next, we investigated the effect of intravenous administration of glucose (400 mg/kg) or lactic acid (negative control; 400 mg/kg) on orexin A-induced inhibition of pulsatile LH secretion. We found that orexin A did not affect pulsatile LH secretion in the presence of food, although it increased feeding behavior. Injection of orexin A significantly inhibited pulsatile LH secretion when food was withheld during blood sampling ($p < 0.05$); this inhibitory effect was rapidly reversed by intravenous injection of glucose but not lactic acid. Because orexin A did not seem to affect pulsatile LH secretion when food was available ad libitum, we speculate that orexin A has an effect on LH secretion when orexin A-induced hunger is accompanied by stress, such as the absence of food. Furthermore, glucose as well as food may act as a satiety factor in gonadotropin-releasing hormone pulse generation.

Introduction

Nutrient availability plays an important role in the maintenance of reproductive functions [1]. For example, fasting and insulin-induced hypoglycemia inhibit pulsatile luteinizing hormone (LH) secretion [2, 3] by inhibiting the electrical activity of the gonadotropin-releasing hormone (GnRH) pulse generator in the hypothalamus [4, 5]. Thus, the site of action of fasting and insulin-induced hypoglycemia is most likely the hypothalamus. Cellular depletion of ATP due to cellular glycopenia could result in inhibition of the GnRH pulse generator activity. However, this may not be the case, since glucose availability, rather than a simple measure of metabolism, such as ATP level, is essential for maintaining the electrical activity of the GnRH pulse generator in insulin-induced hypoglycemia [6]. Therefore, hypoglycemia-sensing mechanisms in the brain play an important role in conveying information

KARGER

Fax +41 61 306 12 34
E-Mail karger@karger.ch
www.karger.com

0028–3835/10/0911–0041$26.00/0

Accessible online at:
www.karger.com/nen

Toshiya Funabashi
Department of Physiology, Yokohama City University Graduate School of Medicine
3-9 Fukuura, Kanazawa-ku
Yokohama 236-0004 (Japan)
Tel. +81 45 787 2579, Fax +81 45 787 2578, E-Mail toshiya@med.yokohama-cu.ac.jp

about the metabolic state to the GnRH pulse generating system, and the underlying key factor may be more complex than ATP level alone. Fasting may cause stress in rats [7]; however, in monkeys, it has been suggested that the suppression of pulsatile LH secretion by fasting is not caused by the psychological stress of food deprivation [5].

The lateral hypothalamic area of the brain is known as a hunger center [8] that contains orexin/hypocretin neurons [9, 10]. Orexins/hypocretins were first identified as neuropeptides that regulated feeding behavior [9, 10]. Subsequently, these neuropeptides were found to play a critical role in regulating the sleep/wake cycle [11], and it was suggested that they also mediated sleep and metabolic imbalances [12]. Regarding neuroendocrine functions, orexin inhibits LH secretion in ovariectomized (OVX) rats [13, 14], and this inhibitory effect is markedly enhanced by a low dose of estrogen that does not itself induce an LH surge [15]. However, orexin also stimulates LH secretion as part of a positive feedback cycle in which estrogen induces an LH surge [13]. Thus, orexin can either inhibit or suppress LH secretion, depending on other physiological conditions. Orexin also acts in a stimulatory manner in the rostral preoptic area and in an inhibitory manner in the medial preoptic area or arcuate/median eminence region, suggesting that it acts in a site-specific manner [16]. Although the precise mechanisms underlying orexin's distinct roles in LH secretion are unknown, orexins may act directly on GnRH neurons [17].

Preliminary experiments suggested that orexin A did not inhibit pulsatile LH secretion when the blood samples were collected under conditions where the rats had access to food ad libitum. In our previous report of the inhibitory effect of orexin A on LH secretion, the rats were under conditions where food was not available during the sampling [15]. We hypothesized that the inhibitory effect of orexin A was due to the absence of food, since orexin-induced hunger might be accompanied by stress stemming from the absence of food. We reasoned that if orexins acted as physiological feeding signals, orexin neurons would be activated at night, since rats eat more at night than in the daytime. It would follow that LH would thus be secreted less frequently at night. However, the LH pulse frequency increased rather than decreased at night [18], even though the rats should have been hungrier then.

The aim of the present study was to systematically determine whether orexin induces inhibition of pulsatile LH secretion when food is available ad libitum. We also examined whether a single satiety factor, such as glucose, can abolish the inhibitory effect of orexins in female rats.

Materials and Methods

Animals

Seven-week-old female Wistar rats (Charles River, Yokohama, Japan) were maintained under controlled temperature (24–26°C) and lighting conditions (light on from 05:00 to 19:00 h) with food (Oriental Yeast Co., Ltd., Tokyo, Japan) and water available ad libitum. The rats were OVX at 8 weeks of age. All animal housing conditions and surgical procedures were in line with the guidelines provided by the Institutional Animal Care and Use Committee of the Yokohama City University School of Medicine.

Two weeks after ovariectomy, a stainless steel guide cannula (outer diameter, 0.7 mm; length, 13 mm) was stereotaxically placed into the third ventricle of each rat (stereotaxic coordinates: A = 6.0, V = 2.0 and L = 0.0 [19]) under sodium pentobarbital anesthesia (31.5 mg/kg body weight). The animals were allowed to recover for more than 10 days.

Estrogen treatment was performed under ether anesthesia around noon on the day before the sampling experiment. A silicone tube (inner diameter, 1.5 mm; outer diameter, 2.5 mm; length, 25 mm) containing 17β-estradiol (E_2; Sigma Chemical Co., St. Louis, Mo., USA) dissolved in sesame oil at a concentration of 20 μg/ml was implanted subcutaneously. We previously showed that this procedure results in serum estradiol levels that are equivalent to those observed on the day of diestrus in intact female rats [15]. An intra-atrial cannula was implanted through the jugular vein at the same time that the silicone tube was implanted.

Experimental Protocols

We first examined the effect of orexin A on pulsatile LH when food was available ad libitum during blood sampling. Blood samples were collected in a sound-attenuated room. Approximately 120 μl of blood was collected under free-moving conditions at 6-min intervals from 09:00 to 12:00 h. After each blood sample was taken, the blood was replaced by an equal volume of heparinized saline (2 IU/ml). One hour after the first blood sample was collected, 0.3 nmol of orexin A (Peptide Institute Inc., Osaka, Japan) dissolved in 3 μl artificial cerebrospinal fluid (aCSF) was injected into the third ventricle of each rat. The same volume of aCSF was injected into control animals.

In the next experiments, food was removed from individual cages just before the start of blood collection; there was no longer any food in the room with these rats, ensuring that the rats could neither see nor smell food. Blood samples were collected as described above. Orexin A (0.3 nmol) was injected i.c.v. after 1 h had passed, and glucose or lactic acid (as a negative control) were injected i.v. at a dose of 400 mg/kg [6], dissolved in 0.5 ml saline, through the same intracardiac cannula 2 h after the experiment started. We used lactic acid as a negative control because its effect on pulsatile LH secretion is identical to that of saline [6]; however, it maintains an ATP level similar to that maintained by glucose [20].

LH Assay and Pulse Analysis

Serum concentrations of LH were measured by double antibody radioimmunoassay with materials supplied by the National Institute of Diabetes and Digestive and Kidney Diseases (NIDDK). The reference standard was NIDDK rat LH-RP-3, but the LH levels were expressed in terms of NIH LH-S1.

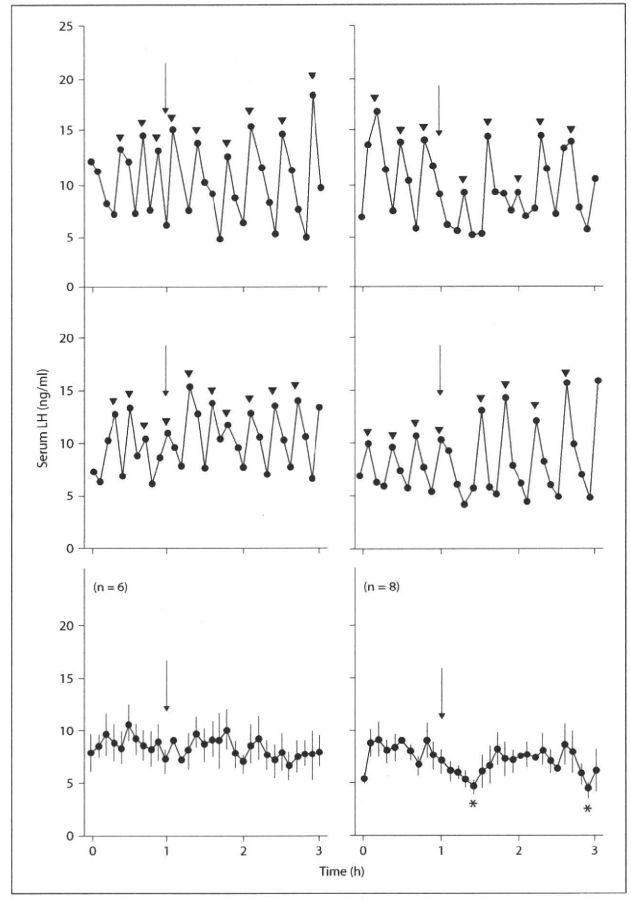

Fig. 1. Representative examples of the effects of i.c.v. injection of aCSF alone (left panels) or aCSF plus orexin A (right panels) on the serum concentrations of LH in rats when food was available ad libitum. Data are shown as mean ± SEM in the bottom two panels. Arrowheads indicate statistically defined LH pulses. Arrows indicate injections (i.c.v.) of aCSF or aCSF plus orexin A. * $p < 0.05$ versus the LH value during the 1st hour.

LH pulse detection was based on a method reported previously [6]. The analysis of LH pulsatility included the determination of pulse frequency (number of LH pulses per hour) and pulse amplitude (the difference between the peak and the pre-peak nadir). Group data of serum LH concentrations over a 3-hour period were also obtained by averaging values at each time point (fig. 1). Analysis of variance (ANOVA) followed by Fisher's PLSD post-hoc comparison was used to test for statistical significance, and significance was accepted at $p < 0.05$. The mean LH concentration was analyzed by a paired t test (fig. 1, fig. 3).

Results

Effect of Orexin on Pulsatile LH Secretion in Rats in the Presence of Food

Blood samples were collected every 6 min for 3 h from female rats that had free access to food. One group of rats was injected with 0.3 nmol of orexin A after 1 h, while another group was injected with vehicle (aCSF) alone (fig. 1). In the aCSF group, each rat exhibited pulsatile LH

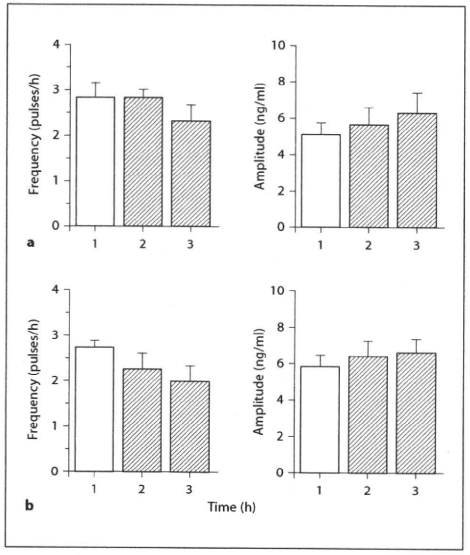

Fig. 2. Effects of i.c.v. injection of aCSF alone (**a**; n = 6) or aCSF plus orexin A (**b**; n = 8) on LH pulse frequency and pulse amplitude with food available ad libitum. Data are expressed as mean ± SEM for the 1st hour, 2nd hour, and 3rd hour. Orexin A was injected after the 1st hour. No statistically significant differences were observed (ANOVA, $p > 0.05$).

secretion, which is normal for OVX rats (fig. 1). We did not observe orexin-induced suppression of pulsatile LH secretion in these conditions, i.e., when food was available ad libitum (fig. 1). However, orexin injection induced feeding behavior (data not shown), indicating that the orexin A was injected correctly and had a biological effect. LH pulse frequency in the aCSF group was not significantly different before versus after injection of aCSF (ANOVA, $p > 0.5$, fig. 2). In the orexin group, the LH pulse frequency decreased slightly but not significantly (ANOVA, $p > 0.1$, fig. 2). Thus, orexin A did not affect pulsatile LH secretion when food was available ad libitum during blood sampling. Neither the aCSF nor the orexin group showed a significant change in the amplitude of the LH pulses before and after injection (ANOVA, $p > 0.5$, fig. 2). As shown in the lower panels in figure 1, injection of orexin A resulted in small but statistically significant decreases in the mean LH concentration at two time points (paired t test, $p < 0.05$).

Effect of Lactic Acid or Glucose Injection on Orexin-Induced Suppression of Pulsatile LH Secretion in the Absence of Food

Next, blood samples were collected every 6 min for 3 h from rats without access to food (fig. 3). Rats were injected with 0.3 nmol of orexin A after 1 h. After 2 h, glucose or lactic acid (as a negative control) was injected i.v. In both groups, each rat exhibited a spontaneous pulsatile LH secretion during the 1st hour of blood sampling (fig. 3), as in figure 1. This indicated that pulsatile LH secretion was observed regardless of whether food was available or not; this makes sense because rats normally eat very little food during this time of day (09:00–12:00 h). However, in both the lactic acid and the glucose groups, pulsatile LH secretion was markedly inhibited by i.c.v. injection of orexin A during the 2nd hour of blood samplings because food was withheld (fig. 3). Thus, orexin A did not affect LH pulse frequency (fig. 1, 2, the 2nd hour) but did decrease it (fig. 3, 4, the 2nd hour). The difference between these experiments was food availability: it was either available ad libitum (fig. 1) or was withheld during blood sampling (fig. 3). During the 3rd hour of blood sampling, after lactic acid or glucose injection, some LH pulses were observed (fig. 3). Analysis showed that LH pulse frequency decreased in both groups after orexin injection but immediately recovered in the 3rd hour after glucose injection (compared with the 1st hour, $p > 0.5$), but not after lactic acid injection (fig. 4, compared with the 1st hour, $p < 0.001$). LH pulse amplitude in the groups was not significantly changed during blood sampling ($p > 0.5$, fig. 4).

Discussion

In the present study, we confirmed that orexin A inhibited pulsatile LH secretion in estrogen-primed OVX rats when food was not available during blood sampling. We further showed that i.c.v. injection of orexin A did not inhibit pulsatile LH secretion when food was available ad libitum. When food was not available, the inhibitory effect of orexin A disappeared rapidly after i.v. injection of glucose. These data lead us to speculate that when orexin A is accompanied by stress due to the absence of food, LH secretion is affected. In general, if food is not available when rats want to eat, the result can be death. The stress due to the combination of absence of food plus injection

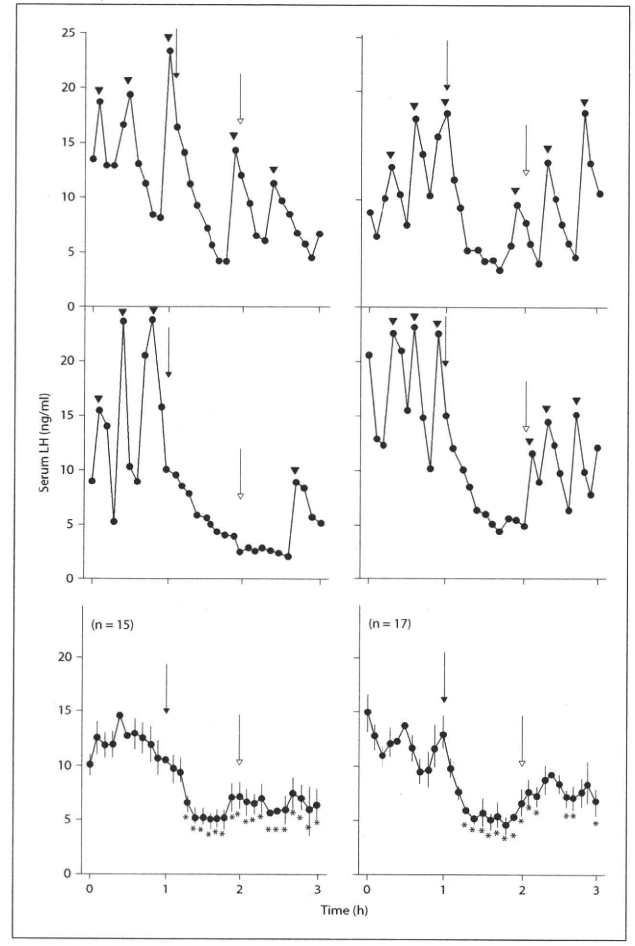

Fig. 3. Representative examples of the effects of i.v. injection of lactic acid (left panels) or glucose (right panels) on the serum concentration of LH after i.c.v. injection of orexin A. Data are shown as mean ± SEM in the bottom two panels. Arrowheads indicate statistically defined LH pulses. Solid arrows indicate orexin A injection (i.c.v.). Open arrows indicate lactic acid or glucose injection (i.v.). * $p < 0.05$ versus the LH value during the 1st hour.

of orexin A can be eliminated by glucose as well as by food.

In contrast to the present results showing no effect of orexin A on pulsatile LH secretion in the presence of food, treatment with either neuropeptide Y (NPY) [21] or 2-deoxyglucose [3] inhibits pulsatile LH secretion even if food is available ad libitum. The effect of 2-deoxyglucose is probably mediated by NPY [22]. Thus, both NPY and orexin A generate hunger and drive a feeding response, but only NPY [21] inhibits pulsatile LH secretion in the presence of food. This discrepancy is puzzling since NPY neurons are thought to mediate the inhibitory effect of

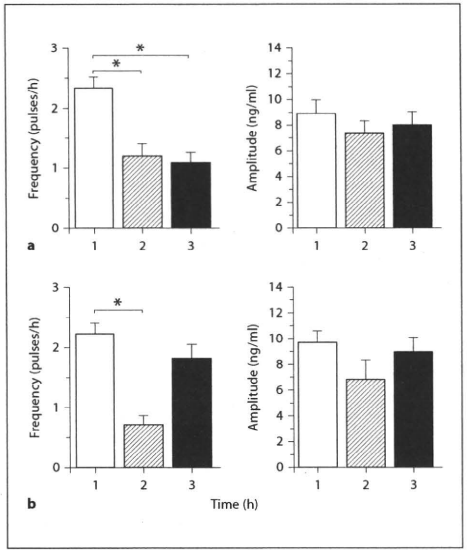

Fig. 4. Effects of i.v. injection of lactic acid (**a**; n = 15) or glucose (**b**; n = 17) on LH pulse frequency and pulse amplitude after i.c.v. orexin A injection. Data are expressed as mean ± SEM for the 1st hour, 2nd hour, and 3rd hour. Orexin A was injected after the 1st hour, and lactic acid or glucose was injected after the 2nd hour. * $p < 0.05$ versus the value during the 1st hour.

orexin A on pulsatile LH secretion and the stimulatory role of orexin A in feeding [23].

Consequently, we speculate that orexin A inhibits LH secretion in the absence of food, such as in the fasting state, but does not affect LH secretion in the presence of food. This raises the question of when orexin A acts to inhibit LH secretion. At present, it is not known whether orexin neurons are activated under physiological conditions, such as during spontaneous feeding when food is available ad libitum. We have preliminary data which suggest that orexin neurons are activated by fasting but not during free-feeding conditions (data not shown). Furthermore, orexin neurons are activated by subnormal glucose levels when food is absent (as in 48-hour fasting), but the activation of orexin neurons was not simply due to increased appetite [24]. Thus, we hypothesize that orexin A is activated by stressful conditions, such as fasting. This stress can be relieved not only by food but also by glucose. In line with this hypothesis, it has been suggested that in addition to affecting feeding behavior and wakefulness [25], orexin neurons are part of the circuitry that mediates the hypothalamic response to acute stress [26], although fasting-induced inhibition of LH secretion cannot be attributed solely to stress [27].

Acknowledgments

We are grateful to the NIDDK for providing radioimmunoassay materials. This work was supported by the Umehara Prize, which was awarded by the Yokohama Foundation for the Advancement of Medical Science.

References

1 Wade GN, Schneider JE: Metabolic fuels and reproduction in female mammals. Neurosci Biobehav Rev 1992;16:235–272.

2 Cagampang FRA, Maeda KI, Tsukamura H, Ohkura S, Ota K: Involvement of ovarian steroids and endogenous opioids in the fasting-induced suppression of pulsatile LH release in ovariectomized rats. J Endocrinol 1991;129:321–328.

3 Nagatani S, Tsukamura H, Murahashi K, Maeda KI: A rapid suppressive effect of estrogen in the paraventricular nucleus on pulsatile LH release in fasting-ovariectomized rats. J Neuroendocrinol 1996;8:267–273.

4 Chen MD, O'Byrne KT, Chiappini SE, Hotchkiss J, Knobil E: Hypoglycemic 'stress' and gonadotropin-releasing hormone pulse generator activity in the rhesus monkey: role of the ovary. Neuroendocrinology 1992;56:666–673.

5 Goubillon ML, Thalabard JC: Insulin-induced hypoglycemia decreases luteinizing hormone secretion in the castrated male rat: involvement of opiate peptides. Neuroendocrinology 1996;64:49–56.

6 He D, Funabashi T, Sano A, Uemura T, Minaguchi H, Kimura F: Effects of glucose and related substrates on the recovery of the electrical activity of gonadotropin-releasing hormone pulse generator which is decreased by insulin-induced hypoglycemia in the estrogen-primed ovariectomized rat. Brain Res 1999;820:71–76.

7 Maeda K, Nagatani S, Estacio MA, Tsukamura H: Novel estrogen feedback sites associated with stress-induced suppression of luteinizing hormone secretion in female rats. Cell Mol Neurobiol 1996;16:311–324.

8 Bernardis LL, Bellinger LL: The lateral hypothalamic area revisited: ingestive behavior. Neurosci Biobehav Rev 1996;20:189–287.

9 de Lecea L, Kilduff TS, Peyron C, Gao X, Foye PE, Danielson PE, Fukuhara C, Battenberg EL, Gautvik VT, Bartlett FS, 2nd, Frankel WN, van den Pol AN, Bloom FE, Gautvik KM, Sutcliffe JG: The hypocretins: hypothalamus-specific peptides with neuroexcitatory activity. Proc Natl Acad Sci USA 1998;95:322–327.

10 Sakurai T, Amemiya A, Ishii M, Matsuzaki I, Chemelli RM, Tanaka H, Williams SC, Richarson JA, Kozlowski GP, Wilson S, Arch JR, Buckingham RE, Haynes AC, Carr SA, Annan RS, McNulty DE, Liu WS, Terrett JA, Elshourbagy NA, Bergsma DJ, Yanagisawa M: Orexins and orexin receptors: a family of hypothalamic neuropeptides and G protein-coupled receptors that regulate feeding behavior. Cell 1998;92:1 page following 696.

11 Ohno K, Sakurai T: Orexin neuronal circuitry: role in the regulation of sleep and wakefulness. Front Neuroendocrinol 2008;29:70–87.

12 Adamantidis A, de Lecea L: The hypocretins as sensors for metabolism and arousal. J Physiol 2009;587:33–40.

13 Pu S, Jain MR, Kalra PS, Kalra SP: Orexins, a novel family of hypothalamic neuropeptides, modulate pituitary luteinizing hormone secretion in an ovarian steroid-dependent manner. Regul Pept 1998;78:133–136.

14 Tamura T, Irahara M, Tezuka M, Kiyokawa M, Aono T: Orexins, orexigenic hypothalamic neuropeptides, suppress the pulsatile secretion of luteinizing hormone in ovariectomized female rats. Biochem Biophys Res Commun 1999;264:759–762.

15 Furuta M, Funabashi T, Kimura F: Suppressive action of orexin a on pulsatile luteinizing hormone secretion is potentiated by a low dose of estrogen in ovariectomized rats. Neuroendocrinology 2002;75:151–157.

16 Small CJ, Goubillon ML, Murray JF, Siddiqui A, Grimshaw SE, Young H, Sivanesan V, Kalamatianos T, Kennedy AR, Coen CW, Bloom SR, Wilson CA: Central orexin a has site-specific effects on luteinizing hormone release in female rats. Endocrinology 2003;144:3225–3236.

17 Campbell RE, Grove KL, Smith MS: Gonadotropin-releasing hormone neurons coexpress orexin 1 receptor immunoreactivity and receive direct contacts by orexin fibers. Endocrinology 2003;144:1542–1548.

18 Hiruma H, Nishihara M, Kimura F: Hypothalamic electrical activity that relates to the pulsatile release of luteinizing hormone exhibits diurnal variation in ovariectomized rats. Brain Res 1992;582:119–122.

19 Albe-Fessard D, Stutinsky F, Libouban S: Atlas stéréotaxique du diencéphale du rat blanc. Paris, Editions du Centre National de la Recherche Scientifique, 1966.

20 Saitoh M, Okada Y, Nabetani M: Effect of mannose, fructose and lactate on the preservation of synaptic potentials in hippocampal slices. Neurosci Lett 1994;171:125–128.

21 Kalra SP, Kalra PS: Nutritional infertility: the role of the interconnected hypothalamic neuropeptide Y-galanin-opioid network. Front Neuroendocrinol 1996;17:371–401.

22 He B, White BD, Edwards GL, Martin RJ: Neuropeptide Y antibody attenuates 2-deoxy-D-glucose induced feeding in rats. Brain Res 1998;781:348–350.

23 Yamanaka A, Kunii K, Nambu T, Tsujino N, Sakai A, Matsuzaki I, Miwa Y, Goto K, Sakurai T: Orexin-induced food intake involves neuropeptide Y pathway. Brain Res 2000;859:404–409.

24 Cai XJ, Widdowson PS, Harrold J, Wilson S, Buckingham RE, Arch JR, Tadayyon M, Clapham JC, Wilding J, Williams G: Hypothalamic orexin expression: modulation by blood glucose and feeding. Diabetes 1999;48:2132–2137.

25 Kotz CM: Integration of feeding and spontaneous physical activity: role for orexin. Physiol Behav 2006;88:294–301.

26 Winsky-Sommerer R, Boutrel B, de Lecea L: Stress and arousal: the corticotrophin-releasing factor/hypocretin circuitry. Mol Neurobiol 2005;32:285–294.

27 Cameron JL, Helmreich DL, Schreihofer DA: Modulation of reproductive hormone secretion by nutritional intake: stress signals versus metabolic signals. Hum Reprod 1993;(suppl 2):162–167.

Contents lists available at ScienceDirect

Neuroscience Letters

journal homepage: www.elsevier.com/locate/neulet

Age- and sex-specific changes in naloxone-induced luteinizing hormone secretion and Fos expression in gonadotropin-releasing hormone neurons of gonadectomized rats

Toahiya Funabashi[a,*,1], Miyako Furuta[a,b], Atsushi Fukushima[a], Fukuko Kimura[a,c]

[a] Department of Physiology, Yokohama City University Graduate School of Medicine, 3-9 Fukuura, Kanazawa-ku, Yokohama 236-0004, Japan
[b] Department of Physiology, St. Marianna University School of Medicine, 2-16-1 Sugao, Mihyamae-ku, Kawasaki 216-8511, Japan
[c] International University of Health and Welfare, Amity-Nogizaka-Bldg 1-21-1, Minamiaoyama, Minato-ku, Tokyo 107-0062, Japan

ARTICLE INFO

Article history:
Received 14 November 2009
Received in revised form
29 December 2009
Accepted 15 January 2010

Keywords:
Opioid
Pulse
Luteinizing hormone
Gonadotropin-releasing hormone
Immediate early genes

ABSTRACT

In the present study, we examined sex-specific changes in luteinizing hormone (LH) secretion and Fos expression in gonadotropin-releasing hormone (GnRH) neurons in response to naloxone in young (3 months old) and old (24 months old), gonadectomized male and female rats. We revealed by immunocytochemistry that, regardless of age and sex, naloxone significantly increased the number of GnRH neurons expressing Fos, which was associated with increased LH secretion. Additionally, although the magnitude of the increase in Fos-expressing GnRH neurons did not change in old males compared to young males, it was attenuated by almost half in old females compared to young females. LH levels decreased 60% in old males compared to young males and 15% in old females compared to young females. These results suggest LH secretion is impaired with age, but the ability of GnRH neurons to be stimulated by naloxone is preserved. However, the opioid-controlling mechanism is more fragile in females than males during aging.

The gonadotropin-releasing hormone (GnRH) pulse generator includes a neuronal circuit and components for controlling pulsatile GnRH secretion. It is manifested by a characteristic increase in electrical neuronal activities in the hypothalamus accompanied by the initiation of each luteinizing hormone (LH) pulse. This event is called a multi-unit activity (MUA) volley [20,30,36], although the nature of the electrical activity and anatomically detailed evidence of the GnRH pulse generator are still uncertain.

The frequency of GnRH pulses is an important determinant of LH secretion from the anterior pituitary [21]. Estrogen can act in a negative feedback loop by decreasing the frequency of MUA volleys [19,20,25]. In rats, this effect of estrogen is at least partly mediated by opioid neurons [16]. The effects of the opioid receptor antagonist, naloxone, are also observable without estrogen [20]; therefore, changes in the frequency of MUA volleys in response to naloxone may reflect an important function of the GnRH pulse generator related to opioid neurons.

On the other hand, anatomical evidence has suggested that β-endorphin neurons make direct contact with GnRH neurons located in the preoptic area [4], an important site for regulating cyclic release of gonadotropin [10]. Since opioid neurons and receptors are densely localized in the hypothalamus [3], they are involved in inducing preovulatory LH secretion [2,13].

Age-related changes in LH secretion may be characterized by age-related alteration of GnRH pulse frequencies. In males, the frequency of LH pulses, which probably reflect GnRH pulses, reportedly decreases with age in rodents [6,15]. The suppressive activity of androgens, via a negative feedback effect, is suggested to increase with age [37]. However, normal negative feedback effects of gonadal steroids were shown during aging [31] using deconvolution analysis. These findings suggest that the GnRH-LH pulsing mechanism maintains an increased frequency and lower amplitude in healthy older men [17,32].

The patterns of LH secretion are different in females from those observed in males due to the presence of phasic LH secretion, but the female GnRH pulse generating system is likely the same as the male system with regard to pulse generation. The LH pulse frequency reportedly decreases with age in rats [29] and the feedback mechanism is also attenuated [27]. Furthermore, the electrical activity of the GnRH pulse generator decreases with age in rats [28], while GnRH secretion in the monkey does not decrease with age [9].

It is unclear whether or not the GnRH pulse generator is impaired with age; yet in general, the GnRH pulse generator is more fragile with age in females than males. This is at least partly due to

* Corresponding author. Tel.: +81 45 787 2578; fax: +81 45 787 2578.
E-mail address: toshiya@med.yokohama-cu.ac.jp (T. Funabashi).
[1] Present address: Department of Physiology, St. Marianna University School of Medicine, 2-16-1 Sugao, Miyamae-ku, Kawasaki 216-8511, Japan.

0304-3940/$ – see front matter © 2010 Elsevier Ireland Ltd. All rights reserved.
doi:10.1016/j.neulet.2010.01.032

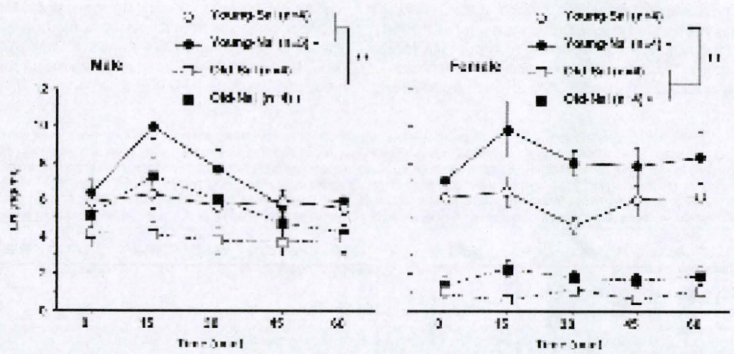

Fig. 1. Naloxone-induced changes in LH secretion during aging. Naloxone (filled circle with solid line for young and filled square with dashed line for old rats) was injected into males (left panel) and females (right panel). Control rats were injected with saline (open circle with solid line for young and open square with dashed line for old rats). Each point and vertical line indicate mean and SEM, respectively. Numbers in parentheses indicate numbers of rats. * and ** indicate $p < 0.05$ vs. saline control and old rats, respectively.

the influence of estrogen on pulse frequency in females, because estrogen decreases drastically with age. The aim of the present study was to determine whether the responsiveness of GnRH neurons to naloxone changed with age when negative feedback by gonadal steroid hormones was interrupted. GnRH responsiveness was measured by counting the number of GnRH neurons that expressed Fos in male and female gonadectomized rats.

Intact male ($n = 9$) and female Wistar rats ($n = 8$) were obtained (Charles River, Yokohama, Japan) at 7–8 weeks of age and were maintained under controlled lighting conditions (7:00–19:00 lights on) with food and water available ad libitum. Two weeks after castration and the day before the experiment, young (3 months old) and old (24 months old) rats were implanted with an intraventricular cannula. Naloxone (5 mg/kg) was intravenously injected after the first blood sampling in half of the rats, and thereafter blood samples were obtained through the cannula 15, 30, 45, and 60 min after injection. The remaining rats were controls and received saline injections. All animal housing and surgical procedures were in accordance with the guidelines of the Institutional Animal Care and Use Committee of the Yokohama City University School of Medicine.

Serum concentrations of LH were measured by double-antibody radioimmunoassay with materials supplied by the National Institute of Diabetes and Digestive and Kidney Disease (NIDDK). The reference standard was NIDDK rat LH-RP-3, but the amounts of LH are expressed in terms of NIH LH-S1. Changes in LH concentrations were analyzed by analyses of variance (ANOVA) for repeated measures, followed by the Fisher's protected LSD *post hoc* test and significance was attained at $p < 0.05$.

After blood sampling, the rats were killed by intravenous injection of an overdose of pentobarbital (70 mg/kg, bw) and prepared for the dual-immunocytochemical study, according to a previously reported method [8]. Briefly, the rats were perfused through the cardiac ventricle with ice-cold 4% paraformaldehyde in phosphate buffer (pH 7.5). Frozen coronal sections were cut 30 μm thick and incubated overnight with rabbit polyclonal antibody to Fos (Oncogene Science, PC-05 Lot#2940101, 0.05 μg/ml). The next day, sections were incubated with biotinylated anti-rabbit IgG (diluted 1:200) and then incubated with an avidin–biotin–peroxidase complex (Vectastain Elite ABC Kit, Vectastain Lab., Burlingame, USA). The sections were then incubated for 5 min in 0.05% 3,3′-diaminobenzidine with H_2O_2. Following the detection of Fos immunoreactivity, the sections were rinsed well, incubated overnight with mouse monoclonal antibody to GnRH (LRH13 [26]) (diluted 1:4000), and further incubated for 1 h with biotinylated anti-mouse IgG (diluted 1:200) and for 2 h with streptavidin-FITC (30 μg/ml). The sections were rinsed and cover slipped with aqueous medium and then examined under a light microscope equipped with appropriate filters for the visualization of the fluorescent signal. Omission of primary antibodies eliminated all staining. Secondary anti-mouse IgG and anti-rabbit IgG antibodies did not bind to the rabbit polyclonal antibody and mouse monoclonal antibody, respectively.

The counting was performed by an investigator unaware of the experimental conditions and expectations. The GnRH-immunoreactive (GnRH-ir) cells, in which a nucleus was visible as a clear halo surrounded by cytoplasmic fluorescent staining, were counted. GnRH-ir cells were defined as double-labeled for both Fos-ir and GnRH-ir when a blue-black nucleus signaling a Fos-ir cell was surrounded by cytoplasmic fluorescent staining. The forebrain was arbitrarily divided as shown in Fig. 2a: the rostral part of the forebrain was defined as the region including the diagonal band of the Broca (DBB), the organum vasculosum of the lamina terminalis (OVLT), the anterior preoptic area (aPOA), the POA, the supraoptic nucleus-paraventricular nucleus (SON-PVN), and the caudal part of the mediobasal hypothalamic nucleus (MBH). The mean number of sections for each area was approximately 5.8, 3.9, 2.8, 8.6, 15.9, or 18.3 for the DBB, the OVLT, the aPOA, the POA, the SON-PVN, or the MBH, respectively. The number of immunoreactive cells was summed in each rat and the mean numbers were then calculated for each treatment group. Statistical comparisons were carried out by ANOVA followed by the Fisher's protected LSD *post hoc* test, and considered significant at $p < 0.05$.

Regardless of sex and treatment, LH secretion appeared to decrease with age; yet, naloxone seemed to induce LH secretion (Fig. 1). In male rats, repeated ANOVA showed a significant effect of treatment (saline vs. naloxone, $p < 0.001$) and age (young vs. old, $p < 0.0001$) without interaction ($p > 0.4$). Therefore, LH secretion significantly decreased with age and naloxone significantly induced LH secretion regardless of age (Fig. 1, left panel). In saline-injected rats, mean LH levels in old males were 62% of the LH levels in young males.

In female rats, repeated ANOVA showed a significant effect of treatment (saline vs. naloxone, $p < 0.0001$) and age (young vs. old, $p < 0.0001$) with interaction ($p < 0.02$). Since the interaction was significant, we further analyzed the data by one-way ANOVA ($p < 0.0001$). Naloxone significantly increased LH secretion in both young and old female rats (young $p < 0.0001$, old $p < 0.05$). Regard-

less of treatment, LH secretion in old females was significantly less than in young females ($p < 0.0001$). In saline-injected rats, mean LH levels in old females were only 15% of the LH levels in young females.

In Fig. 2b, the number of GnRH-ir cells (upper panels) is expressed as the mean number per section for each area, and the number of GnRH-ir cells also expressing Fos-ir (lower panels) are presented for each area (as schematized in Fig. 2a). The overall distribution of GnRH-ir cells in the forebrain was similar to that reported previously [38]. As we noted previously, a small number of GnRH-ir cells existed in the MBH. It was obvious that the number of GnRH-ir cells decreased with age, regardless of sex. In both the male and female rats, ANOVA revealed a significant effect of age (young vs. old males, $p < 0.0001$; young vs. old females, $p < 0.02$) but not of treatment (males: saline vs. naloxone, $p > 0.3$; females: saline vs. naloxone, $p > 0.7$) without interaction (males: $p > 0.3$; females: $p > 0.9$). These results suggested that aging caused a loss of GnRH neurons in male rats. Similar results have previously been reported in female rats lacking gonadal hormones [8].

There were Fos-ir cells throughout the forebrain in saline-injected rats, but few GnRH-ir cells were also Fos-ir, regardless of age or sex. However, the number of Fos-ir cells seemed to be increased in all subdivisions, extending from the rostral to the caudal part of the forebrain, in naloxone-injected rats (data not shown). For the total number of GnRH-ir cells that were also Fos-ir in male rats, two-way ANOVA revealed a significant effect of treatment (saline vs. naloxone, $p < 0.05$) but not of age (young vs. old, $p > 0.5$) without interaction ($p > 0.9$). These results suggested that naloxone-induced Fos expression in GnRH neurons regardless of age. There was no significant difference between young and old rats in the number of naloxone-induced Fos-ir cells in male rats.

For the total number of GnRH-ir cells that were also Fos-ir in female rats, ANOVA revealed a significant effect of treatment (saline vs. naloxone, $p < 0.0005$) and age (young vs. old, $p < 0.04$) with significant interaction ($p < 0.04$). Further analysis by one-way ANOVA ($p < 0.0009$) revealed that the number of GnRH-ir cells expressing Fos-ir was significantly larger in naloxone-injected young females than in saline-injected young females ($p < 0.0003$) or naloxone-injected old females ($p < 0.007$). There were significantly more GnRH-ir cells that were also Fos-ir in naloxone-injected old females than in saline-injected old females ($p < 0.05$). These results suggested that naloxone treatment induced Fos expression in GnRH neurons, but the effect was larger in young females than in old females.

Finally, we analyzed the total number of double-labeled cells in each age to see a possible sex difference. In young rats, ANOVA revealed a significant effect of treatment (saline vs. naloxone, $p < 0.0005$) and sex (male vs. female, $p < 0.003$) with significant interaction ($p < 0.003$). Further analysis by one-way ANOVA ($p < 0.0005$) revealed the number of GnRH-ir cells that were also Fos-ir was significantly larger in naloxone-injected females than in saline-injected females or naloxone-injected males. This result suggested that naloxone treatment in young rats induced Fos expression in GnRH neurons, but the effect was larger in females than in males. In old rats, two-way ANOVA revealed a significant effect of treatment (saline vs. naloxone, $p < 0.002$) but not of sex (male vs. female, $p > 0.1$) without interaction ($p > 0.06$). This result suggested that naloxone-induced Fos expression in old rats regardless of sex.

The present study demonstrated, in females, the number of GnRH-ir cells that expressed Fos in response to naloxone was approximately two times larger in young rats than old rats; while, no difference was observed between young and old male rats. However, there was a sex-specific difference in the response of GnRH neurons to naloxone in young rats that disappeared in old rats. We concluded, in the absence of gonadal steroid hormones, the GnRH pulse generator does not differ between older males and older females and does not change with age in male rats. Furthermore, LH levels in old rats dropped 40% in males and 85% in females, compared to young rats. The LH secretion data suggest that reproductive aging is due primarily to aging of the anterior pituitary function.

There are approximately 20% fewer GnRH-ir cells in old rats compared to young rats, irrespective of sex, suggesting age-related loss of GnRH neurons. This result is in good accord with our previous report [8], but contradictory to others [11,22]. Differences in the ages of animals used in the studies may be one reason for the variation; we used approximately 2-year-old rats, while other studies used rats approximately 10–12 months old. A more likely factor may be differences in the hormonal milieu of the animals; we used castrated rats, while other studies used intact animals.

We previously reported the percentage of GnRH-ir cells that express Fos in response to naloxone is 2.4% in male rats [24] and 6.8% in female rats [7]. In the present study, we found approximately 1.9% and 3.4% of GnRH-ir cells in young and old male rats, respectively, and 16.2% and 7.6% of GnRH-ir cells in young and old female rats, respectively, express Fos in response to naloxone. Small differences in the number of Fos-expressing GnRH-ir cells between the previous and present study are probably due to differences in the methods of naloxone administration (bulk intravenous injection in the present study and intravenous infusion in the previous study) and the time after naloxone treatment. We consider our overall results in the present study to be in accord with our previous results [7,24]. We conclude the population of GnRH neurons that express Fos is larger in young female rats than in young male rats, and there is no sex-specific difference in GnRH populations among old rats. Of note, both the percentage and distribution pattern of GnRH-ir cells that are also Fos-ir in the present study are in good accord with our previous studies; GnRH neurons located in the caudal region (i.e. the MBH) are more likely to express Fos in response to naloxone. This distribution pattern may suggest an important difference between GABAergic neurons and opioid neurons, which control GnRH secretion [7].

Opioid peptides are critically involved in the regulation of LH secretion via control of GnRH secretion [13]. Naloxone induces LH secretion by increasing GnRH secretion from the hypothalamus in rats [5]. Opioid peptides at least partly mediate the negative feedback of gonadal steroid hormones in both sexes of rats [13,23], as well as in human men [33] and women [34]. This suggests that the response to naloxone is due to the side of the hypothalamo-pituitary-gonadal axis related to the negative feedback of gonadal steroid hormones. Furthermore, in rats, opioid neurons play a distinct role in the control of GnRH secretion; naloxone stimulates the electrical activity of the GnRH pulse generator both in the presence and absence of gonadal hormones [12,20]. This phenomenon is also reported in goats [12], but not in monkeys [18]. Although the nature of the electrical activity of the GnRH pulse generator is not known, naloxone-induced Fos expression in GnRH neurons suggests activation of GnRH neurons. In support of this speculation, it has been reported that naloxone induces GnRH secretion in ovariectomized rats [14]. Thus, naloxone induces GnRH secretion [14], likely by increasing the GnRH pulse frequency, which is reflected as an increase in MUA volleys [20] and the resultant induction of Fos expression in GnRH neurons [7]. However, whether naloxone treatment induces Fos expression by directly activating GnRH neurons or by modulating other neurons is unclear from the present study, since naloxone was administered by an intravenous injection. Anatomical evidence [4] suggests direct action but we cannot deny the possibility that excitatory neurons activate GnRH neurons due to disinhibition by opioid neurons.

What is the physiological meaning of this sex-specific difference in Fos expression of GnRH neurons in young rats? Why is the GnRH pulse generator more active in females than males, as the present study in young rats demonstrates? We do not have

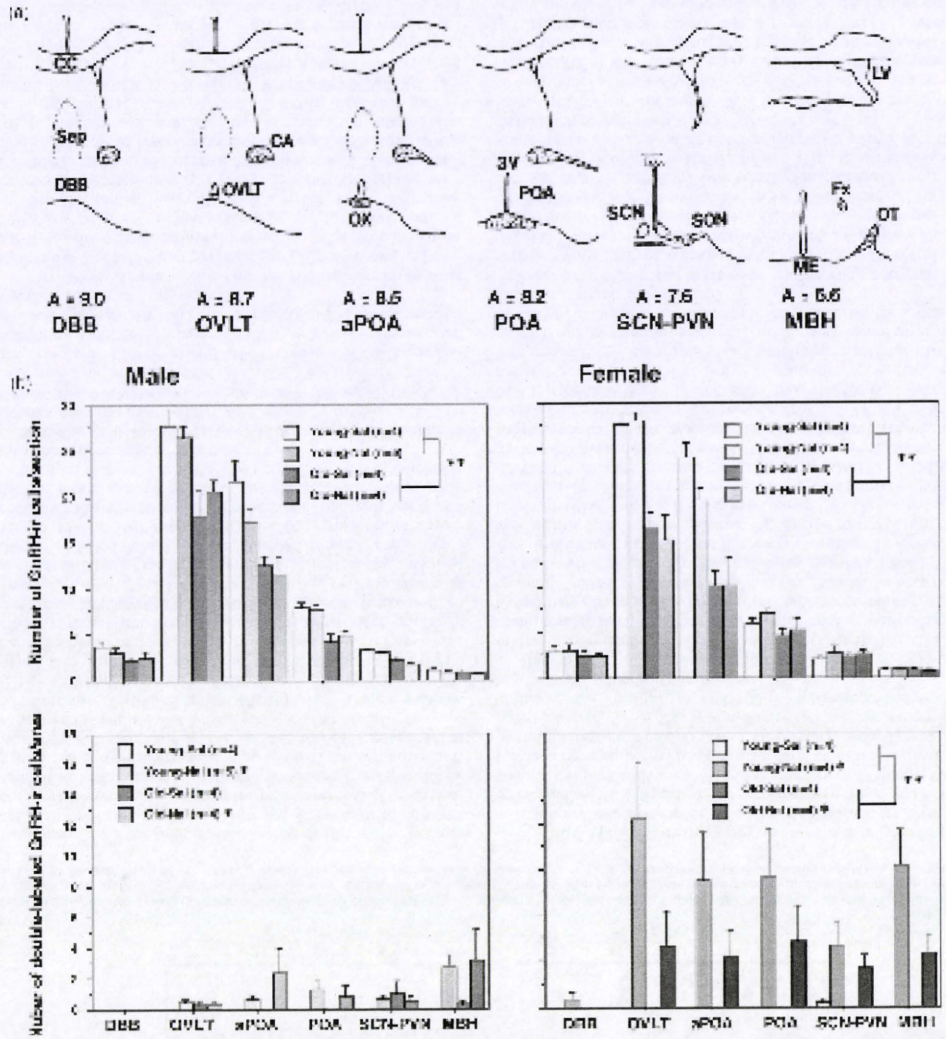

Fig. 2. Naloxone-induced Fos expression in GnRH-ir cells in young and old rats. (a) Schematic illustration of a coronal section showing the brain area where GnRH-ir cell expressing Fos-ir were quantified (modified from Albe-Fessard et al., 1996 [1]); aPOA, anterior preoptic area; CA, anterior commissure; DBB, diagonal band of the Broca; Fx, fornix; LV, lateral ventricle; ME, median eminence; MBH, mediobasal hypothalamus; OT, optic tract; OX, optic chiasm; OVLT, organum vasculosum of the lamina terminalis; POA, preoptic area; SCN, suprachiasmatic nucleus; Sep, septum; SON, supraoptic nucleus; 3V, third ventricle. (b) The number of GnRH-ir cells (upper panels) and GnRH-ir cells that also express Fos-ir (lower panels) in each brain area in males (left panels) and females (right panels). Values are the mean ± SEM and the numbers of rats are indicated in parentheses. * and ** indicate $p < 0.05$ vs. saline-injected rats at each age and saline-injected rats regardless of age, respectively.

answers to these questions yet, but one possible explanation is that GnRH neurons in females are active to maintain estrous cyclicity. The LH pulse frequency is influenced by the milieu of gonadal steroid hormones. Without testosterone in males and estrogen in females, the frequency of the GnRH pulse generator could theoretically be the same. In keeping with this hypothesis, the MUA volley intervals are identical in ovariectomized and orchidectomized rats ([20], Kato and Kimura personal communications). Therefore, basal pulse generator activity might be essentially the same in both sexes. However, the frequency is obviously higher in the follicular phase

compared to the luteal phase in female rats. This leads us to speculate that the GnRH pulse generator has the capacity to generate a higher frequency in females than in males, and this ability is lost during reproductive senescence. In female rats, the GnRH pulse generator is for the ovary, which shows phasic changes in function. After loss of ovary function due to reproductive senescence, it is quite reasonable there would be no sex-specific difference in the GnRH pulse generator in old rats, as found in the present study.

A simple interpretation of the present study may be that the pulse generator is not aged in both sexes, but rather GnRH neurons involved in surge generation are impaired with age. It has been suggested that opioid neurons are involved in the surge of LH secretion [2,13]. The mechanism that governs aging of the GnRH pulse generator in females is unknown at this time. GnRH neurons may be aged by definition [35]. An important point is that the effects of aging on the hypothalamus, in regard to GnRH neurons or other neural components of the GnRH pulse generator, are mild compared to age-related effects on the anterior pituitary.

Acknowledgment

This study was supported in part by a Grant-in-Aid for Scientific Research (C: 17590209 to TF) from the Ministry of Education, Culture, Sports, Science and Technology, Japan.

References

[1] D. Albe-Fessard, F. Stutinsky, S. Libouban, Atlas Stéréotaxique du Diencéphale du Rat Blanc, Centre National de la Recherche Scientifique, Paris, 1966.
[2] L.G. Allen, E. Hahn, D. Caton, S.P. Kalra, Evidence that a decrease in opioid tone on proestrus changes the episodic pattern of luteinizing hormone (LH) secretion: implications in the preovulatory LH hypersecretion, Endocrinology 122 (1988) 1004–1013.
[3] R.J. Bicknell, Endogenous opioid peptides and hypothalamic neuroendocrine neurones, J. Endocrinol. 107 (1985) 437–446.
[4] W.-P. Chen, J.W. Witkin, A.J. Silverman, Sexual dimorphism in the synaptic input to gonadotropin releasing hormone neurons, Endocrinology 126 (1990) 695–702.
[5] T.J. Cicero, P.F. Schmoeker, E.R. Meyer, B.T. Miller, Luteinizing hormone releasing hormone mediates naloxone's effects on serum luteinizing hormone levels in normal and morphine-sensitized male rats, Life Sci. 37 (1985) 467–474.
[6] A. Coquelin, C. Desjardins, Luteinizing hormone and testosterone secretion in young and old male mice, Am. J. Physiol. 243 (1982) E257–E263.
[7] T. Funabashi, K. Jinnai, F. Kimura, Fos expression by naloxone in LHRH neurons of the mediobasal hypothalamus and effects of pentobarbital sodium in the proestrous rat, J. Neuroendocrinol. 9 (1997) 87–92.
[8] T. Funabashi, F. Kimura, The number of luteinizing hormone-releasing hormone immunoreactive neurons is significantly decreased in the forebrain of old-aged female rats, Neurosci. Lett. 189 (1995) 85–88.
[9] A.C. Gore, B.M. Windsor-Engnell, E. Terasawa, Menopausal increases in pulsatile gonadotropin-releasing hormone release in a nonhuman primate (*Macaca mulatta*), Endocrinology 145 (2004) 4653–4659.
[10] R.A. Gorski, Gonadal hormones and the perinatal development of neuroendocrine function, Front. Neuroendocrinol. 2 (1971) 237–290.
[11] G.E. Hoffman, C.E. Finch, LHRH neurons in the female C57BL/6J mouse brain during reproductive aging: no loss up to middle age, Neurobiol. Aging 7 (1986) 45–48.
[12] K. Ito, T. Tanaka, Y. Mori, Opioid peptidergic control of gonadotropin-releasing hormone pulse generator activity in the ovariectomized goat, Neuroendocrinology 57 (1993) 634–639.
[13] S.P. Kalra, Neural circuits involved in the control of LHRH secretion: a model for estrous cycle regulation, J. Steroid Biochem. 23 (1985) 733–742.
[14] D.G. Karahalios, J.E. Levine, Naloxone stimulation of in vivo LHRH release is not diminished following ovariectomy, Neuroendocrinology 47 (1988) 504–510.
[15] A.E. Karpas, W.J. Bremner, D.K. Clifton, R.A. Steiner, D.M. Dorsa, Diminished luteinizing hormone pulse frequency and amplitude with aging in the male rat, Endocrinology 112 (1983) 788–792.
[16] A. Kato, H. Hiruma, F. Kimura, Acute estradiol modulation of electrical activity of the LHRH pulse generator in the ovariectomized rat: restoration by naloxone, Neuroendocrinology 59 (1994) 426–431.
[17] D.M. Keenan, J.D. Veldhuis, Disruption of the hypothalamic luteinizing hormone pulsing mechanism in aging men, Am. J. Physiol. Regul. Integr. Comp. Physiol. 281 (2001) R1917–R1924.
[18] J.S. Kesner, J.M. Kaufman, R.C. Wilson, G. Kuroda, E. Knobil, The effect of morphine on the electrophysiological activity of the hypothalamic luteinizing hormone-releasing hormone pulse generator in the rhesus monkey, Neuroendocrinology 43 (1986) 686–688.
[19] J.S. Kesner, R.C. Wilson, J.M. Kaufman, J. Hotchkiss, Y. Chen, H. Yamamoto, R.R. Pardo, E. Knobil, Unexpected responses of the hypothalamic gonadotropin-releasing hormone "pulse generator" to physiological estradiol inputs in the absence of the ovary, Proc. Natl. Acad. Sci. U.S.A. 84 (1987) 8745–8749.
[20] F. Kimura, M. Nishihara, H. Hiruma, T. Funabashi, Naloxone increases the frequency of the electrical activity of luteinizing hormone-releasing hormone pulse generator in long-term ovariectomized rats, Neuroendocrinology 53 (1991) 97–102.
[21] E. Knobil, The neuroendocrine control of the menstrual cycle, Recent Prog. Horm. Res. 36 (1980) 53–88.
[22] B.H. Miller, A.C. Gore, N-methyl-D-aspartate receptor subunit expression in GnRH neurons changes during reproductive senescence in the female rat, Endocrinology 143 (2002) 3568–3574.
[23] M.A. Miller, W.J. Bremner, D.K. Clifton, D.M. Dorsa, R.A. Steiner, Opioid regulation of luteinizing hormone secretion in the male rat, Biol. Reprod. 35 (1986) 17–26.
[24] D. Mitsushima, T. Funabashi, F. Kimura, Fos expression in gonadotropin-releasing hormone neurons by naloxone or bicuculline in intact male rats, Brain Res. 839 (1999) 209–212.
[25] Y. Mori, M. Nishihara, T. Tanaka, T. Shimizu, M. Yamaguchi, Y. Takeuchi, K. Hoshino, Chronic recording of electrophysiological manifestation of the hypothalamic gonadotropin-releasing hormone pulse generator activity in the goat, Neuroendocrinology 53 (1991) 392–395.
[26] M.K. Park, K. Wakabayashi, Preparation of a monoclonal antibody to common amino acid sequence of LHRH and its application, Endocrinol. Jpn. 33 (1986) 257–272.
[27] W.G. Rossmanith, C. Reichelt, W.A. Scherbaum, Neuroendocrinology of aging in humans: attenuated sensitivity to sex steroid feedback in elderly postmenopausal women, Neuroendocrinology 59 (1994) 355–362.
[28] A. Sano, F. Kimura, Electrical activity of the pulse generator of gonadotropin-releasing hormone in 26-month-old female rats, Neuroendocrinology 72 (2000) 199–207.
[29] K. Scarbrough, P.M. Wise, Age-related changes in pulsatile luteinizing hormone release precede the transition to estrous acyclicity and depend upon estrous cycle history, Endocrinology 126 (1990) 884–890.
[30] T. Tanaka, Y. Mori, K. Hoshino, Hypothalamic GnRH pulse generator activity during the estradiol-induced LH surge in ovariectomized goats, Neuroendocrinology 56 (1992) 641–645.
[31] J.D. Veldhuis, A. Iranmanesh, E. Samojlik, R.J. Urban, Differential sex steroid negative feedback regulation of pulsatile follicle-stimulating hormone secretion in healthy older men: deconvolution analysis and steady-state sex-steroid hormone infusions in frequently sampled healthy older individuals, J. Clin. Endocrinol. Metab. 82 (1997) 1248–1254.
[32] J.D. Veldhuis, D.M. Keenan, P.Y. Liu, A. Iranmanesh, P.Y. Takahashi, A.X. Nehra, The aging male hypothalamic-pituitary-gonadal axis: pulsatility and feedback, Mol. Cell Endocrinol. 299 (2009) 14–22.
[33] J.D. Veldhuis, A.D. Rogol, E. Samojlik, N.H. Ertel, Role of endogenous opiates in the expression of negative feedback actions of androgen and estrogen on pulsatile properties of luteinizing hormone secretion in man, J. Clin. Invest. 74 (1984) 47–55.
[34] M. Vermesh, P.D. Silva, R.A. Lobo, Endogenous opioids modulate the inhibitory effects of androgen on the hypothalamic-pituitary axis of normal women, J. Clin. Endocrinol. Metab. 65 (1987) 1183–1186.
[35] Y. Wang, M. Garro, H.A. Dantzler, J.A. Taylor, D.D. Kline, M.C. Kuehl-Kovarik, Age affects spontaneous activity and depolarizing after potentials in isolated gonadotropin-releasing hormone neurons, Endocrinology 149 (2008) 4938–4947.
[36] R.C. Wilson, J.S. Kesner, J.M. Kaufman, T. Uemura, T. Akema, E. Knobil, Central electrophysiologic correlates of pulsatile luteinizing hormone secretion in the rhesus monkey, Neuroendocrinology 39 (1984) 256–260.
[37] S.J. Winters, R.J. Sherins, P. Troen, The gonadotropin-suppressive activity of androgen is increased in elderly men, Metabolism 33 (1984) 1052–1059.
[38] J.W. Witkin, C.M. Paden, A.J. Silverman, The luteinizing hormone-releasing hormone (LHRH) systems in the rat brain, Neuroendocrinology 35 (1982) 429–438.

Physiology & Behavior 100 (2010) 101–104

Contents lists available at ScienceDirect

Physiology & Behavior

journal homepage: www.elsevier.com/locate/phb

Formalin-induced nociceptive behavior and c-Fos expression in middle-aged female rats

Hiroko Hagiwara [a], Fukuko Kimura [a,b], Dai Mitsushima [a], Toshiya Funabashi [a,*]

[a] Department of Physiology, Yokohama City University Graduate School of Medicine, 3-9 Fukuura, Kanazawa-ku, Yokohama 236-0004, Japan
[b] International University of Health and Welfare, Amity-Nogizaka-Bldg 1-21-1, Minamiaoyama, Minato-ku, Tokyo 107-0062, Japan, Japan

ARTICLE INFO

Article history:
Received 30 March 2009
Received in revised form 1 February 2010
Accepted 3 February 2010

Keywords:
Formalin
Middle age
Estrous cycle
Lateral septum
c-Fos
Female

ABSTRACT

The impact of the estrous cycle on the nociceptive response in middle-aged female rats was assessed using the formalin test and c-Fos immunoreactivity as a marker of neural activation. Young (2-month-old) and middle-aged (11-month-old) rats were examined, dividing the middle-aged rats into two groups based on their estrous cycle: regular 4-day estrous cycle and irregular estrous cycle. The right hind paw was subcutaneously injected with 50 μl of 2% formalin or saline as a control. Behavioral changes were observed for 1 h. Cycling rats were used during proestrus. Middle-aged female rats had a significantly higher score for nociceptive behavior compared to young rats, irrespective of estrous cyclicity, which suggests that aging, not the ability to maintain estrous cyclicity, causes hypersensitivity to the formalin injection. Immunohistochemical analysis found that the brain response to formalin injection was also more sensitive in middle-aged rats than young rats; a significant increase in the number of c-Fos immunoreactive cells was found in the ventral portion of the lateral septum of middle-aged rats injected with formalin compared to young and middle-aged rats injected with saline, irrespective of estrous cyclicity. Based on these results, we conclude that the sensitivity to painful stimuli in middle-aged female rats, which are in a neuroendocrine state similar to pre- and peri-menopausal women, is associated with age and not affected by reproductive ability.

1. Introduction

Women often report pain-related symptoms during menopause [1,2], and pain is a significant health problem for middle-aged women [3]. However, the factors that affect the pain response in menopausal females are not clear. A lack of understanding regarding these factors and mechanisms is mostly due to limited studies on age-related changes in nociception and pain behavior, which have only been performed in males [4]; no studies have focused on females during the arrest of spontaneous ovulation. For example, an age-associated change has been demonstrated in the sensitivity to formalin-induced tonic pain, which peaks at mid-life [5], but the study only used male rats.

Reproductive aging in female rodents is characterized by an arrest of spontaneous ovulation, with a transition from regular to irregular cycling in middle age [6,7]. Because the menopausal transition in women and female rats share significant characteristics, including patterns of luteinizing hormone secretion and responsiveness to estradiol, middle-aged female rats are an appropriate model for studying reproductive aging [7]. Importantly, changes in the blood estrogen levels of pre- and peri-menopausal women during aging [8] are similar to those of middle-aged rats [9–11]; the responsiveness to estrogen in the brain plays an essential role in the initiation of reproductive senescence before any changes in circulating estrogens [7].

In females, estrogens are not only essential for reproduction [12], but they are also an important factor in the modulation of pain responses. Interestingly, although the formalin test is a model of behavioral responses to tissue injury (phase 1) and inflammation (phase 2) [13,14], an estrogen effect is evident during interphase [15–18]. Thus, estrogens, the responsiveness to estrogens, and/or aging per se may alter pain responses in aged female rats, and the formalin test is suitable for measuring these alterations.

If 17β-estradiol is an important factor for pain responses, a change in pain-related behavior would not be observed unless serum 17β-estradiol is altered. If the responsiveness to 17β-estradiol is important, pain-related behavior would be different between regular-cycling and irregular-cycling groups of female rats. If aging itself is important, female rats would exhibit altered pain responses regardless of reproductive state. Therefore, the present study examined changes in the response to formalin-induced nociceptive stimuli using a behavioral test and focusing on the effect of the estrous cycle in middle-aged rats with unchanged serum 17β-estradiol levels [9–11]. In addition to behavioral examinations, we analyzed c-Fos expression

* Corresponding author. Department of Physiology, Yokohama City University Graduate School of Medicine, 3-9 Fukuura, Kanazawa-ku, Yokohama 236-0004, Japan. Tel./fax: +81 45 787 2578.
E-mail address: toshiya@med.yokohama-cu.ac.jp (T. Funabashi).

0031-9384/$ – see front matter © 2010 Elsevier Inc. All rights reserved.
doi:10.1016/j.physbeh.2010.02.004

as a marker of neural activity in order to determine the cerebral region associated with middle-age-related changes in the pain response.

2. Methods

2.1. Animals

Female 2-month-old (young) and 11-month-old (middle-aged) Wistar rats (Charles River, Yokohama, Japan) were maintained at a constant temperature of 24–26 °C under controlled lighting conditions (lights on 05:00–19:00) with food and water available ad libitum. Daily vaginal smears were obtained, and rats exhibiting three or more consecutive 4-day estrous cycles were defined as having a regular cycle. For young rats, only those exhibiting a regular cycle were used. Middle age was defined as 11 months of age because it is when rats transition from a regular estrous cycle to an irregular cycle [7]. The middle-aged rats were divided into two groups: rats exhibiting a regular 4-day estrous cycle (R group) and those that had ceased cycling (IR group). Regular-cycling rats were used on the day of proestrus. Irregular-cycling rats exhibiting persistent estrus or persistent diestrus were examined on these days. Twenty-four hours before formalin injection, a silicone cannula for intravenous anesthetic injection was implanted into the right atrium of all rats under ether anesthesia. This procedure did not interfere with the estrous cycle. The right hindpaws of some young (173 ± 3.3 g, $n=8$) and middle-aged rats (R group 376.3 ± 3.4 g, $n=8$; IR group 374.3 ± 4.5 g, $n=11$) were injected with 50 µl of 2% formalin and behavioral changes observed for 1 h. The remaining young (172.1 ± 4.1 g, $n=7$) and regular middle-aged rats (375 ± 7.6 g, $n=6$) were injected with saline on the day of proestrus as a control. All rats were sacrificed by an overdose of intravenous pentobarbital (100 mg/kg) and subjected to immunohistochemical analysis.

Heparinized phosphate buffer (PB; pH 7.5) at approximately 4 °C was perfused through the cardiac ventricle, followed by paraformaldehyde (4%) in PB. After perfusion, the brain was removed from the cranium, fixed at 4 °C overnight in PB containing 4% paraformaldehyde, and incubated at 4 °C overnight in 25% sucrose in PB. The brains were then frozen with powdered dry ice and stored at −70 °C until processed for immunohistochemistry.

Blood samples were taken before the injection and the serum 17β-estradiol concentrations determined using an EIA kit (Cayman Chemical Co., Ann Arbor, MI, USA). Serum samples were extracted once with diethyl ether and reconstituted with assay buffer. All animal housing and surgical procedures were in accordance with the guidelines specified by the institutional animal care and use committee of Yokohama City University School of Medicine. The experiments followed the ethical guidelines of the International Association for the Study of Pain [10].

2.2. Behavioral test

Immediately after the formalin injection, the rat was placed in a transparent Plexiglas box ($30 \times 30 \times 30$ cm) with a transparent floor positioned over a mirror angled at 45° to allow for observations of nociceptive behavior. The nociceptive behavior assessment [13,14] was performed on a single parameter by scoring the time of elevation for the injected paw. This simple method successfully detects sex differences in the formalin test [18] and was chosen because changes in single behavioral responses may be overlooked when using the weight-scores method [19]. We determined the length of time that the paw was elevated from the floor every 5 min for 1 h, and a mean response was calculated for each phase. For statistical purposes, the data were separated into three phases: phase I (0–5 min after formalin injection), interphase (5–15 min after injection), and phase II (15–60 min after injection).

2.3. Immunohistochemistry

Frozen coronal sections (30 µm) were cut using a Bright cryostat and washed with 0.1 M phosphate buffered saline (PBS). Samples were incubated overnight with rabbit polyclonal c-Fos antibody diluted 1:40,000 (PC38, Ab-5, Calbiochem) in PBS containing 1.5% normal goat serum and 0.1% Triton X-100. The next day, sections were incubated with biotinylated anti-rabbit IgG (1:200), followed by incubation with streptavidin–biotin–peroxidase complex (Vectastain Elite ABC Kit, Vectastain Lab).

Bound peroxidase was visualized by incubating the sections for 8 min in 0.05% 3,3′-diaminobenzidine with H_2O_2. Samples were then mounted on glass slides, dehydrated in graded alcohol, cleared in xylene, and coverslipped with Permount.

The lateral septal nucleus (LS) was subdivided into the dorsal (LSD), intermediate (LSI), and ventral (LSV) regions [20] (Fig. 1), and the number of c-Fos immunoreactive (c-Fos-ir) cells in each region was determined by an investigator blinded to the experimental conditions. Two sections per rat were selected and matched across all animals in all experimental groups. Microscopic images (5×10 magnification) were imported into a computer with a Penguin 600CL digital camera (Pixera Corporation, Los Gatos) and analyzed using Image-Pro plus version 5.1 (MedikaCybernetics, Inc.). The cut-off value was defined so that the number of nuclei obtained by this method was consistent with the number obtained by visual inspection.

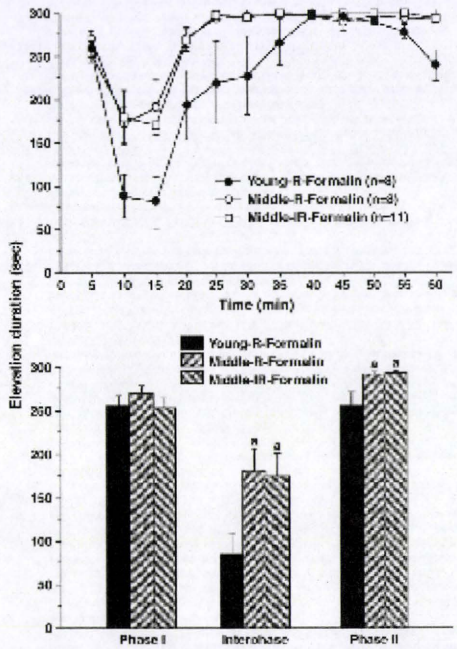

Fig. 1. Behavioral responses of young and middle-aged female rats during the formalin test. R, regular 4-day estrous cycle; IR, irregular estrous cycle. Each data point in the upper panel represents the amount of time the animals raised the injected paw (elevation duration) every 5 min during 1 h of observation. For statistical purposes, the data were separated into three phases in the lower panel: phase I (0–5 min after formalin injection), interphase (5–15 min after injection), and phase II (15–60 min after injection). The data are presented as mean ± SEM. a $P<0.05$ vs. young rats.

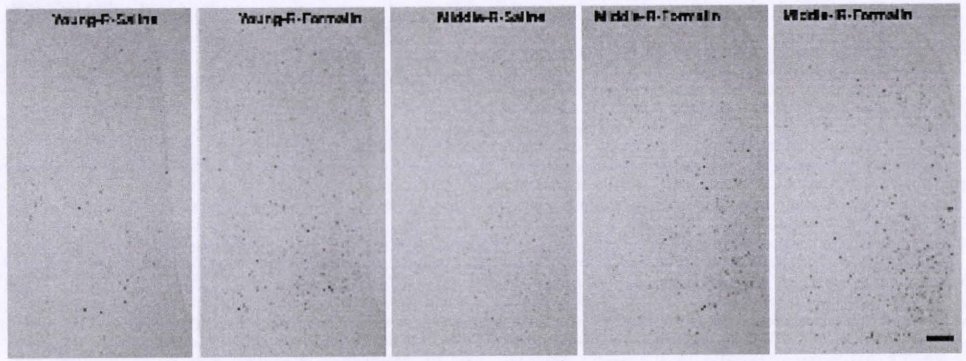

Fig. 2. Representative photographs of the lateral septum 1 h after saline or formalin injection. The c-Fos-immunoreactive cells are shown in a saline-injected young rat (Young-R-Saline), formalin-injected young rat (Young-R-Formalin), saline-injected middle-aged rat with a regular estrous cycle (Middle-R-Saline), formalin-injected middle-aged rat with a regular estrous cycle (Middle-R-Formalin), and a formalin-injected middle-aged rat with an irregular estrous cycle (Middle-IR-Formalin). Scale bar = 100 µm.

All counting parameters, including the cut-off value and microscopic illumination, were unchanged throughout the counting procedure. The number of c-Fos-ir cells in a square region ($600\ \text{mm} \times 600\ \text{mm}$) in the LSI and LSV and a rectangular region ($300\ \text{mm} \times 600\ \text{mm}$) on the LSD was counted bilaterally. The average number of c-Fos-ir cells per area in each rat was used for statistical analysis. Data were analyzed by repeated or one-way analysis of variance (ANOVA), followed by Fisher's protected least significant difference post-hoc test. Differences were considered significant if $P<0.05$.

3. Results

The serum concentrations of 17β-estradiol in the young-R-formalin ($n=8$), middle-R-formalin ($n=6$), and middle-IR-formalin ($n=6$) groups were $21.6 + 3.0$ pg/ml, $23.3 + 4.2$ pg/ml, and $26.4 + 4.1$ pg/ml, respectively. No significant difference in the serum concentrations was found (ANOVA, $P>0.6$).

3.1. Behavioral test

Formalin-injected rats exhibited two typical phases of nociceptive behavior (Fig. 1), which is in agreement with what was previously reported [13,14,18]. This pattern was similar in young and middle-aged rats, but we observed a different length of nociceptive behavior during interphase and phase II. Repeated measures ANOVA indicated a significant difference among the groups ($F_{2,\ 24}=4.950$, $P<0.05$) and phases ($F_{2,\ 48}=69.297$, $P<0.0001$) with a significant interaction ($F_{4,\ 48}=2.895$, $P=0.0317$). Because the interaction was significant, the groups were compared at each phase. We did not detect any significant differences among the groups during phase I ($F_{2,\ 24}=0.691$, $P>0.5$). In interphase ($F_{2,\ 24}=4.273$, $P<0.05$) and phase II ($F_{2,\ 24}=5.880$, $P<0.01$), ANOVA revealed significant differences among the groups. In both phases, the post-hoc comparison indicated that the duration of elevation in middle-aged rats was significantly longer than the duration in young rats, irrespective of the estrous cycle (interphase $P<0.05$, phase II $P<0.01$).

3.2. Number of c-Fos-ir cells

Based on visual inspection, the number of c-Fos-ir cells in the LS, but not other brain areas, including the paraventricular nucleus, the pre-optic area, and the bed nucleus stria terminalis, was associated with age. Formalin injection appeared to increase the expression of c-Fos in the cells of the lateral septum (Fig. 2), particularly in the LSV. ANOVA indicated a significant difference in the number of c-Fos cells in the LSV among the groups ($F_{4,\ 35}=6.326$, $P<0.001$; Fig. 3). The post-hoc comparison revealed that the number of c-Fos-ir cells in the middle-aged rats was significantly greater than in the control groups of young and middle-aged rats, irrespective of estrous cycle ($P<0.02$). We did not detect any significant differences in the number of c-Fos-ir cells between young saline- and formalin-injected rats

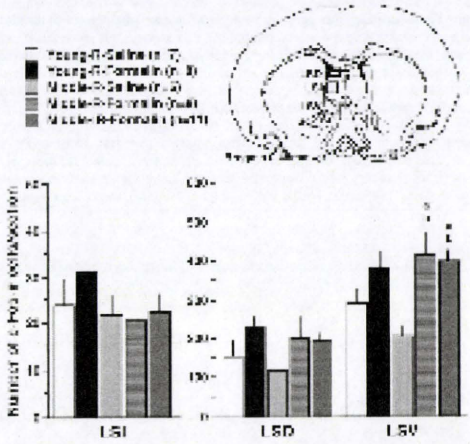

Fig. 3. Quantification of c-Fos immunoreactive cells in the lateral septum. Brain sections were from saline-injected young rats (Young-R-Saline), formalin-injected young rats (Young-R-Formalin), saline-injected middle-aged rats with a regular estrous cycle (Middle-R-Saline), formalin-injected middle-aged rats with a regular estrous cycle (Middle-R-Formalin), and formalin-injected middle-aged rats with an irregular estrous cycle (Middle-IR-Formalin). An illustration of the coronal region of the rat brain is shown in the upper right panel. The areas with bold and hatched lines indicate the regions in which c-Fos immunoreactive cells were counted and those taken for photographs in Fig. 2, respectively. Ac, anterior commissura; cc, corpus callosum; LSD, lateral septum dorsal; LSI, lateral septum intermediate; LSV, lateral septum ventral; n, optic nerve. Data are presented as mean ± SEM. a, $P<0.05$ vs. young rats injected with saline; b, $P<0.05$ vs. middle-aged rats injected with saline.

($P>0.09$). In the LSI, changes in the number of c-Fos-ir cells were similar to the changes in the LSV, but ANOVA found no significant difference ($F_{4,36}=2.411$, $P>0.05$). ANOVA also found no significant difference in the number of c-Fos-ir cells in the LSD among the groups ($F_{4,36}=0.758$, $P>0.5$; Fig. 3).

4. Discussion

We used the formalin test and immunohistochemical analysis to demonstrate that middle-aged female rats are more sensitive to formalin-induced nociceptive stimuli, irrespective of estrous cyclicity. We speculate that the brain response of the middle-aged rats, whose neuroendocrine status is similar to that of pre- and peri-menopausal women, exhibit hypersensitivity to nociceptive stimuli due to age, and this response is unrelated to reproductive ability.

Studies have suggested that females are sensitive to formalin-induced pain due to the influence of ovarian steroid hormones [15]. For example, normal female rats exhibit more nociceptive responses to formalin than ovariectomized rats, suggesting modulatory roles of ovarian steroid hormones [16]. Ovarian steroid hormone replacement in ovariectomized rats restores the ovariectomy-induced decline in nociceptive response [21], though contradictory results have been reported [22]. Thus, age-related changes in blood 17β-estradiol levels and/or responses to 17β-estradiol might determine pain hypersensitivity in middle-aged rats. However, 17β-estradiol levels of middle-aged rats, not only on the day of proestrus during regular-cycling, but also on another day during irregular cycling, are similar to the levels in young rats on the day of proestrus. These results are consistent with previous reports [9–11]. Therefore, we speculate that 17β-estradiol levels are not an important factor for hyperalgesia in middle age, and the pain response is elevated in association with age not only in males [5], but also in females. If this situation is the case, we would like to note that the aging effects are also related to phase in the formalin test; middle-aged rats were hyperalgesic in interphase and phase 2 but not in phase 1. The absence of age effects in phase 1 of the formalin test suggests that the tissue injury induced by formalin injection in middle-aged rats is not different from the injury induced in young rats. Middle age may be too early to see changes in phase 1, but previous results in old male rats may eliminate this possibility [5]. Currently, the mechanism for the phase-specific effects of age is not known, but the results of the present study support the idea that age differences in the pain responses are not linear in models of tissue injury and inflammation [4].

Another finding from the present study is that the activation of the LSV after formalin injection is stronger in middle-aged female rats than young female rats. This observation is in accordance with previous findings in male rats [23]. However, in young female rats, we observed a tendency of increased c-Fos expression after formalin injection, but it was not significantly different from the expression in saline-injected rats. This finding is contradictory to previous reports, which found increased c-Fos expression in the LS of male rats [24]. This discrepancy may be due to the assessment time after injection; we examined expression 1 h after injection, whereas the other report analyzed expression 2 h after injection [24]. In addition, Aloisi et al. [25] did not find a significant difference 90 min after injection. Nevertheless, our results suggest that pain responses are elevated in middle age. This speculation is supported not only by the results from our behavioral examination, but also the morphological study.

How the LSV is associated with the pain response in the brain after formalin injection is not yet known. Because pain is an emotional experience, and the lateral septum plays an important role in regulating emotional processes [18,26–28], we speculate that middle-aged females are hypersensitive to a pain-induced emotional process. Future studies should address the role of the LSV and the underlying mechanisms in the pain response in middle-aged females.

Acknowledgment

This work was supported by a Grant-in-Aid for Scientific Research (C: 17590208 to FK) from the Ministry of Education, Culture, Sports, Science and Technology of Japan.

References

[1] Peat G, Thomas E, Handy J, Croft P. Social networks and pain interference with daily activities in middle and old age. Pain 2004;112:397–405.
[2] Barnabei VM, Cochrane BB, Aragaki AK, Nygaard I, Williams RS, McGovern PG, et al. Menopausal symptoms and treatment-related effects of estrogen and progestin in the Women's Health Initiative. Obstet Gynecol 2005;105:1063–73.
[3] Rousseau ME, Gottlieb SF. Pain at midlife. J Midwifery Womens Health 2004;49:529–38.
[4] Gagliese L, Melzack R. Age differences in nociception and pain behaviours in the rat. Neurosci Biobehav Rev 2000;24:843–54.
[5] Gagliese L, Melzack R. Age differences in the response to the formalin test in rats. Neurobiol Aging 1999;20:699–707.
[6] Lu JK, Anzalone CR, LaPolt PS. Relation of neuroendocrine function to reproductive decline during aging in the female rat. Neurobiol Aging 1994;15:541–4.
[7] Downs JL, Wise PM. The role of the brain in female reproductive aging. Mol Cell Endocrinol 2009;299:32–8.
[8] Santoro N, Brown JR, Adel T, Skurnick JH. Characterization of reproductive hormonal dynamics in the perimenopause. J Clin Endocrinol Metab 1996;81:1495–501.
[9] Lerner SP, Meredith S, Thayne WV, Butcher RL. Age-related alterations in follicular development and hormonal profiles in rats with 4-day estrous cycles. Biol Reprod 1990;42:633–8.
[10] Rubin BS, Mitchell S, Lee CE, King JC. Reconstructions of populations of luteinizing hormone releasing hormone neurons in young and middle-aged rats reveal progressive increases in subgroups expressing Fos protein on proestrus and age-related deficits. Endocrinology 1995;136:3823–30.
[11] Gore AC, Yeung G, Morrison JH, Oung T. Neuroendocrine aging in the female rat: the changing relationship of hypothalamic gonadotropin-releasing hormone neurons and N-methyl-D-aspartate receptors. Endocrinology 2000;141:4757–67.
[12] Morrison JH, Brinton RD, Schmidt PJ, Gore AC. Estrogen, menopause, and the aging brain: how basic neuroscience can inform hormone therapy in women. J Neurosci 2006;26:10332–48.
[13] Henry JL, Yashpal K, Pitcher GM, Coderre TJ. Physiological evidence that the 'interphase' in the formalin test is due to active inhibition. Pain 1999;82:57–63.
[14] Tjolsen A, Berge OG, Hunskaar S, Rosland JH, Hole K. The formalin test: an evaluation of the method. Pain 1992;51:5–17.
[15] Aloisi AM, Bonifazi M. Sex hormones, central nervous system and pain. Horm Behav 2006;50:1–7.
[16] Gaumond I, Arsenault P, Marchand S. The role of sex hormones on formalin-induced nociceptive responses. Brain Res 2002;958:139–45.
[17] Spooner MF, Robichaud P, Carrier JC, Marchand S. Endogenous pain modulation during the formalin test in estrogen receptor beta knockout mice. Neuroscience 2007;150:675–80.
[18] Hagiwara H, Funabashi T, Mitsushima D, Kimura F. Effects of neonatal testosterone treatment on sex differences in formalin-induced nociceptive behavior in rats. Neurosci Lett 2007;412:264–7.
[19] Capone F, Aloisi AM. Refinement of pain evaluation techniques. The formalin test. Ann Ist Super Sanita 2004;40:223–9.
[20] Alonso JR, Frotscher M. Organization of the septal region in the rat brain: a Golgi/EM study of lateral septal neurons. J Comp Neurol 1989;286:472–87.
[21] Gaumond I, Arsenault P, Marchand S. Specificity of female and male sex hormones on excitatory and inhibitory phases of formalin-induced nociceptive responses. Brain Res 2005;1052:105–11.
[22] Kuba T, Quinones-Jenab V. The role of female gonadal hormones in behavioral sex differences in persistent and chronic pain: clinical versus preclinical studies. Brain Res Bull 2005;66:179–88.
[23] Lei LG, Zhang YQ, Zhao ZQ. Pain-related aversion and Fos expression in the central nervous system in rats. NeuroReport 2004;15:67–71.
[24] Ohtori S, Takahashi K, Chiba T, Takahashi Y, Yamagata M, Sameda H, et al. Fos expression in the rat brain and spinal cord evoked by noxious stimulation to low back muscle and skin. Spine 2000;25:2425–30.
[25] Aloisi AM, Zimmermann M, Herdegen T. Sex-dependent effects of formalin and restraint on c-Fos expression in the septum and hippocampus of the rat. Neuroscience 1997;81:951–8.
[26] Mongeau R, Miller GA, Chiang E, Anderson DJ. Neural correlates of competing fear behaviors evoked by an innately aversive stimulus. J Neurosci 2003;23:3855–68.
[27] Keefe FJ, Rumble ME, Scipio CD, Giordano LA, Perri LM. Psychological aspects of persistent pain: current state of the science. J Pain 2004;5:195–211.
[28] Sheehan TP, Chambers RA, Russell DS. Regulation of affect by the lateral septum: implications for neuropsychiatry. Brain Res Brain Res Rev 2004;46:71–117.

commentary

The chemical biology of synapses and neuronal circuits

Haruhiko Bito

Excitatory synapses are located in confined chemical spaces called the dendritic spines. These are atypical femtoliter-order microdomains where the behavior of even single molecules may have important biological consequences. Powerful chemical biological techniques have now been developed to decipher the dynamic stability of the synapses and to further interrogate the complex properties of neuronal circuits.

More than a century ago,the visionary anatomist (and later Nobel laureate) Santiago Ramon y Cajal uncovered the immense potential that the central nervous system acquires during development when innumerable connections, rather than fusions, are formed between diverse neuronal cells[1]. These connections are called synapses, and their anatomical, physiological, biochemical and pharmacological characteristics have been studied extensively for more than 100 years. It is estimated that there are about 10^{14} synapses formed between 10^{11} neurons in each and every human brain[2]. Through the explosion of knowledge we have gained over the past few decades, we are now able to pin down the locations of most synaptic proteins and even identify the favorite binding partners of many. Intense efforts are currently being devoted to cataloging the physical arrays of synaptic connections in the cerebral cortex and to extracting the organizing principles that govern these connectivities[3].

Synapses are subcellular microcompartments that are essential for a digital form of transneuronal communication, mediated by chemical mediators termed neurotransmitters. At excitatory synapses in the cerebral cortex, the most numerous synapses in our brain, the presynaptic nerve ending contains several tens to a few hundreds of synaptic vesicles filled with the neurotransmitter glutamate. Each time a terminal receives an electrical impulse from the cell soma, within one to a few milliseconds several vesicles fuse to presynaptic membrane zones and release a large amount of glutamate into the intersynaptic space. Released glutamate traverses this space by passive diffusion, and because its target glutamate receptors in the postsynaptic neuron are heavily enriched in specialized membrane structures that are directly apposed to the glutamate release sites, it will take no more than a few milliseconds for the postsynaptic ligand-gated channels to open and trigger a cascade of electrochemical signaling pathways.

This postsynaptic reception of neurotransmitter signals is carried out at the surface of very tiny (<1 fl; 1 fl = $(1\ \mu m)^3$) specialized protrusions[4] emanating from dendritic branches (**Fig. 1a**), which are termed dendritic 'spines'. Since Cajal's time, what we have learned about the spatial and structural regularity of these postsynaptic specializations strongly suggests that this synaptic apparatus (**Fig. 1b**) could serve as an elementary signal-generating (and perhaps also signal-processing) unit of a neuron. Here, I will discuss the growing impact of chemical biology in improving our understanding of the biology of the dendritic spines, with a view toward modeling, measuring and manipulating the dynamic functions of the synapses. Indeed, we have recently witnessed a tremendous amount of excitement on this subject, fueled by the ever-growing availability of new chemical and molecular tools that allow the thought experiments of the past to become reality today.

Spines are odd chemical reaction spaces

Information transmitted by synaptic activity is first received at the dendritic

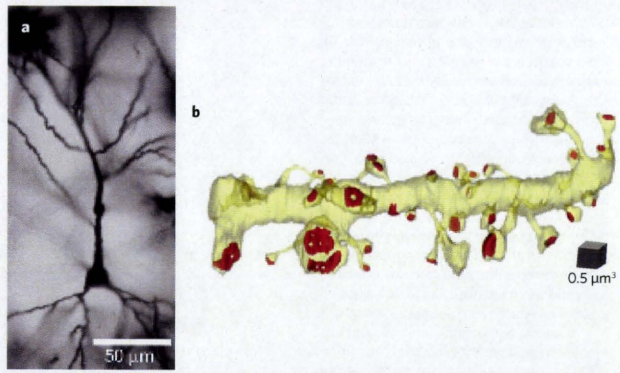

Figure 1 | Dendritic spines are highly atypical chemical reaction spaces at the boundary between mass and stochastic reaction schemes. (**a**) Golgi staining of dendritic branches in a typical neuron (courtesy of H. Okuno). (**b**) On the basis of the standard size of three-dimensionally reconstructed dendritic spines, we can estimate that in each spine, most signaling molecules are likely to be present only in small numbers (1 to about 100). The image in panel **b** is reproduced from ref. 33, with permission from Elsevier.

spines. But despite the fundamental importance of these structures, neuroscientists have yet to answer some of the simplest questions about the spines.

For example, let us consider the physical scale of the dendritic spines (**Fig. 2a**), where the synapses are. A rough estimate of the mean volume of the dendritic spines, obtained through serial electron microscopic reconstructions of excitatory synapses, shows them to be smaller than 1 fl (ref. 4) (**Fig. 1b**). A back-of-the-envelope calculation (**Box 1**) will then reveal that a decently enriched synaptic protein, such as glutamate receptor, at about 1 μM concentration will represent about 100 molecules per synapse. Strikingly, this also means that the presence of one single molecule in an average spine will represent a 10 nM concentration. A dissociation constant of this order is frequently observed in *in vitro* reactions between a pair of high-affinity interacting proteins or between an enzyme and a substrate. Thus, one might imagine that in a femtoliter-order space such as the spines, the addition or loss of each single molecule may perhaps be biologically important.

This is assuming that a chemical mass reaction based on free reaction and diffusion can occur in spines at the nano-to-meso scale. However, we do not actually know how diffuse synaptic proteins enriched in the spines are, as many of them are bound to either membrane-spanning proteins (such as channels and receptors) or cytoskeletal proteins (such as actin and actin-interacting) or both (**Fig. 2b**). It has been speculated that stochastic processes might be important in such tiny biological spaces, and indeed, models of stochastic reactions have been shown to reliably predict some of the signal transduction outcomes within a spine[5]. Conversely, experimental data suggest that the opening of a single presynaptic Ca^{2+} channel, for instance, can trigger neurotransmitter release[6], whereas even at the peak of a synaptic response, less than one NMDA receptor channel may be open on average[7], thus lending support to a possible stochastic scenario of synaptic transmission–triggered Ca^{2+} signaling. On the other hand, classical models of actin remodeling still remain useful for describing actin polymerization states within a spine[8], and a simple linear inverse correlation was found between spine length and PDZ domain–based interactions of PSD-95 and SynGAP, two dominantly expressed proteins at maturing synapses[9].

Thus, the truth may be a mixture of these two possibilities, to say the least, and dendritic spines appear to represent highly atypical chemical reaction spaces at the boundary between mass and stochastic reaction schemes. As these tiny synapses may behave quite distinctly from continuous fluids or ideal gas, one may need to go beyond the classical Boltzman equation and adopt other frameworks, such as the Langevin[10] or Focker-Planck equations[11], in order to more accurately describe and model the chemistry of synapses.

Box 1 | Back-of-the-envelope calculations

Estimating the number of molecules in a standard spine (~0.16 fl), given that concentration × volume × Avogadro constant = number of molecules:

At 1 μM, 1×10^{-6} (mol l^{-1}) × 0.16×10^{-15} (l) × $6.02 \times 10^{23} = 1 \times 10^{2}$ molecules

At 10 nM, 10×10^{-9} (mol l^{-1}) × 0.16×10^{-15} (l) × $6.02 \times 10^{23} = 1$ molecule

The dynamic stability of the synapses

For many decades, *in vivo* and *in vitro* recordings of synaptic transmission in many brain areas have shown remarkable stability in the magnitude of the electrical responses that can be elicited at synapses. Recent *in vivo* live imaging studies of dendritic spines in superficial layers of the cerebral cortex confirms that a large majority of synapses are indeed stable over a long period of time[12,13]. Similarly, the molecular make-up of the synapses appears to be quite stable and uniform across synapses, both presynaptically and postsynaptically, when measured in fixed brain tissues and cells that have already reached adulthood and maturity. However, given that most neurons in our brain lose their ability to divide during early development, how can such regularity of structures and molecular components persist over many months, if not years or a whole lifetime, in a majority of synapses?

Clearly, the replacement of both structural (membrane lipids and cytoskeleton) and proteinous components of the synapses has to take place under rigorous control, as most neuronal proteins degrade within hours to a few days once translated. In such a self-organized system, regulation of protein trafficking, as well as mRNA transcription and translation, may be truly vital.

Even more surprising, however, are recent measurements taken within the dendritic spines, both *in vitro* and *in vivo*, indicating that the turnover of synaptic proteins can be very fast, on the order of seconds to minutes[14,15]. Proteins may even travel across—and be shared between—neighboring spines within the same dendritic tree, without losing their activity[16]. Furthermore, during synaptic plasticity, which is a sudden change in the efficacy of the synaptic transmission that has been postulated to be a cellular correlate of memory, glutamate receptor numbers were shown to change substantially in accordance with the size and the direction of the plasticity[17].

To further complicate the picture, spine morphology is intrinsically fluctuating when measured over days, and this morphing can be strongly facilitated and biased into enlargement immediately after induction of plasticity[10,18]. Such an increase in spine size could be fast (within a few minutes) and substantial (>100%). The efficacy of chemical reactions could thus be modulated by a factor of 2–3 by such dynamic morphing of the spines.

How do neurons manage to become self-organized, accurately balancing protein removal from synapses and trafficking into synapses on demand, when the spine volume is dynamically modulated? What are the activation and inactivation kinetics of signal transduction enzymes in a living spine undergoing such dynamic morphing? Addressing these daunting issues is now a high priority in the context of understanding the pathology of many neuropsychiatric disorders. Indeed, dysregulation of the balance sheet of synaptic proteins (such as neuregulin, neurexin and shank), aberrant spine morphology and the associated defects in signal transduction have been correlated with several forms of cognitive dysfunction[10,17].

Recent advances in fluorescent protein-labeling techniques both chemical and genetic (such as tetracysteine tag, SNAP tag, HaloTag, quantum dot (QD)–tagged antibody and fluorescent protein tags) and in biophysical optical recording methods (such as total internal reflection microscopy and two-photon laser scanning microscopy) have been of immense help in addressing these questions[19,20]. Using these new technologies, we are able to get inside or near the synapses and spy on the dynamics of individual synaptic protein species one at a time while also recording spine shape. Local turnover of synaptic proteins inside a spine can be measured with fluorescence recovery after photobleaching techniques or through the use of photoconvertible fluorescent proteins. Tracking of membrane-bound surface glutamate receptors at single-molecule resolution using QD- or

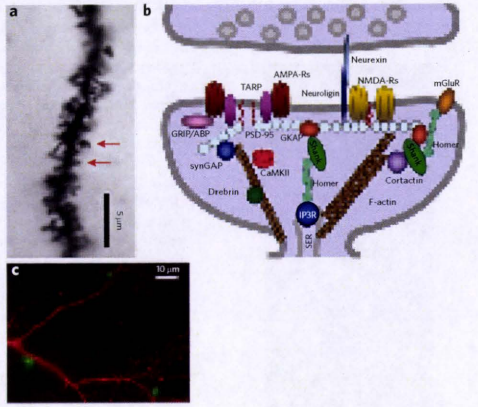

Figure 2 | Going inside the spines and exploring synaptic proteins that support the function of individual synapses. (**a**) Golgi stain of individual spines (courtesy of H. Okuno). (**b**) Analyzing one synapse at a time. Proteins expressed in dendritic spines are highly organized and form clusters; scaffolding proteins are directly and indirectly associated with membrane-spanning proteins such as channels and receptors, while also interacting with F-actin or F-actin-interacting proteins. (**c**) Localized distribution of activated caged fluorescein isothiocyanate (FITC) near the synaptic sites where focused UV light was shined.

fluorophore-labeled antibodies has revealed that lateral diffusion of synaptic receptors can be unexpectedly fast. Quantitative imaging using fluorescence resonance energy transfer (and fluorescence lifetime measurement) has also proven to be very effective in measuring signal transduction at single-synapse resolution.

Although not all the mysteries have been solved, these experiments collectively provide an increasingly quantitative picture of the protein machines that are present at synapses. Through engineering brighter dyes and tags with improved cell penetration, enhancing protein labeling techniques and using new single-molecule imaging methods with better signal-to-noise ratio, we will undoubtedly further our insights into how these synaptic machines are set in motion so that synapses can reliably generate robust and stable baseline electrical responses while also allowing dramatic changes in synaptic efficacy and spine volumes to occur in parallel.

Clicking synapses 'on' and 'off'

As discussed above, the dendritic spines represent one of the most interesting challenges for scientists elucidating the elementary chemical interface at the intersection of neural circuitry and intracellular signal transduction cascades. There are, however, many practical issues that need to be overcome to expand our knowledge in this area. We still do not even know the basic anatomical rules governing interaction and interference between physically proximal and distal synapses. Are there any mechanisms to amplify chemical signaling across distance? Do topologically organized chemical gradients exist inside dendrites, and do they play a significant role in modulating synaptic information processing?

Furthermore, we currently have little understanding of the functional states of synapses on a cell-assembly basis. What is the overall signaling impact of synaptic inputs at physically non-adjacent, yet temporally correlated, connections between neurons in an active cell assembly? What are the exact numbers (few or many?) and the locations (random or topologically organized?) of the synapses that are usually engaged in performing any given neuronal or cognitive task?

To address these questions, we clearly need to push the current limits of data acquisition and promote massively parallel imaging approaches using a battery of sensors of synaptic activity and of specific signal transduction pathways (obtained through careful chemical biological designs or encoded genetically), with both synaptic and cellular resolutions.

Our current ability to deconstruct the chemistry inside the synapses in depth gives hope that we will soon be able to reconstruct the function of a synapse and causally connect the networks of chemical reactions inside synapses with the encoding and representation of information within the neuronal circuit. The most direct way to do this is to choose a synapse of interest, identify unitary events and artificially manipulate them, preferably mimicking them so as to replace endogenous information inputs, and test how one has managed to alter (compromise or ameliorate) the neuronal circuitry's outputs.

Pioneering chemists have previously designed 'caged' molecules, in which photosensitive reaction moieties such as carboxy-2-nitrobenzyl (CNB), 4-methoxy-7-nitroindolinyl (MNI), carboxymethoxy-5,7-dinitroindolinyl (CDNI) or ruthenium-bipyridine-trimethylphosphine (RUBI) groups mask the functional groups of the molecule[21–23]. Exposure to light of a specific wavelength triggers photocatalysis of these moieties, thereby revealing the protected groups and 'activating' the molecules instantaneously (**Fig. 2c**). Shining light on synapses bathed with caged neurotransmitters has provided a powerful

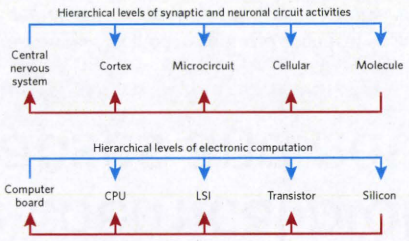

Figure 3 | Deconstructing and reconstructing cognition. Manipulating and interrogating synapses and neuronal circuits, by triggering and altering synaptic activity, has simultaneous effects at several distinct hierarchical levels: behavioral, systems, microcircuits, cellular and molecular. Intuitively, these levels can be compared to various complexities of electronic computation.

means to demonstrate the role of glutamate as a neurotransmitter, to map functional circuit connectivities *in vitro*[24] and *in vivo*[25] and to uncover mechanisms of synaptic plasticity at single-spine resolution[10,18,26] at millisecond to second temporal resolution. Additionally, chemical genetic strategies such chemical dimerization[27], inducible protein stabilization[28] or molecular re-engineering[29] are actively sought after to dissect the role of specific chemical signaling pathways.

Systematically manipulating a specific set of synapses *in vivo* will unavoidably modify neural function at all levels: molecular, cellular, circuits, systems, and behavioral (**Fig. 3**). Spectacular achievements using optogenetic technologies[30] demonstrate the critical importance of precisely targeting specific sets of synapses within a neuronal circuit. Clearly, finding the most astute combination of remotely activatable chemicals, circuit-oriented genetic manipulation and massively parallel high-throughput readouts at multiple levels, *ex vivo* or *in vivo*, will pave the way for a successful chemical biology exploration of the synapses and neuronal circuits.

What lies ahead?

More and more, our efforts to tease apart the principles of chemistry and how they pertain to communication inside and across synapses are met with success. Through these continuing efforts, we will better resolve the molecular states and kinetics of the most basic chemical events, events that are central to the computation carried out in each of the 10^{14} synapses. This level of deconstruction of the chemical nature of the synapses now provides us with an unprecedented window of opportunity to address a fundamental desire of a synaptologist: can we sneak into the synapses' 'design' and even perhaps reprogram them?

Although constructing and designing synapses may have sounded preposterous five years ago, it does not sound so far-fetched in 2010. In fact, a tremendous amount of translational research money is now being devoted to the study of the malfunction of so-called "induced synapses" formed *in vitro* between neuron-like cells massively derived from human induced pluripotent stem cells, which were obtained from living neuropsychiatric patients. If we could identify the faulty information processing event involved at induced synapses in such disease neurons, we might think of using drugs to correct synaptic dysregulation there. The possibility of *en masse* reprogramming of embryonic stem cells into "induced neurons"[31] and of building layered neuronal structures among them[32] in fact, provides hope that drug screening and pre-preclinical trials performed to study neuronal activity in human induced neuronal circuits *in vitro* may become a reality in the not-too-distant future. ■

Haruhiko Bito is in the Department of Neurochemistry at University of Tokyo Graduate School of Medicine, Tokyo, Japan.
e-mail: hbito@m.u-tokyo.ac.jp

References

1. Ramón y Cajal, S. *Textura del sistema nervioso del hombre y de los vertebrados* (Librería de Nicolás Moya, Madrid, 1899).
2. Kandel, E.R. Schwartz., J. H. & Jessell T. M. *Principles of Neural Science*. 4th ed. (McGraw-Hill, New York, 2000)
3. Markram, H. *Nat. Rev. Neurosci.* **7**, 153–160 (2006).
4. Harris, K.M. & Stevens, J.K. *J. Neurosci.* **9**, 2982–2997 (1989).
5. Bhalla, U.S. *Biophys. J.* **87**, 745–753 (2004).
6. Stanley, E.F. *Neuron* **11**, 1007–1011 (1993).
7. Nimchinsky, E.A., Yasuda, R., Oertner, T.G. & Svoboda, K. *J. Neurosci.* **24**, 2054–2064 (2004).
8. Honkura, N., Matsuzaki, M., Noguchi, J., Ellis-Davies, G.C. & Kasai, H. *Neuron* **57**, 719–729 (2008).
9. Nonaka, M., Doi, T., Fujiyoshi, Y., Takemoto-Kimura, S. & Bito, H. *J. Neurosci.* **26**, 763–774 (2006).
10. Kasai, H., Fukuda, M., Watanabe, S., Hayashi-Takagi, A. & Noguchi, J. *Trends Neurosci.* **33**, 121–129 (2010).
11. Harrison, L.M., David, O. & Friston, K.J. *Phil. Trans. R. Soc. Lond. B* **360**, 1075–1091 (2005).
12. Yang, G., Pan, F. & Gan, W.B. *Nature* **462**, 920–924 (2009).
13. Holtmaat, A. & Svoboda, K. *Nat. Rev. Neurosci.* **10**, 647–658 (2009).
14. Kuriu, T., Inoue, A., Bito, H., Sobue, K. & Okabe, S. *J. Neurosci.* **26**, 7693–7706 (2006).
15. Gray, N.W., Weimer, R.M., Bureau, I. & Svoboda, K. *PLoS Biol.* **4**, e370 (2006).
16. Tsuriel, S. *et al. PLoS Biol.* **4**, e271 (2006).
17. Kessels, H.W. & Malinow, R. *Neuron* **61**, 340–350 (2009).
18. Matsuzaki, M., Honkura, N., Ellis-Davies, G.C. & Kasai, H. *Nature* **429**, 761–766 (2004).
19. Giepmans, B.N., Adams, S.R., Ellisman, M.H. & Tsien, R.Y. *Science* **312**, 217–224 (2006).
20. Miyawaki, A. *Neuron* **48**, 189–199 (2005).
21. Canepari, M., Nelson, L., Papageorgiou, G., Corrie, J.E.T. & Ogden, D. *J. Neurosci. Methods* **112**, 29–42 (2001).
22. Ellis-Davies, G.C. *Nat. Methods* **4**, 619–628 (2007).
23. Fino, E. *et al. Front. Neural Circuits* **3**, 2 (2009).
24. Yoshimura, Y., Dantzker, J.L. & Callaway, E.M. *Nature* **433**, 868–873 (2005).
25. Matsuzaki, M., Ellis-Davies, G.C. & Kasai, H. *J. Neurophysiol.* **99**, 1535–1544 (2008).
26. Tanaka, K. & Augustine, G.J. *Neuron* **59**, 608–620 (2008).
27. Pruschy, M.N. *et al. Chem. Biol.* **1**, 163–172 (1994).
28. Banaszynski, L.A., Chen, L.C., Maynard-Smith, L.A., Ooi, A.G. & Wandless, T.J. *Cell* **126**, 995–1004 (2006).
29. Bishop, A.C. *et al. Nature* **407**, 395–401 (2000).
30. Gradinaru, V. *et al. Cell* **141**, 154–165 (2010).
31. Vierbuchen, T. *et al. Nature* **463**, 1035–1041 (2010).
32. Eiraku, M. *et al. Cell Stem Cell* **3**, 519–532 (2008).
33. Bourne, J. & Harris, K.M. *Curr. Opin. Neurobiol.* **17**, 381–386 (2007).

Acknowledgments

This commentary is based on past and ongoing works that received support from grants-in-aid from the Japan Society for Promotion of Science, the Ministry of Education, Culture, Sports, Science and Technology of Japan, the Ministry of Health, Labor and Welfare of Japan, a Global Center of Excellence program "Comprehensive Center for Education and Research of the Chemical Biology of Disease" and awards from the Astellas Foundation for Research on Metabolic Disorders, the Cell Science Foundation, the Takeda Science Foundation and the Toray Science Foundation. The author thanks H. Okuno, S. Takemoto-Kimura and H. Fujii for critical comments on an earlier version of the manuscript.

Competing interests statement

The author declares no competing financial interests.

NeuroToxicology 31 (2010) 85–93

Contents lists available at ScienceDirect

NeuroToxicology

Up-regulation of neurotrophin-related gene expression in mouse hippocampus following low-level toluene exposure

Tin-Tin Win-Shwe [a], Shinji Tsukahara [a], Shoji Yamamoto [a], Atsushi Fukushima [a], Naoki Kunugita [b], Keiichi Arashidani [b], Hidekazu Fujimaki [a,*]

[a] *Research Center for Environmental Risk, National Institute for Environmental Studies, 16-2 Onogawa, Tsukuba, Ibaraki 305-8506, Japan*
[b] *University of Occupational and Environmental Health, Japan 1-1 Iseigaoka, Yahatanishi-ku, Kitakyushu, Fukuoka 807-8555, Japan*

ARTICLE INFO

Article history:
Received 8 May 2009
Accepted 17 November 2009
Available online 22 November 2009

Keywords:
Neurotrophins
Toluene
Brain
Mice
Allergy
Strain difference

ABSTRACT

To investigate the role of strain differences in sensitivity to low-level toluene exposure on neurotrophins and their receptor levels in the mouse hippocampus, 8-week-old male C3H/HeN, BALB/c and C57BL/10 mice were exposed to 0, 5, 50, or 500 ppm toluene for 6 h per day, 5 days per week for 6 weeks in an inhalation chamber. We examined the expressions of neurotrophin-related genes and receptors in the mouse hippocampus using real-time reverse transcription polymerase chain reaction (RT-PCR). The expression of nerve growth factor (NGF), brain-derived neurotrophic factor (BDNF), tyrosine kinase (Trk) A, and TrkB mRNAs in the C3H/HeN mice hippocampus was significantly higher in the mice exposed to 500 ppm toluene. Among the three strains of mice, the C3H/HeN mice seemed to be sensitive to toluene exposure. To examine the combined effect of toluene exposure and allergic challenge, the C3H/HeN mice stimulated with ovalbumin were exposed to toluene. The allergy group of C3H/HeN mice showed significantly elevated level of NGF mRNA in the hippocampus following exposure to 50 ppm toluene. Then, we also examined the expression of transcription factor, dopamine markers and oxidative stress marker in the hippocampus of sensitive strain C3H/HeN mice and found that the expression of CREB1 mRNA was significantly increased at 50 ppm toluene. In immunohistochemical analysis, the density of the NGF-immunoreactive signal was significantly stronger in the hippocampal CA3 region of the C3H/HeN mice exposed to 500 ppm toluene in non-allergy group and 50 ppm in allergy group. Our results indicate that low-level toluene exposure may induce up-regulation of neurotrophin-related gene expression in the mouse hippocampus depending on the mouse strain and an allergic stimulation in sensitive strain may decrease the threshold for sensitivity at lower exposure level.

1. Introduction

Toluene is a well-known neurotoxicant and the central nervous system is a primary target in both acute and chronic exposure of toluene-toxicity (US EPA, 1994). Previous data from *in vivo* and *in vitro* animal studies strongly support that the hippocampus is target for toluene (Korbo et al., 1996; Terashi et al., 1997; Gelazonia et al., 2006). In addition, we had measured brain toluene levels by solid-phase microextraction technique and reported the hippocampal toluene levels following inhalation exposure (Nakajima et al., 2006) and intraperitoneal administration (Win-Shwe et al., 2007a). Little is known about the role of hippocampus in allergic sensitivity. Toluene exposure may cause alterations in the hippocampal functions of individuals with underlying allergic or stressful conditions (Lindvall et al., 1992). The number of corticotrophin-releasing hormone (CRH)-immunoreactive (ir) neurons in the hypothalamus, the number of adrenocorticotropic hormone (ACTH)-ir cells, and ACTH-mRNA expression in the anterior pituitary of allergy (AG) group mice were significantly higher than those of non-allergy (NAG) group mice (Sari et al., 2004, 2006). Recently, we have reported that the ovalbumin (OVA) immunization may enhance the sensitivity to toluene exposure by modulating the NMDA receptor subunit expressions in the olfactory bulb of allergic mouse model (Win-Shwe et al., in press). Therefore, in the present study, we used OVA as a stressor to investigate whether exposure to low levels of toluene, in combination with OVA, might also affect hippocampal neurotrophin-related gene expression.

Neurotrophins are a group of structurally related polypeptides that support the survival, differentiation, and maintenance of neuronal populations expressing appropriate high-affinity neurotrophin receptors. Neurons in the hippocampus are maintained by neurotrophins, such as nerve growth factor (NGF), brain-derived neurotrophic factor (BDNF), and the tyrosine kinase (Trk) family of neurotrophin receptors. Neurotrophins and their related receptors have been identified as targets for neurotoxicants and are known to play a role in bidirectional signaling between cells of the

* Corresponding author. Tel.: +81 29 850 2518; fax: +81 29 850 2518.
E-mail address: fujimaki@nies.go.jp (H. Fujimaki).

0161-813X/$ – see front matter © 2009 Elsevier Inc. All rights reserved.
doi:10.1016/j.neuro.2009.11.004

immune and nervous systems. Recently, many researchers have examined the functions of neurotrophic factors and their receptors in the brain, because these factors and receptors might be possible targets for neurotoxicants like lead (Kidd et al., 2008) and chlorpyrifos (Betancourt et al., 2006).

While the neurobehavioral and neurotoxic effects of toluene have been thoroughly examined, the mechanisms whereby toluene exerts its effects in the brain are not fully understood. The occupational exposure limit for toluene is 50 ppm in Japan (Japan Society for Occupational Health, 1994) and recently updated threshold limit value is 20 ppm in United States (ACGIH, 2006). Exposure to low concentrations of toluene leads to persistent deficits in spatial learning and memory function in a rat model (von Euler et al., 1993, 2000). From a dosimetric analysis of behavioral effects of acute toluene exposure in rat and humans, behavioral outcomes depend on internal dose rather than external dose and duration of exposure (Benignus et al., 1998). Recently, a study using a mouse model showed that mice exposed to a low level of toluene showed little change in the number of rewards obtained in a waiting-for-reward task, whereas mice exposed to a high concentration of toluene exhibited a significantly poorer performance, suggesting that exposure to high concentrations of toluene had a significant impact on cognitive and/or psychomotor function (Bowen and McDonald, 2009). Toluene also affects the neurotransmitter systems in the hippocampus. Our previous study indicates that the extracellular levels of neurotransmitter glutamate and taurine in the mice hippocampus were rapidly and reversibly increased within 30 min after the toluene administration in a dose-dependent manner and returned to the basal level by 1 h, however, the glycine and GABA were stable and no significant changes were observed (Win-Shwe et al., 2007a).

We hypothesized that toluene exposure may affect the function of the hippocampus via the modulation of neurotrophin-related genes and signaling pathway in strain-dependent manner and allergic stimulation may influence the threshold for sensitivity. Therefore, the present study was designed to investigate the intra-species variation in sensitivity to the expression of toluene-mediated neurotrophins and related receptors in the mouse hippocampus and examine the combined effect of toluene exposure and allergic challenge on neurogenesis-related markers in the hippocampus of sensitive mouse strain.

2. Materials and methods

2.1. Animals

Seven-week-old male C3H/HeN, BALB/c and C57BL/10 mice were obtained from Japan SLC Inc. (Shizuoka, Japan) and were used at an age of 8 weeks. Food and water were given *ad libitum*. The mice were housed in plastic cages under controlled environmental conditions (temperature, 23 ± 0.5 °C; humidity, 50 ± 5%; lights on between 07:00 and 19:00 h). This study was approved by the Ethics Committee for Experimental Animals of the University of Occupational and Environmental Health, Japan.

2.2. Experimental design

To detect the strain differences in response to toluene exposure, C3H/HeN, BALB/c and C57BL/10 mice ($n = 9$ each) were exposed to either a filtered air control (0 ppm) or 5, 50, or 500 ppm of toluene for 6 h (from 10:00 to 16:00 h) per day, 5 days per week for 6 weeks. One day following the final toluene inhalation, the hippocampi from nine mice (six for mRNA analysis and three for immunohistochemical analysis) from each strain were collected. Among the three strains of mice, C3H/HeN mice seemed to be most sensitive to toluene exposure and this mouse strain was used to detect the combined effect of toluene exposure and OVA immunization. C3H/HeN mice ($n = 9$ each, six for mRNA analysis and three for immunohistochemical analysis) were exposure to toluene as same schedule and the AG groups were treated with OVA on days 0, 7, 21 and 42 approximately 1 h before toluene exposure. These mice were injected with 10 μg of OVA plus 2 mg of alum intraperitoneally on day 0 and 10 μg of OVA only on day 7. Each of these mice was then challenged with nebulized OVA as a booster once every 3 weeks (days 21 and 42) during the exposure period, as described previously (Fujimaki et al., 2007). Fig. 1 shows the detail experimental schedule for the present study.

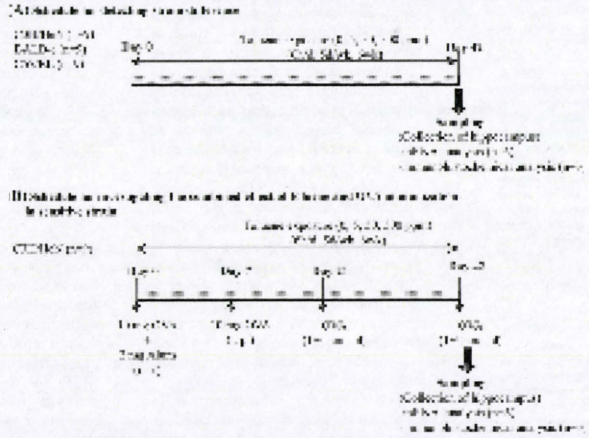

Fig. 1. (A) Experimental schedule for detecting different sensitivity in three strains of mice and (B) experimental schedule for investigating the combined effect of toluene and OVA immunization in C3H/HeN mice. Mice were exposed to a filtered air control (0 ppm), 5, 50, or 500 ppm of toluene for 6 h (from 10:00 to 16:00 h) per day, 5 days per week for 6 weeks. The allergy (AG) groups were treated with OVA on days 0, 7, 21 and 42 approximately 1 h before toluene exposure.

2.3. Generation of toluene

Toluene vapor was generated using an organic solvent gas generator (Shibata Scientific Technology, Ltd.) and was diluted with clean, filtered air to achieve the desired gas concentrations; the vapor was then introduced into a stainless steel and glass chamber, as described previously (Hori et al., 1999). The average toluene levels (mean ± S.D.) in the 5-, 50- and 500-ppm exposure groups were 4.9 ± 0.6, 49.5 ± 4.4, and 496.7 ± 17.9 ppm, respectively.

2.4. Quantitative real-time PCR

One day following the final toluene inhalation, the mice were sacrificed under deep pentobarbital anesthesia and the hippocampus was collected from each group of three strains of mice, frozen quickly in liquid nitrogen, and then stored at −80 °C until the total RNA was extracted. The expression levels of NGF, BDNF, TrkA, TrkB, calcium/calmodulin-dependent protein kinase (CaMK)-IV, cyclic AMP responsive element binding protein (CREB)-1, CREB2, D1, D2, tyrosine hydrolase (TH), heme oxygenase (HO)-1, Bax, Bbc3 and 18S mRNA in the hippocampus were estimated using quantitative real-time PCR analysis with the ABI Prism 7000 Sequence Detection System (Applied Biosystems Inc., USA), as described previously (Win-Shwe et al., 2007b). The tissue 18S level was examined as an internal control. The primer sequences used in the present study were shown in Table 1. Some primers (BDNF, ID_12064; TrkA, ID_18211; TrkB, ID_18212; D1, ID_13488; D2, ID_13489; TH, ID_21823; Bbc3, ID_170770; Bax, ID_12028; HO-1, ID_15368) were purchased from Qiagen, Sample & Assay Technologies (Qiagen GmbH, Germany). Data were analyzed using the comparative threshold cycle method. The relative expression levels of each mRNA were normalized individually according to the 18S content in the respective samples and were expressed as mRNA signals per 18S.

2.5. Immunohistochemistry

On the day after the final toluene exposure, the brains were removed from three C3H/HeN mice from each group of control and toluene-exposed non-allergy and AG groups after the animals had been deeply anesthetized with sodium pentobarbital; the brains were then fixed with 10% formalin. The fixed brains were dehydrated using a graded series of ethanol, cleared with xylene, and embedded in paraffin. Coronal paraffin sections were cut at a thickness of 10 μm using a cryostat and were mounted on 3-aminopropyltriethoxysilane-coated glass slides. Cells containing NGF polypeptide in the hippocampus were detected immunohistochemically.

To determine the expression levels of NGF polypeptide in the hippocampus, series of NGF-immunostained sections taken from 3 mice in each group (4 sections for each mouse) were used to analyze the density of NGF-immunoreactive signals in the hippocampus. Photomicrographic digital images (150 dpi, 256 scales) of the hippocampal regions were taken using a CCD camera connected to a light microscope. In the pyramidal cell layer of the CA1 and CA3 regions, the granular cell layer of the DG, and all of these regions combined, the densities of the NGF-immunoreactive signals were determined with the aid of a computer running image-analysis software (ImageJ 1.38X; National Institutes of Health, Bethesda, MD, USA). The density of the NGF-immunoreactive signal was expressed as a percentage of the NGF-immunoreactive area darker than 70 of the 256 units in the total area of interest.

Table 1
Primer sequences used in real-time PCR.

Gene	Primer	Sequence
18S rRNA	Forward	5′-TACCACATCCAAGAAGGCAG-3′
	Reverse	5′-TGCCCTCCAATGGATCCTC-3′
NGF	Forward	5′-TGGGCTTCAGGGACAGAGTC-3′
	Reverse	5′-CAGCTTTCTATACTGGCCGCAG-3′
CREB1	Forward	5′-GGAATCTGGAGCAGACAACC-3′
	Reverse	5′-ATAACGCCATGGACCTGGAC-3′
CREB2	Forward	5′-AATTGGCCATCTCCCAGAAA-3′
	Reverse	5′-GAATGCTCTGGAGTGGAAGAC-3′
CaMKIV	Forward	5′-AAATCAGCCTGGTCCTTGAG-3′
	Reverse	5′-TCTGGTTTGAGGTCACGATG-3′

2.6. Statistical analysis

All data were expressed as the mean ± standard error (S.E.). The statistical analysis was performed using the StatMate II statistical analysis system for Microsoft Excel, Version 5.0 (Nankodo Inc., Tokyo, Japan). Dose–response data were analyzed using a one-way analysis of variance with a Bonferroni/Dunn post-hoc analysis. A value of $P < 0.05$ was considered statistically significant.

3. Results

3.1. Detection of intra-species variation of sensitivity to toluene exposure

To explore the sensitive strain of mice to toluene exposure, we compared the expression of various marker mRNA in the hippocampus of C3H/HeN, BALB/c and C57BL/10 mice.

3.1.1. Neurotrophins and related receptors

NGF mRNA expression in the hippocampus of the C3H/HeN mice was significantly increased in mice exposed to 500 ppm of toluene ($P < 0.01$, Fig. 2a). The mRNA expression of TrkA, a receptor for NGF, was also significantly increased in mice exposed to 500 ppm of toluene ($P < 0.01$, Fig. 2d). In BALB/c mice, however, no significant change in NGF or TrkA receptor expression was observed after toluene exposure (Fig. 2b and e). Moreover, no significant difference in NGF or TrkA receptor expression was observed in C57BL/10 mice after toluene exposure (Fig. 2c and f).

BDNF mRNA expression in the hippocampus of C3H/HeN mice was significantly increased in mice exposed to 500 ppm of toluene ($P < 0.01$, Fig. 3a). The mRNA expression of TrkB, the receptor for BDNF, was also significantly increased in mice exposed to 500 ppm of toluene ($P < 0.01$, Fig. 3d). In BALB/c mice, BDNF mRNA expression was significantly increased in the mice exposed to 500 ppm of toluene, compared with expression in the control group ($P < 0.01$, Fig. 3b). No significant change in TrkB receptor expression was observed in BALB/c mice after toluene exposure (Fig. 3e). Furthermore, no significant difference in BDNF or TrkB receptor expression was observed in C57BL/10 mice after toluene exposure (Fig. 3c and f).

3.1.2. Transcription factor

In NGF signal transduction pathways, multiple protein kinases translocate to the nucleus to activate transcriptional activator CREB. One of these kinases is CaMKIV, which phosphorylates CREB. We examined the expression of CaMKIV, and did not observe any difference of CaMKIV mRNA expression between the mice exposed to toluene and filtered air (data not shown). We also detected the expression of NGF-related transcriptional factors, CREB1 mRNA in the hippocampus of C3H/HeN mice after toluene exposure. An increased CREB1 mRNA was found in mice exposed to 50 ppm of toluene compared to that of mice exposed to filtered air ($P < 0.05$,

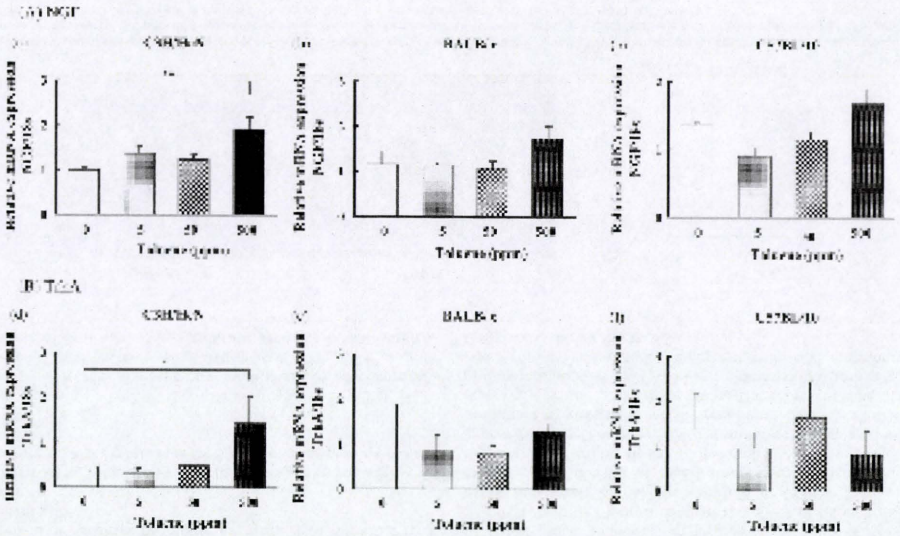

Fig. 2. Expression of NGF and TrkA in the hippocampus of three strains of mice. (a) NGF and (d) TrkA in C3H/HeN mice; (b) NGF and (e) TrkA in BALB/c mice; and (c) NGF and (f) TrkA in C57BL/10 mice following exposure to 0, 5, 50 or 500 ppm of toluene for 6 weeks. Each bar represents the mean ± S.E. ($n = 6$) (**$P < 0.01$, *$P < 0.05$).

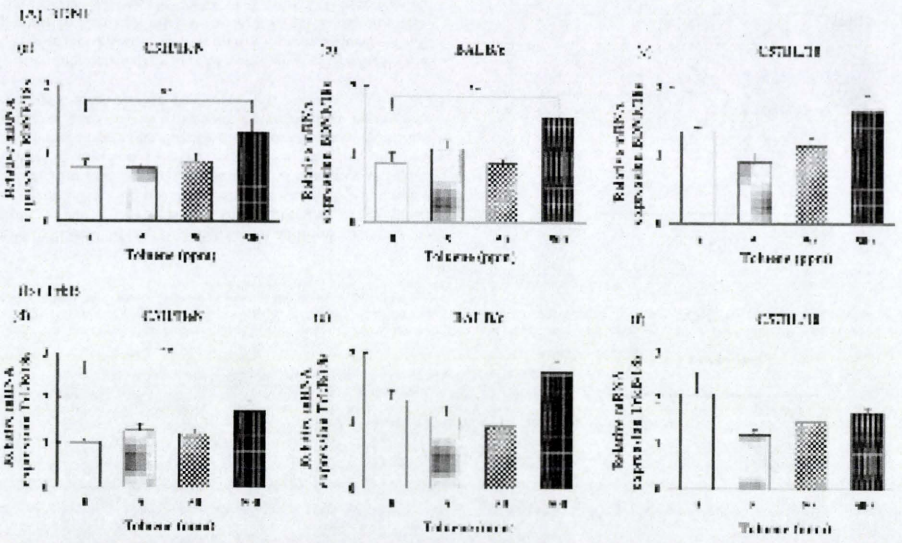

Fig. 3. Expression of BDNF and TrkB in the hippocampus of three strains of mice. (a) BDNF and (d) TrkB in C3H/HeN mice; (b) BDNF and (e) TrkB in BALB/c mice; and (c) BDNF and (f) TrkB in C57BL/10 mice following exposure to 0, 5, 50 or 500 ppm of toluene for 6 weeks. Each bar represents the mean ± S.E. ($n = 6$) (**$P < 0.01$).

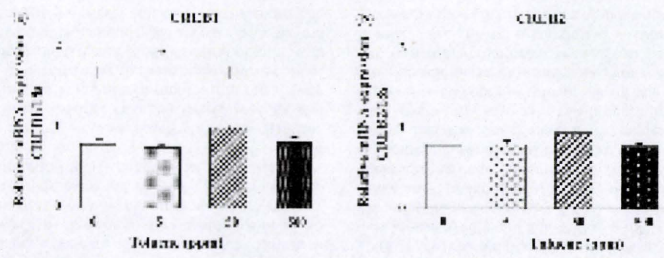

Fig. 4. Expression of CREB1 and CREB2 in the hippocampus of C3H/HeN mice. (a) CREB1 and (b) CREB2 mRNAs in mice following exposure to 0, 5, 50 or 500 ppm of toluene for 6 weeks. Each bar represents the mean ± S.E. ($n = 6$) (*$P < 0.05$).

Fig. 4a). In addition, we examined the expression of CREB2 mRNA, which functions to repress CREB1 activity. We did not observe any significant change of CREB2 mRNA (Fig. 4b).

3.1.3. Dopamine markers

Then, we postulated that the signaling pathway mediating the effect of toluene may be common or specific in the hippocampus for this C3H/HeN of mice. It is possible that the dopamine receptor signaling pathway may cross-talk with neurotrophin signaling pathways following exposure to toluene. We did not find any difference of D1 mRNA expression between mice exposed to toluene and filtered air (Fig. 5a). Although statistically insignificant, the results indicate a trend of increased D2 mRNA expression in mice exposed to 50 ppm of toluene (Fig. 5b). Tyrosine hydroxylase (TH) has a link with dopamine receptor activity. Therefore, we examined the expression of TH mRNA in the hippocampus of mice exposed to toluene. There was a tendency of higher TH mRNA expression in mice exposed to toluene as compared to that of mice exposed to filtered air (Fig. 5c).

3.1.4. Oxidative stress marker and apoptotic markers

NGF served as a growth factor as well as a regulator for cell survival. Balance of NGF-TrkA-MEK1-ERK1/2-CREB and NGF-TrkA-MEK3/6-p38 MAP pathway could contribute to NGF-induced cell death (Yan et al., 2002). To investigate the effect of toluene exposure on oxidative stress in the hippocampus of C3H/HeN mice, we examined the expression of oxidative stress marker, HO-1 mRNA. We found a significantly increased HO-1 mRNA expression in mice exposed to 500 ppm toluene as compared to that of mice

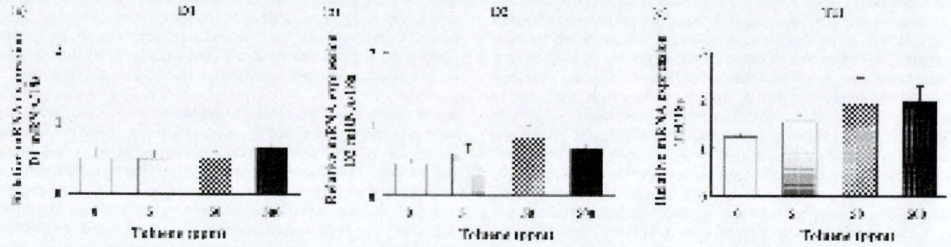

Fig. 5. Expression of D1, D2 and TH in the hippocampus of C3H/HeN mice. (a) D1, (b) D2 and (c) TH mRNAs in mice following exposure to 0, 5, 50 or 500 ppm of toluene for 6 weeks. Each bar represents the mean ± S.E. ($n = 6$).

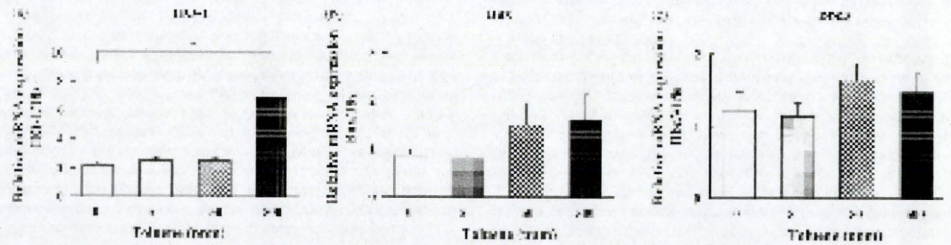

Fig. 6. Expression of HO-1, Bax and Bbc in the hippocampus of C3H/HeN mice. (a) HO-1, (b) Bax and (c) Bbc mRNAs in mice following exposure to 0, 5, 50 or 500 ppm of toluene for 6 weeks. Each bar represents the mean ± S.E. ($n = 6$) (*$P < 0.05$).

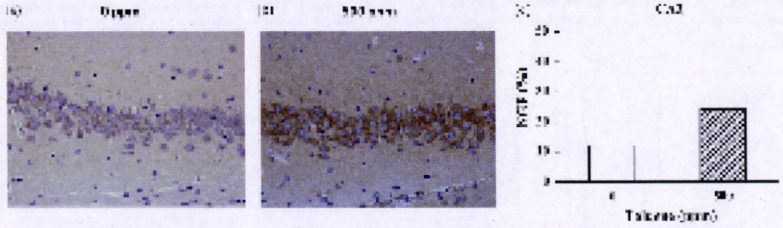

Fig. 7. Representative digital photomicrographs of NGF-immunostained sections taken from the hippocampal CA3 region in C3H/HeN mice following exposure to toluene (a) 0 ppm and (b) 500 ppm for 6 weeks (Scale bars = 50 μm). (c) Density of NGF-immunoreactivity in the hippocampal CA3 region of C3H/HeN mice following exposure to 0 and 500 ppm of toluene for 6 weeks. Each bar represents the mean ± S.E. ($n = 3$).

exposed to filtered air ($P < 0.05$, Fig. 6a). In addition, to assess the apoptotic activity, we measured the expression of apoptotic related genes (Bax for pro-apoptosis and Bbc3 (Bcl-2 binding component) for anti-apoptosis). There was a tendency of higher Bax mRNA expression in mice exposed to toluene, but not statistically significant (Fig. 6b). We did not observe any significant difference of Bbc3 mRNA expression between mice exposed to toluene and filtered air (Fig. 6c).

3.1.5. NGF-immunoreactivity in the hippocampus of C3H/HeN mice

To confirm the effect of toluene on the expression levels of NGF polypeptide in C3H/HeN mice, we examined the density of NGF-immunoreactive signals in the CA1–3 and DG hippocampal regions. In the hippocampus of 500 ppm toluene-exposed C3H/HeN mice, intense immunoreactive signals for NGF were found in the pyramidal cell layers of the CA1–3 regions and in the granular cell layer of the DG. The representative digital photomicrograph of the CA3 of mice exposed to 0 ppm (Fig. 7a) and 500 ppm (Fig. 7b) and, the percentage of NGF-immunoreactivity (Fig. 7c) were shown.

Taken together, our findings indicate that C3H/HeN mice seemed to be sensitive to toluene exposure than the other two strains of mice.

3.2. Detection of combined effect of toluene exposure and allergic stimulation on NGF expression in the hippocampus of sensitive mouse strain

To examine whether the allergic condition affect NGF expression in the hippocampus modulated by exposure to toluene, C3H/HeN mice were stimulated with OVA during toluene exposure period. A significant increase in NGF mRNA

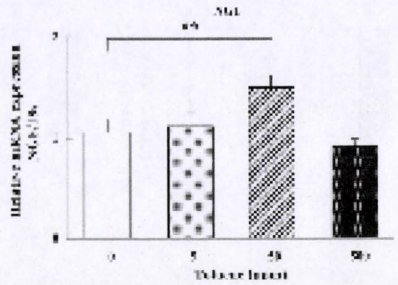

Fig. 8. Expression of NGF in the hippocampus of AG group of C3H/HeN mice following exposure to 0, 5, 50 or 500 ppm of toluene for 6 weeks. Each bar represents the mean ± S.E. ($n = 6$) (**$P < 0.01$, AG = allergy).

expression was observed in the hippocampus of the AG group of C3H/HeN mice following exposure to 50 ppm of toluene ($P < 0.01$, Fig. 8). Then, to confirm the effect of toluene on the expression levels of NGF polypeptide in C3H/HeN mice, we examined the density of NGF-immunoreactive signals in the hippocampal regions. In the hippocampus of 50 ppm toluene-exposed C3H/HeN mice with OVA stimulation, significant intense immunoreactive signals for NGF were found in the pyramidal cell layers of the CA1 and CA3 regions. The representative digital photomicrograph of the CA3 of mice exposed to 0 ppm (Fig. 9a) and 50 ppm (Fig. 9b) and, the percentage of NGF-immunoreactivity were shown in Fig. 9c.

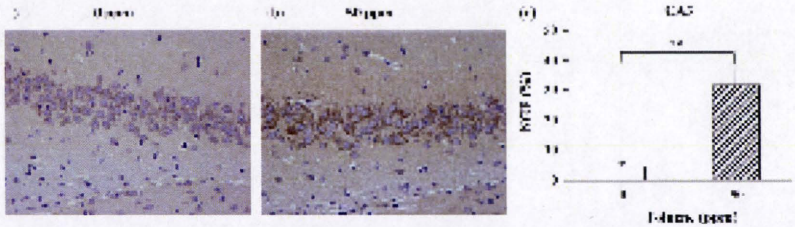

Fig. 9. Representative digital photomicrographs of NGF-immunostained sections taken from the hippocampal CA3 region in AG group of C3H/HeN mice following exposure to toluene (a) 0 ppm and (b) 500 ppm for 6 weeks (Scale bars = 50 μm). (c) Density of NGF-immunoreactivity in the hippocampal CA3 region of AG group of C3H/HeN mice following exposure to 0 and 500 ppm of toluene for 6 weeks. Each bar represents the mean ± S.E. ($n = 3$). (**$P < 0.01$, AG = allergy).

4. Discussion

The major findings of our present study are that low levels of toluene exposure can up-regulate the expressions of neurotrophins and their related receptors in the mouse hippocampus in strain-dependent manner, and allergic stimulation lower the threshold for the sensitivity to toluene in the most sensitive strain C3H/HeN mice. Little is known about differences in sensitivity to volatile organic compounds (VOCs) among mouse strains. Immunological studies have indicated that C3H mice are more resistant to infection with *Salmonella*, *Leishmania*, or *Mycobacterium avium* than C57BL/6 mice (Kamath et al., 2004). Acute restraint stress has also been reported to decrease the infiltration of inflammatory cells in BALB/c mice, but not in C57BL/6 mice (Okuyama et al., 2007). Neurological studies have also demonstrated that different sensory abilities may influence strain differences in learning and memory performances (Brown and Wong, 2007). In toxicological aspect, our research group showed that the strain differences influence the extracellular amino acid neurotransmitter levels in the hippocampus of major histocompatibility complex (MHC) congenic mice (Win-Shwe et al., 2009) and NMDA receptor subunit expression in olfactory bulb of an allergic mouse model (Win-Shwe et al., in press) following toluene exposure. In view of these previous results, the three above-mentioned mice strains were used to compare the effect of low-level toluene on neurotrophin-related gene expression in the hippocampus.

Our present data clearly showed that toluene exposure alone significantly increased the mRNA expressions of NGF, TrkA, BDNF and TrkB in the hippocampus of C3H/HeN mice exposed to 500 ppm of toluene, but not in the BALB/c and C57BL mice. It may be due to different sensitivities of three strains of mice to brain neurotrophins in response to low-level toluene exposure. However, it is not known the exact mechanism for different sensitivity to toluene-mediated neurotrophin expressions in the hippocampus of three mice strains in the present study. It has been reported that MHC class I protein perform crucial roles outside the immune system, specifically in activity-dependent development and plasticity of the vertebrate nervous system (Huh et al., 2000; Goddard et al., 2007). Currently, our research group showed the strain differences in extracellular amino acid neurotransmitter levels in the hippocampus of H-2 haplotype congenic mice [C57BL/10 (H-2^b) and B10.BR/Sg (H-2^k)] in response to toluene exposure (Win-Shwe et al., 2009). Therefore, it may be suggested that H-2 haplotype plays a role in different sensitivity to environmental chemical exposure.

In our present study, using sensitive model of mice, we examined brain NGF level in the hippocampus and found that up-regulation of NGF level in non-allergic mice exposed to 500 ppm toluene whereas in AG mice exposed to 50 ppm toluene. Our findings indicate that toluene exposure at lower level up-regulates the expression of neurotrophins in an allergic mouse model. However, a dose-dependency in adjuvant activity was not found. Some discrepancies were found between high and low dose effect of toluene on NGF expression in mouse hippocampus. No mechanism has been proposed to explain the above stimulatory effect of low-level toluene exposure on NGF expression in the hippocampus. One possibility is that toluene inhalation contributes to neural dysfunction related to sensory stimulation, and this neurotrophin expression and homeostatic mechanisms compensate for toxicant-induced changes. Neurotrophins also take part in neurogenic inflammation by modulating the activity of sensory neurons and enhancing the synthesis and release of neuropeptides (Lindsay and Harmar, 1989). Another possibility is that in OVA-immunized mice, immune system may be activated and may be sensitive to low-level toluene. Furthermore, we previously reported that OVA immunization acts as a stressor to activate hypothalamo-pituitary adrenal axis (Sari et al., 2004) and then that signal further activates some of immune cells and neural cells in the hippocampus and these neuroimmune interactions promote to up-regulate the neurotrophin expressions. Toluene exposure alone induces NGF synthesis at higher exposure level (500 ppm) and co-exposure of toluene and OVA, like double stressors may induce NGF synthesis at lower exposure level (50 ppm). This finding was consistent with our previous study that showed increased sensitivity of CRH-ir neurons in the hypothalamus and ACTH-ir neurons and mRNA expression in AG mice were higher than those of non-allergic mice in response to toluene (Sari et al., 2006).

We also suggested that the NGF endogenously released after toluene and/or OVA stimulation possibly participates in promoting cell repair and the remodeling of damaged tissue due to acute and chronic stressful events (Aloe et al., 2002). Taken together, brain NGF may represent a link between nervous, endocrine and immune systems and may translate environmental messages into pathophysiological responses. In our previous study, we demonstrated an increased NGF protein level in the hippocampus of C3H/HeN mice following exposure to low levels of formaldehyde (400 ppb) after OVA stimulation (Fujimaki et al., 2004). NGF and BDNF play a key role in the fine tuning of learning and memory performances and in some behavioral processes associated with stress situations (Aloe et al., 2002; Chao et al., 2006). In the immunohistochemical analysis, we observed significantly denser NGF-immunoreactivities in the CA1 and CA3 regions of the hippocampus of C3H/HeN mice in the AG group after exposure to 50 ppm of toluene. This finding is consistent with the expression of NGF mRNA levels in the hippocampus in AG group of C3H/HeN mice. Taken together, our findings strongly suggest that low levels of toluene exposure up-regulated the expression of NGF in the hippocampus at both the mRNA and protein levels in AG C3H/HeN mice.

Currently, neurotrophins and their related receptors have been identified as targets for neurotoxicant. NGF can regulate allergic airway inflammation as well as neural hyper-responsiveness (Bonini et al., 1996; Sanico et al., 1999), indicating that NGF is involved in both neural and immune sensitization. Under physiologic conditions, the local production of neurotrophins is low in both human and animal studies (Nockher and Renz, 2006). Among the neurotrophins, NGF and BDNF play a crucial role in the survival and development of specific peripheral and brain neurons (Chao et al., 2006; Allen and Dawbarn, 2006). They are produced and released by a variety of cells localized in the central and peripheral nervous systems and by cells of the immune and endocrine systems (Levi-Montalcini et al., 1990; Barde, 1994). As mentioned above, the exact mechanism behind the alterations in neurotrophins and their receptors in the mouse hippocampus following toluene exposure is not clear. Using PC 12 cells, Bedogni and colleagues demonstrated the dual role of reactive oxygen species (ROS) in survival signaling and in cell death (Bedogni et al., 2003). They reported that ROS rapidly generated in the cell cytosol in response to NGF and Rac-1 have a role in survival signaling to Akt and CREB, whereas harmful mitochondrial oxidants produced at the onset of apoptotic death are reduced by the neurotrophin, likely through the induction of the mitochondrial scavenger manganese-dependent superoxide dismutase. In the present study, oxidative stress maker, the expression of HO-1 mRNA was significantly higher in the hippocampus of C3H/HeN mice exposed to 500 ppm of toluene. There was a tendency of higher proapoptotic Bax mRNA expression in mice exposed to toluene, but not statistically significant. At least in part, our present study showed that the up-regulation of neurotrophins and related receptors in the C3H/HeN mice hippocampus may be occurred to

compensate or to protect neurodegeneration induced by exposure to 500 ppm toluene.

In our previous study, we found a significant up-regulation of N-methyl D-aspartate (NMDA) receptor subunit NR2B expression associated with a simultaneous induction of CaMKIV, CREB1 and FosB/ΔFosB in the hippocampus of mice exposed to 50 ppm toluene for 12 weeks (Ahmed et al., 2007). In the present study, although the exposure to 50 ppm toluene for 6 weeks increased the expression of CREB1 mRNA in the hippocampus of mice, we did not observe any difference of CaMKIV expression. Therefore, activation of CREB-mediated gene transcription may require a prolonged period of exposure to toluene. Bale et al. (2005) suggested that the up-regulation of the functional expression of NMDA receptor subunits in the hippocampal neurons treated in vitro with toluene chronically, at human abusive level, as a compensatory response. Further study is needed to identify the hippocampus-specific upstream regulators or downstream targets of CREB that serve as Ca^{2+} dependent kinases. To the best of our knowledge, only a few studies have examined the effects of long-term toluene exposure on the expression of dopamine receptors in adult mouse hippocampus. Dopamine D1/D5 receptors have a novel neuromodulatory role in regulating hippocampal synaptic plasticity, i.e., time-dependent reversal of NMDAR-dependent long-term depression (Mockett et al., 2007). Recently, it has been reported that ciliary neurotrophic factor mediates dopaminergic innervations and D2 receptor-induced neurogenesis in the adult brain (Yang et al., 2008). However, a link between NGF and dopaminergic system is not clear. Therefore, we also examined the dopamine receptors D1, D2 and related enzyme TH gene expressions in this study. However, we did not observe any significant difference between treatment groups. One of the possibilities is NGF mediates different mechanism to induce neurogenesis in the hippocampus independent of dopaminergic system in the mouse hippocampus.

Although many epidemiological studies have demonstrated the causative factors, susceptible populations and clinical implications for multiple chemical sensitivity (MCS) (Graveling et al., 1999; Ross et al., 1999; Bolt and Kiesswetter, 2002), the pathophysiology of the disease is still unclear. It is assumed that the affected individuals react to widely different types of chemical stimuli in very low concentrations that would not cause any reaction in the general population (Cullen, 1987). However, genetic factors may play a role in the etiology of MCS and analysis of genetic factors becomes possible and new approaches to identify the mechanism of MCS.

An increased NGF level was occurred in plasma of MCS patients (Kimata, 2004). Then, the MCS patients showed significantly higher capsaicin cough sensitivity than the healthy controls, supporting a hypothesis that NGF-related neurogenic mechanisms are involved in MCS (Ternesten-Hasseus et al., 2002). Our results indicate that low-level toluene exposure may induce up-regulation of neurotrophin-related gene expression in the mouse hippocampus depending on the mouse strain and an allergic stimulation in sensitive strain may decrease the threshold for sensitivity at lower exposure level.

In conclusion, this is the first study to demonstrate that exposure to low levels of toluene up-regulated the expression of neurotrophins and their receptors in adult mouse hippocampus in a strain-dependent manner and in accordance with the allergic condition. Further studies are needed to evaluate the existence of a positive relation between NGF–TrkA-signal transduction pathway and neurobehavioral alterations following toluene exposure.

Conflict of interest statement

We have no conflicting interests to declare.

Acknowledgments

This research was partly supported by a grant from the Ministry of Education, Culture, Sports, Sciences and Technology, Japan (#18390189, #21390198) to H.F. We thank Ms. K. Ohnishi and K. Taki for their technical assistance.

References

Ahmed S, Win-Shwe TT, Yamamoto S, Tsukahara S, Kunugita N, Arashidani K, Fujimaki H. Increased hippocampal mRNA expression of neuronal synaptic plasticity related genes in mice chronically exposed to toluene at a low-level human occupational-exposure. Neurotoxicology 2007;28:168–74.
Allen SJ, Dawbarn D. Clinical relevance of the neurotrophins and their receptors. Clin Sci (Lond) 2006;110:175–91.
Aloe L, Alleva E, Fiore M. Stress and nerve growth factor: findings in animal models and humans. Pharmacol Biochem Behav 2002;73:159–66.
American Conference of Governmental Industrial Hygienists (ACGIH). Threshold limit values and biological exposure indices guide; 2006. www.acgih.org/TLV/Studies.htm.
Bale AS, Tu Y, Carpenter-Hyland EP, Chandler LJ, Woodward JJ. Alterations in glutamatergic and GABAergic ion channel activity in hippocampal neurons following exposure to the abused inhalant toluene. Neuroscience 2005;130:197–206.
Barde YA. Neurotrophins: a family of proteins supporting the survival of neurons. Prog Clin Biol Res 1994;390:45–56.
Bedogni B, Pani G, Colavitti R, Riccio A, Borrello S, Murphy M, Smith R, Eboli ML, Galeotti T. Redox regulation of cAMP-responsive element-binding protein and induction of manganous superoxide dismutase in nerve growth factor-dependent cell survival. J Biol Chem 2003;278:16510–9.
Benignus VA, Boyes WK, Bushnell PJ. A dosimetric analysis of behavioral effects of acute toluene exposure in rats and humans. Toxicol Sci 1998;43:186–95.
Betancourt AM, Burgess SC, Carr RL. Effect of developmental exposure to chlorpyrifos on the expression of neurotrophin growth factors and cell-specific markers in neonatal rat brain. Toxicol Sci 2006;92:500–6.
Bolt HM, Kiesswetter E. Is multiple chemical sensitivity a clinically defined entity? Toxicol Lett 2002;128:99–106.
Bonini S, Lambiase A, Bonini S, Angelucci F, Magrini L, Manni L, Aloe L. Circulating nerve growth factor levels are increased in humans with allergic diseases and asthma. Proc Natl Acad Sci U S A 1996;93:10955–60.
Bowen SE, McDonald P. Abuse pattern of toluene exposure alters mouse behavior in a waiting-for-reward operant task. Neurotoxicol Teratol 2009;31:18–25.
Brown RE, Wong AA. The influence of visual ability on learning and memory performance in 13 strains of mice. Learn Mem 2007;14:134–44.
Chao MV, Rajagopal R, Lee FS. Neurotrophin signalling in health and disease. Clin Sci (Lond) 2006;110:167–73.
Cullen MR. The worker with multiple chemical sensitivities: an overview. Occup Med 1987;2:655–61.
Fujimaki H, Kurokawa Y, Kunugita N, Kikuchi M, Sato F, Arashidani K. Differential immunogenic and neurogenic inflammatory responses in an allergic mouse model exposed to low levels of formaldehyde. Toxicology 2004;197:1–13.
Fujimaki H, Yamamoto S, Win-Shwe TT, Hojo R, Sato F, Kunugita N, Arashidani K. Effect of long-term exposure to low-level toluene on airway inflammatory response in mice. Toxicol Lett 2007;168:132–9.
Gelazonia L, Japaridze N, Svanidze I. Pyramidal cell loss in hippocampus of young rats exposed to toluene. Georg Med News 2006;135:126–8.
Goddard CA, Butts DA, Shatz CJ. Regulation of CNS synapses by neuronal MHC class I. Proc Natl Acad Sci U S A 2007;104:6828–33.
Graveling RA, Pilkington A, George JP, Butler MP, Tannahill SN. A review of multiple chemical sensitivity. Occup Environ Med 1999;56:73–85.
Hori H, Ishidao T, Oyabu T, Yamato H, Morimoto Y, Tanaka I. Effect of simultaneous exposure to methanol and toluene vapor on their metabolites in rats. J Occup Health 1999;41:149–53.
Huh GS, Boulanger LM, Du H, Riquelme PA, Brotz TM, Shatz CJ. Functional requirement for class I MHC in CNS development and plasticity. Science 2000;290:2155–9.
Japan Society for Occupational Health. Toluene. Ind Med 1994;36:103–10.
Kamath AB, Alt J, Debbabi H, Taylor C, Behar SM. The major histocompatability complex haplotype affects T-cell recognition of Mycobacterial antigens but not resistance to *Mycobacterium tuberculosis* in C3H mice. Infect Immun 2004;72:6790–8.
Kidd SK, Anderson DW, Schneider JS. Postnatal lead exposure alters expression of forebrain p75 and TrkA nerve growth factor receptors. Brain Res 2008;1195:113–9.
Kimata H. Effect of exposure to volatile organic compounds on plasma levels of neuropeptides, nerve growth factor and histamine in patients with self-reported multiple chemical sensitivity. Int J Hyg Environ Health 2004;207(2):159–63.
Korbo L, Ladefoged O, Lam HR, Ostergaard G, West MJ, Arlien-Søborg P. Neuronal loss in hippocampus in rats exposed to toluene. Neurotoxicology 1996;17:359–66.
Levi-Montalcini R, Aloe L, Alleva E. A role for nerve growth factor in nervous, endocrine and immune systems. Prog Neurol Endocrinol Immunol 1990;3:1–10.
Lindsay RM, Harmar AJ. Nerve growth factor regulates expression of neuropeptide genes in adult sensory neurons. Nature 1989;337:362–4.
Lindvall O, Ernfors P, Bengzon J, Kokaia Z, Smith ML, Siesjö BK, Persson H. Differential regulation of mRNAs for nerve growth factor, brain-derived neurotrophic factor, and neurotrophin 3 in the adult rat brain following cerebral ischemia and hypoglycemic coma. Proc Natl Acad Sci U S A 1992;89:648–52.

Mockett BG, Guévremont D, Williams JM, Abraham WC. Dopamine D1/D5 receptor activation reverses NMDA receptor-dependent long-term depression in rat hippocampus. J Neurosci 2007;27:2918–26.
Nakajima D, Tin-Tin-Win-Shwe. Kakeyama M, Fujimaki H, Goto S. Determination of toluene in brain of freely moving mice using solid-phase microextraction technique. Neurotoxicology 2006;27:615–8.
Nockher WA, Renz H. Neurotrophins in allergic diseases: from neuronal growth factors to intercellular signaling molecules. J Allergy Clin Immunol 2006;117:583–9.
Okuyama K, Ohwada K, Sakurada S, Sato N, Sora I, Tamura G, Takayanagi M, Ohno I. The distinctive effects of acute and chronic psychological stress on airway inflammation in a murine model of allergic asthma. Allergol Int 2007;56:29–35.
Ross PM, Whysner J, Covello VT, Kuschner M, Rifkind AB, Sedler MJ, Trichopoulos D, Williams GM. Olfaction and symptoms in the multiple chemical sensitivities syndrome. Prev Med 1999;28:467–80.
Sanico AM, Koliatsos VE, Stanisz AM, Bienenstock J, Togias A. Neural hyperresponsiveness and nerve growth factor in allergic rhinitis. Int Arch Allergy Immunol 1999;118:154–8.
Sari DK, Kuwahara S, Tsukamoto Y, Hori H, Kunugita N, Arashidani K, Fujimaki H, Sasaki F. Effects of prolonged exposure to low concentrations of formaldehyde on the corticotrophin releasing hormone neurons in the hypothalamus and adrenocorticotropic hormone cells in the pituitary gland in female mice. Brain Res 2004;1013:107–16.
Sari DK, Kuwahara S, Tsukamoto Y, Hori H, Kunugita N, Arashidani K, Fujimaki H, Sasaki F. Effect of subchronic exposure to low concentrations of toluene on the hypothalamo-pituitary adrenal gland axis of female mice. J Jpn Soc Atmos Environ 2006;42:38–43.
Terashi H, Nagata K, Satoh Y, Hirata Y, Hatazawa J. Hippocampal hypoperfusion underlying dementia due to chronic toluene intoxication. Rinsho Shinkeigaku 1997;37:1010–3.
Ternesten-Hasseus E, Bende M, Millqvist E. Increased capsaicin cough sensitivity in patients with multiple chemical sensitivity. J Occup Environ Med 2002;44:1012–7.
United States Environmental Protection Agency. Prepared by the Office of Pollution Prevention and Toxics. Chemicals summary of toluene, EPA; 1994: 749-F-94-021a.
von Euler G, Ogren SO, Li XM, Fuxe K, Gustafsson JA. Persistent effects of subchronic toluene exposure on spatial learning and memory, dopamine-mediated locomotor activity and dopamine D2 agonist binding in the rat. Toxicology 1993;77:223–32.
von Euler M, Pham TM, Hillefors M, Bjelke B, Henriksson B, von Euler G. Inhalation of low concentrations of toluene induces persistent effects on a learning retention task, beam-walk performance, and cerebrocortical size in the rat. Exp Neurol 2000;163:1–8.
Win-Shwe TT, Mitsushima D, Nakajima D, Ahmed S, Yamamoto S, Tsukahara S, Kakeyama M, Goto S, Fujimaki H. Toluene induces rapid and reversible rise of hippocampal glutamate and taurine neurotransmitter levels in mice. Toxicol Lett 2007a;168:75–82.
Win-Shwe TT, Yamamoto S, Nakajima D, Furuyama A, Fukushima A, Ahmed S, Goto S, Fujimaki H. Modulation of neurological related allergic reaction in mice exposed to low-level toluene. Toxicol Appl Pharmacol 2007b;222:17–24.
Win-Shwe TT, Mitsushima D, Yamamoto S, Funabashi T, Fujimaki H. Strain differences in extracellular amino acid neurotransmitter levels in the hippocampi of major histocompatibility complex congenic mice in response to toluene exposure. Neuroimmunomodulation 2009;16:185–90.
Win-Shwe TT, Kunugita N, Yamamoto S, Arashidani K, Fujimaki H. Strain differences influence NMDA receptor subunit gene expression in olfactory bulb of an allergic mouse model following toluene exposure. Neuroimmunomodulation; in press.
Yan C, Liang Y, Nylander KD, Schor NF. TrkA as a life and death receptor: receptor dose as a mediator of function. Cancer Res 2002;62:4867–75.
Yang P, Arnold SA, Habas A, Hetman M, Hagg T. Ciliary neurotrophic factor mediates dopamine D2 receptor-induced CNS neurogenesis in adult mice. J Neurosci 2008;28:5867–9.

Toxicology in Vitro 24 (2010) 2012–2020

Contents lists available at ScienceDirect

Toxicology in Vitro

journal homepage: www.elsevier.com/locate/toxinvit

Use of live imaging analysis for evaluation of cytotoxic chemicals that induce apoptotic cell death

Yoshiko Koike-Kuroda [a], Masaki Kakeyama [b,c], Hidekazu Fujimaki [c], Shinji Tsukahara [a,c,*]

[a] Department of Regulation Biology, Graduate School of Science and Engineering, Saitama University, Shimo-Okubo 255, Sakura-ku, Saitama City, Saitama 338-8570, Japan
[b] Laboratory of Environmental Health Sciences, Graduate School of Medicine, Center for Disease Biology and Integrative Medicine, The University of Tokyo, Hongo 7-3-1, Bunkyo-ku, Tokyo 113-0033, Japan
[c] Research Center for Environmental Risk, National Institute for Environmental Studies, Onogawa 16-2, Tsukuba, Ibaraki 305-8506, Japan

ARTICLE INFO

Article history:
Received 3 March 2010
Accepted 27 July 2010
Available online 1 August 2010

Keywords:
Caspase-3
Apoptosis
Live imaging
Sodium arsenite

ABSTRACT

We carried out live imaging of PC12 cells expressing SCAT3, a caspase-3 cleavage peptide sequence linking two fluorescent proteins, ECFP and Venus, which function respectively as the donor and acceptor for FRET. Live imaging of SCAT3-expressing cells was performed from 60 to 300 min after exposure to sodium arsenite ($NaAsO_2$: 0, 1, 5, or 10 μM) was initiated. We then measured the emission ratio of ECFP to Venus to monitor the activity of caspase-3 and found that the ratio was temporally and dose-dependently increased by $NaAsO_2$. The mean ECFP/Venus emission ratio between 200 and 300 min after exposure to $NaAsO_2$ at a dose of 5 or 10 μM, but not at 1 μM, was significantly higher than that in the control group. We showed by other methods that $NaAsO_2$ significantly increased the amount and activity of mature caspase-3 and the amount of nucleosomes generated from DNA fragmentation, and decreased cell viability. However, methods other than live imaging required a longer time and higher doses of $NaAsO_2$ than did live imaging to detect significant effects. This result suggests that live imaging using SCAT3 is a useful method for the screening of chemical toxicities and for improving the efficiency of toxicity evaluation.

1. Introduction

Apoptosis is a phenomenon that controls cell fate and determines cell survival and cell death. Cell death by apoptosis often, although not always, occurs if the cells are exposed to toxic chemicals. Heavy metal compounds, which are capable of causing numerous acute or chronic pathologies, are known to induce apoptotic cell death (Rana, 2008). For example, the inorganic arsenic compounds, sodium arsenite ($NaAsO_2$) and arsenic trioxide, exhibit cytotoxicity accompanied by the induction of apoptotic cell death in a variety of cells, including immune cells (Bustamante et al., 1997; Hossain et al., 2000), neuronal cells (Namgung and Xia, 2001; Wong et al., 2005; Chattopadhyay et al., 2002), a gastric cancer cell line (Jiang et al., 2001), a leukemia cell line (Iwama et al., 2001), and a neuroblastoma cell line (Watcharasit et al., 2008). In addition, cell death by apoptosis occurs when cells are exposed to other heavy metal compounds, such as lead acetate (Shabani and Rabbani, 2000; Columbano et al., 1985), lead nitrate (Pachauri et al., 2009), hexavalent chromium (Hill et al., 2008; Carlisle et al., 2000; Wang et al., 2000; Azad et al., 2008; Gambelunghe et al., 2006; Rudolf and Cervinka, 2006), methyl mercury (Homma-Takeda et al., 2001; Close et al., 1999; Shenker et al., 1999; Toimela and Tahti, 2004), mercuric chloride (Araragi et al., 2003), and cadmium chloride (Dong et al., 2001; Choi et al., 2002; Gennari et al., 2003; Habeebu et al., 1998). Caspase-3 is an executor proteinase of apoptosis, whose enzymatic activity is stimulated by death signals. It has been reported that the caspase-3 of cells cultured *in vitro* is activated by lead acetate (Dong et al., 2009), hexavalent chromium (Hill et al., 2008; Russo et al., 2005), methyl mercury (Toimela and Tahti, 2004), arsenic trioxide (Jiang et al., 2001; Tse et al., 2008, 2009; Piga et al., 2007) or $NaAsO_2$ (Watcharasit et al., 2008). The combined data suggest that activation of caspase-3 may be a major irreversible step towards apoptotic cell death following exposure to such heavy metal compounds. Thus, the activity of caspase-3 is a suitable end-point for evaluation of the cytotoxicity of chemicals.

Abbreviations: ECFP, enhanced cyan fluorescent protein; FRET, fluorescence resonance energy transfer; $NaAsO_2$, sodium arsenite; NGF, nerve growth factor; PBS, phosphate-buffered saline; PEI, polyethyleneimine; pNA, *p*-nitroanilide; SDS, sodium dodecyl sulfate; Z-VAD-FMK, *N*-benzyloxycarbonyl-Val-Ala-Asp-fluoromethylketone (broad-spectrum caspase inhibitor).

* Corresponding author at: Department of Regulation Biology, Graduate School of Science and Engineering, Saitama University, Shimo-Okubo 255, Sakura-ku, Saitama City, Saitama 338-8570, Japan. Tel./fax: +81 48 858 3420.
E-mail address: stsuka@mail.saitama-u.ac.jp (S. Tsukahara).

0887-2333/$ - see front matter © 2010 Elsevier Ltd. All rights reserved.
doi:10.1016/j.tiv.2010.07.022

The dynamics and temporal patterns of caspase activation can be monitored by fluorescence resonance energy transfer (FRET) methods. In a single living cell undergoing apoptosis, temporal changes in the activity of caspase-3 are profiled by measurement of the extent of FRET within a recombinant substrate composed of enhanced cyan fluorescent protein (ECFP) linked by the caspase-3 cleavage sequence, Asp-Glu-Val-Asp (DEVD), to enhanced yellow fluorescent protein (EYFP) (Tyas et al., 2000; Luo et al., 2001; Rehm et al., 2002). In addition, Takemoto et al. improved such a recombinant substrate by replacing EYFP with a variant of EFYP named Venus (Nagai et al., 2002) and called the improved indicator for caspase-3 activation "SCAT3" (Takemoto et al., 2003). The usefulness of FRET technology using SCAT3 for monitoring caspase-3 activation in living cells both *in vitro* and *in vivo* has been well documented (Takemoto et al., 2003; Kanuka et al., 2005; Kuranaga et al., 2006; Takemoto et al., 2007).

In the present study, we applied live cell imaging analysis using SCAT3 for determination of cytotoxic effects of chemicals on the PC12 cell line, which is a cell line derived from a pheochromocytoma of rat adrenal medulla and which has the potential to differentiate into neuron-like cells. By live imaging of SCAT3-expressing PC12 cells, we profiled the temporal changes in caspase-3 activity after exposure of the cells to $NaAsO_2$. In addition, we examined the effects of $NaAsO_2$ on apoptosis induced by other methods to determine whether the sensitivity and efficiency of detection of toxicity is improved by live imaging analysis using SCAT3. In this study, we performed western blotting analysis for determination of the protein expression of the cleaved, active form of caspase-3, measured the enzymatic activity of caspase-3, the amount of nucleosomes generated from apoptotic DNA fragmentation, and the viability of PC12 cells after they were exposed to $NaAsO_2$.

2. Materials and methods

2.1. Cell culture and reagent preparation

PC12 cells (Collection No. IFO50278; the Health Science Research Resources Bank, Kobe, Japan) were used to test the usefulness of the SCAT3 system for detection of $NaAsO_2$ toxicity. The effects of $NaAsO_2$ on the protein expression and enzymatic activity of caspase-3, on DNA fragmentation, and on cell viability were assayed. PC12 cells were maintained in RPMI 1640 medium (Gibco-Invitrogen, Carlsbad, CA, USA) containing 10% horse serum, 5% fetal bovine serum, 0.1 mM Non-Essential Amino Acids Solution (Invitrogen, Carlsbad, CA, USA), a mixture of penicillin and streptomycin (100 units/ml and 100 μg/ml each; Invitrogen), and 100 μg/ml normocin (InvivoGen, San Diego, CA, USA) in 75-cm^2 flasks coated with poly-D-lysine (Becton Dickinson and Co., Oxford, UK) in an atmosphere containing 5% CO_2 at 37 °C. PC12 cells at passage 7–12 were used for the following experiments.

For each experiment, PC12 cells were cultured in medium that was exclusively used for experiments and not for cell maintenance. This medium hereafter referred to as experimental medium consisted of RPMI 1640 medium (Gibco-Invitrogen) containing 0.01 mM Non-Essential Amino Acids Solution (Invitrogen), a mixture of penicillin and streptomycin (10 units/ml and 10 μg/ml each; Invitrogen) and 10 μg/ml normocin (InvivoGen), with or without supplementation with 1% horse serum and 0.5% fetal bovine serum. PC12 cells cultured in this medium were simultaneously treated with nerve growth factor (NGF; 50 ng/ml) for neuron-like cell differentiation and were exposed to $NaAsO_2$ (Wako Pure Chemical Industries, Osaka, Japan) at a dose of 0, 1, 5, or 10 μM. Crystalline $NaAsO_2$ was dissolved in sterile-filtered water (Sigma–Aldrich, St. Louis, MO, USA) at a concentration of 100 mM. $NaAsO_2$ solution (100 mM) was diluted with experimental medium with or without serum supplementation to generate the indicated concentrations.

2.2. Transfection and imaging analysis of SCAT3

PC12 cells (10^6 cells) were transfected with 2.0 μg of the SCAT3 expression vector pcDNA-SCAT3, provided by Dr. M. Miura (University of Tokyo, Tokyo, Japan) (Takemoto et al., 2003), using Nucleofector™ II (Lonza Cologne AG, Cologne, Germany). PC12 cells (10^4 cells/well) were then seeded onto 8-well chamber slides (LAB-TEK™ Chambered Coverglass; Nalge Nunc International, Rochester, NY, USA) coated with 0.25% polyethyleneimine (PEI; Sigma–Aldrich) and were cultured in the above-described subculture medium (300 μl) under an atmosphere containing 5% CO_2 at 37 °C.

One or two days after transfection, live imaging of SCAT3-expressing PC12 cells was performed using a fluorescent time-lapse microscope BioZero 8100 (Keyence Co., Osaka, Japan) controlled by a computer with a BZ Viewer version 1.0 software installed (Keyence). SCAT3-expressing PC12 cells were simultaneously treated with NGF (50 ng/ml) and exposed to $NaAsO_2$ (0 or 10 μM) in 300 μl of experimental medium with or without serum supplementation. Live imaging of such cells was then carried out in five independent experiments. In some experiments, SCAT3-expressing PC12 cells were simultaneously treated with NGF (50 ng/ml) and exposed to $NaAsO_2$ at a dose of 0, 1, 5, or 10 μM in serum supplemented experimental medium. Live imaging of these cells was then performed in five independent experiments.

SCAT3-expressing PC12 cells were placed in an incubation chamber (Microscope Incubation System INU-KI-F1, Tokai Hit, Shizuoka, Japan) whose temperature was controlled at 37 °C and within which the gas concentration was maintained at 5% CO_2 and 95% air. Fluorescent time-lapse imaging was started at 60 min and ended at 300 min after initiation of $NaAsO_2$ exposure. A 440AF21 excitation filter, a 455DRLP dichroic mirror, and two emission filters 480AF30 for ECFP and 535AF25 for Venus (Opto Science Inc., Tokyo, Japan) were used for imaging of SCAT3-expressing cells. The excitation intensity was attenuated to 40% of the maximum power of a light source with a neutral density filter. Fluorescent images of SCAT3 were captured every 20 min using an objective lens (Plan Fluor ELWD DM 20xC, NA 0.45; Nikon, Tokyo, Japan) and a CCD camera in the KEYENCE BioZero 8100.

After live imaging was completed for each experiment, the intensity of ECFP and Venus emissions of SCAT3-expressing PC12 cells was measured using the digital image data. The region of interest corresponded to from 1.12 to 1.69 mm of the cultured slides (the mean number of SCAT3-expressing PC12 cells: approx. 150). The RGB digital images of ECFP (*cyan blue*) and Venus (*yellow green*) taken from SCAT3-expressing PC12 cells were converted into monochromatic color images (*red* for ECFP; *green* for Venus). These images were merged at each time point in order to determine the intensities of ECFP and Venus of the same region, which were obtained by measuring the brightness of *red* and *green* colors, respectively with the aid of a computer and the KEYENCE BZ Viewer version 1.0 software (Keyence). After the brightness values of *red* and *green* colors in the same region of each merged image were measured, the ECFP/Venus emission ratio was calculated by dividing the brightness value of the *red* color by that of the *green* color. The ECFP/Venus emission ratio at each time point was calibrated using the ratio of the same area at 60 min after $NaAsO_2$ exposure, which was set at a value of 1.

2.3. Western blot analysis of caspase-3

PC12 cells, seeded on 0.25% PEI-coated 12-well plates, (10^5 cells/well) were treated with NGF (50 ng/ml) and exposed to

$NaAsO_2$ (0, 1, 5, or 10 μM) in 1 ml of serum supplemented experimental medium. These cells were rinsed in phosphate-buffered saline (PBS) 360 and 1200 min after exposure to $NaAsO_2$, and were then collected in PBS containing a protease inhibitor cocktail (EDTA-free Complete Mini; Roche Diagnostics, Basel, Switzerland) on ice. After the cells were centrifuged at 1500 rpm for 10 min at 4 °C, the cell pellets were homogenized in lysis buffer (CelLytic; Sigma–Aldrich) containing a protease inhibitor cocktail (1:4000; Sigma–Aldrich). PC12 cells, exposed to $NaAsO_2$ at different doses, were collected from five and four independent experiments for 360-min and 1200-min exposure, respectively.

The cell lysate of each sample was mixed with 1/4 volume of 0.29 M Tris–Hcl (pH 6.8) containing 8.3% sodium dodecyl sulfate (SDS), 25% glycerol, 7.75% dithiothreitol, and 0.01% bromphenol blue, and was then boiled at 95 °C for 4 min. Equal amounts of protein (5 μg) were resolved by electrophoresis on 15% SDS–polyacrylamide gels, and the proteins were transferred to PVDF membranes by semidry transfer using an iBlot module (Invitrogen). After transfer, the membranes were rinsed in TBST (20 mM Tris–HCl containing 0.9% NaCl, and 0.1% Tween-20, pH 7.6) and were treated with a blocking buffer (Blocking One; Nakalai Tesque, Inc., Kyoto, Japan) for 1 h at room temperature. The membranes were incubated with a rabbit anti-caspase-3 antibody (1:2000; Cell Signaling Technology, Beverly, MA, USA), which can detect both cleaved caspase-3 (an active caspase-3) and non-cleaved caspase-3 (procaspase-3), at 4 °C overnight before and after rinsing in TBST. Membranes were successively incubated with horseradish peroxidase-conjugated goat anti-rabbit IgG (1:2000, Cell Signaling) in TBST for 1 h at room temperature. Immunoreactive signals for specific proteins were visualized on an X-ray film using a chemiluminescence reagent.

The levels of immunoreactive signals for caspase-3 were determined using ImageJ 1.31 software (National Institutes of Health, Bethesda, MD, USA). The level of cleaved caspase-3 was normalized by dividing by the total amount of caspase-3 in the same lane of the blotting membrane. The percent of cleaved caspase-3 in total caspase-3 was expressed relative to controls (0 μM of $NaAsO_2$) that were set at 100% for each experiment.

2.4. Caspase-3 activity assay

PC12 cells were cultivated in 0.25% PEI-coated 6-well plates up to 80–90% confluency, and were then treated with NGF (50 ng/ml) and exposed to $NaAsO_2$ (0, 1, 5 or 10 μM) for 360 or 1200 min in 2 ml of serum supplemented experimental medium In addition, some of PC12 cells were exposed to 10 μM of $NaAsO_2$ and were treated with 50 μM of *N*-benzyloxycarbonyl-Val-Ala-Asp-fluoromethylketone (Z-VAD-FMK), a broad-spectrum caspase inhibitor (Promega, Madison, WI, USA) for 1200 min. PC12 cell in each group were collected from four or five independent experiments.

After protein was extracted from the collected cells, an equal amount of total protein (35 μg) from each sample was used for the measurement of caspase-3 activity. The activity of caspase-3 in cell extracts was evaluated by assessing cleavage of the colorimetric substrate, a DEVD peptide-conjugated with *p*-nitroanilide (pNA), using a caspase-3 activity assay kit (CaspACE™ assay system, Colorimetric; Promega) in accordance with the manufacturer's protocol. The activity of caspase-3 was expressed as the amount of free pNA per unit protein (pmol/μg).

2.5. Apoptosis assay

PC12 cells, seeded on 0.25% PEI-coated 96-well plates (10^4 cells/well), were treated with NGF (50 ng/ml) and exposed to $NaAsO_2$ at a dose of 0, 1, 5 or 10 μM for 1200 min in 100 μl of serum supplemented experimental medium. The effect of $NaAsO_2$ on DNA fragmentation was examined using a Cell Death Detection ELISA Plus Assay kit (Roche Diagnostics) in accordance with the manufacturer's protocol. This assay was performed using four independent experiments. The amount of nucleosomes generated from DNA fragmentation was expressed relative to that of controls (0 μM of $NaAsO_2$) that were set at 100% for each experiment.

2.6. Cell viability assay

The effects of $NaAsO_2$ on the viability of PC12 cells were determined in six independent experiments using a colorimetric assay based on the reduction of tetrazolium salt to formazan by mitochondrial dehydrogenase activity. PC12 cells, seeded on 0.25% PEI-coated 96-well plates (10^4 cells/well), were treated with NGF (50 ng/ml) and exposed to $NaAsO_2$ (0, 1, 5 or 10 μM) in triplicate for 1 or 2 days in 100 μl of serum supplemented experimental medium. Ten microliters of Tetrazolium reagent WST-1 (Roche Applied Bioscience, Indianapolis, IN, USA) was then reacted with the cells for 1–3 h at 37 °C, and absorbance at 450 nm was then measured using a reference wavelength of 650 nm. The absorbance at 650 nm was subtracted from the absorbance at 450 nm, and this value was then expressed as a percentage of the value obtained for PC12 cells without $NaAsO_2$ exposure, whose viability was set at 100%.

2.7. Statistical analyses

Overall differences in the temporal changes in the ECFP/Venus emission ratio among groups were analyzed using two-way factorial analysis of variance (ANOVA) for repeated measures. When significant overall effects were detected contrast analyses between groups were then performed. The overall effects of culture conditions and $NaAsO_2$ on the mean of the ECFP/Venus emission ratio were examined using two-way ANOVA. One-way ANOVA was performed to determine differences among groups with respect to the mean of the ECFP/Venus emission ratio, the amount of cleaved caspase-3, the activity of caspase-3, the amount of apoptotic nucleosomes, and cell viability. When significant overall effects were detected by two-way or one-way ANOVA, Fisher's PLSD test was performed for post hoc analysis.

3. Results

3.1. Effects of serum supplementation and $NaAsO_2$ exposure on SCAT3-expressing cells

We first assayed the FRET signal of the caspase-3 cleavage FRET reporter SCAT3, following exposure of SCAT3-expressing PC12 cells to $NaAsO_2$ in the presence or absence of serum. The fluorescence intensities of Venus (*yellow green*) and ECFP (*cyan blue*), and the morphology of SCAT3-expressing PC12 cells, were altered over time by $NaAsO_2$ exposure under all culture conditions (Fig. 1A and C). The ratio of ECFP to Venus emissions was calculated by dividing the brightness value of the *red* signal (ECFP) by that of the *green* signal (Venus), after the images of ECFP and Venus were converted into monochromatic images (ECFP: *cyan blue* to *red*; Venus: *yellow green* to *green*).

This ratio increased as the time of exposure to 10 μM of $NaAsO_2$ under serum-free culture conditions was increased, and peaked at 220–240 min (Fig. 1B). However, under these serum-free culture conditions, the temporal pattern of the ECFP/Venus emission ratio did not significantly [$F(12, 96) = 1.52$, $p = 0.13$] differ between the control and the $NaAsO_2$-exposed groups. This result was due to the fact that there was a gradual increase in this ratio over time even in the control group under serum-free culture conditions.

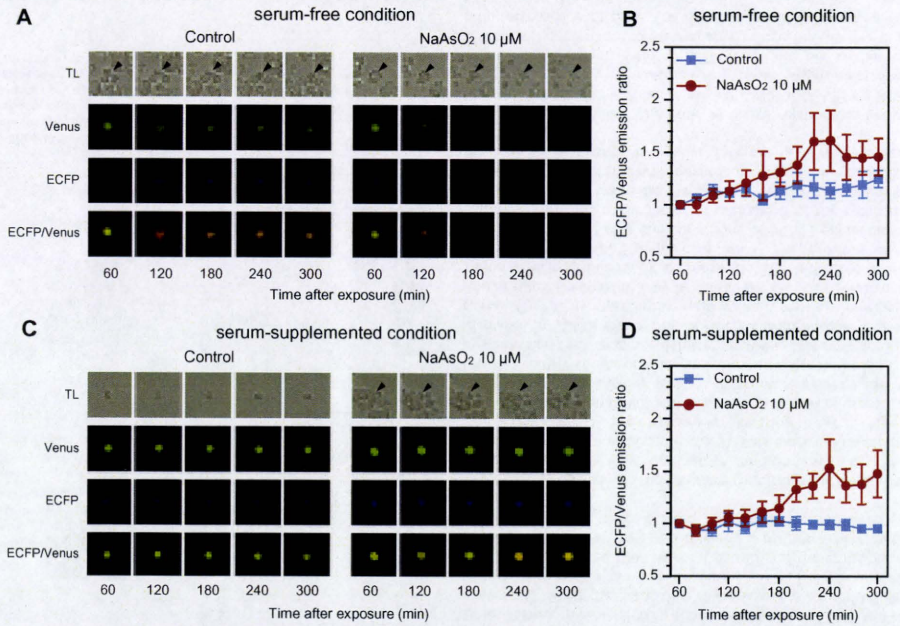

Fig. 1. Effects of culture serum conditions on SCAT3-expressing PC12 cells during exposure to $NaAsO_2$. Imaging analyses of SCAT3-expressing PC12 cells during exposure to $NaAsO_2$ (0 or 10 μM) were performed under serum-free culture conditions (A and B) or serum-supplemented culture conditions (C and D). A and C: Time-lapse images of SCAT3-expressing PC12 cells captured with transmitted light (TL), emissions of ECFP (*cyan blue*) and Venus (*yellow green*), and merged images of Venus and ECFP after conversion of fluorescent colors into pseudo colors (ECFP: *cyan blue* to *red*; Venus: *yellow green* to *green*) arrowheads indicate SCAT3-expressing cells. B and D: temporal changes in the emission ratio of ECFP to Venus of SCAT3-expressing cells. The ratio at each time point was calibrated using the ratio at 60 min after exposure, which was set at 1. Values are the means ± SEM of five independent experiments. (For interpretation of the references to color in this figure legend, the reader is referred to the web version of this article.)

Under serum-supplemented culture conditions, the ECFP/Venus emission ratio began to increase at 180 min, and peaked at 240 min after SCAT3-expressing PC12 cells were exposed to 10 μM of $NaAsO_2$ (Fig. 1D). In contrast, in the control group under serum-supplemented culture conditions, the ECFP/Venus emission ratio did not change over time and was maintained at a stable level. There was a significant difference in the temporal pattern of the ECFP/Venus emission ratio between the control and the $NaAsO_2$-exposed groups under serum-supplemented culture conditions [$F(12, 96) = 3.16$, $p < 0.001$].

In terms of the mean of the ECFP/Venus emission ratio in SCAT3-expressing PC12 cells during 80 to 180 min after exposure to $NaAsO_2$ there was no significant effect of culture condition [$F(1, 16) = 3.09$, $p = 0.10$], $NaAsO_2$ [$F(1, 16) = 0.81$, $p = 0.38$], or the interaction between these two main factors [$F(1, 16) = 0.002$, $p = 0.96$] (Fig. 2). However, two-way ANOVA indicated significant effects of $NaAsO_2$ [$F(1, 16) = 6.87$, $p < 0.05$] on the mean emission ratio during 200–300 min after exposure to $NaAsO_2$. Over this time period the effect of culture conditions [$F(1, 16) = 1.16$, $p = 0.30$] or the interactive effect of $NaAsO_2$ and culture conditions [$F(1, 16) = 0.17$, $p = 0.68$] was not significant. However, post hoc analysis indicated that the mean ECFP/Venus emission ratio was significantly ($p < 0.05$) increased by $NaAsO_2$ under serum-supplemented culture conditions, but not under serum-free culture conditions (Fig. 2).

3.2. Dose–response effects of $NaAsO_2$ on SCAT3-expressing cells

We next investigated the dose–response effects of $NaAsO_2$ on the ECFP/Venus emission ratio of SCAT3-expressing PC12 cells cultured in medium supplemented with serum. The fluorescence intensity of ECFP (*cyan blue*) and Venus (*yellow green*), as well as the morphology of SCAT3-expressing cells, were altered by exposure to $NaAsO_2$ at a concentration of 5 or 10 μM, whereas no dramatic changes in these parameters occurred in the control SCAT3-expressing PC12 cells or in the cells exposed to 1 μM $NaAsO_2$ (Fig. 3A; Supplementary data: Videos 1–4). The ratio of ECFP to Venus emission did not begin to change until 180 min after exposure to $NaAsO_2$ (Fig. 3B). The results by two-way ANOVA for repeated measures indicated that the temporal pattern of the ECFP/Venus emission ratio differed among the different groups [$F(36, 288) = 1.48$, $p < 0.05$]. In contrast analysis between groups, the temporal pattern of the ECFP/Venus emission ratio in the group exposed to 5 μM of $NaAsO_2$ significantly ($p < 0.005$) differed from that of the control group, but the ratio in the group exposed to 1 μM of $NaAsO_2$ did not. The ECFP/Venus emission ratio in the group exposed to 10 μM $NaAsO_2$ also changed over time in a similar manner to the change in the group exposed to 5 μM $NaAsO_2$. The difference in the temporal pattern of the ratio between the control group and the group exposed to 10 μM $NaAsO_2$ was close to significance ($p = 0.052$).

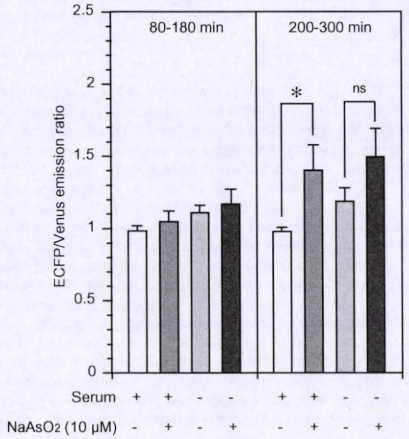

Fig. 2. Effects of $NaAsO_2$ and serum on the mean of the ECFP/Venus emission ratio of SCAT3-expressing PC12 cells. The ECFP/Venus emission ratio was calculated during 80–180 min or 200–300 min after exposure of SCAT3-expressing PC12 cells, in the presence or absence of serum, to the indicated concentrations of $NaAsO_2$. Values are the means ± SEM of five independent experiments. *, $p < 0.05$; ns, not significant.

Fig. 4 shows the means of the ECFP/Venus emission ratios during 80–180 min, and 200–300 min, after SCAT3-expressing PC12 cells were exposed to different doses of $NaAsO_2$. One-way ANOVA indicated that there was no significant difference in the mean of the ECFP/Venus emission ratio during 80–180 min after exposure of SCAT3-expressing PC12 cells to $NaAsO_2$ at any dose [$F(3, 24) = 0.98$, $p = 0.42$]. However, the mean of the ratio was significantly different among the groups [$F(3, 24) = 3.91$, $p < 0.05$] during 200–300 min after exposure. Post hoc analysis indicated that the mean of the ECFP/Venus emission ratio was significantly increased by 5 and 10 μM $NaAsO_2$ ($p < 0.01$ and $p < 0.05$, respectively), but not by 1 μM.

3.3. Effects of $NaAsO_2$ on the protein level of caspase-3

To compare the sensitivity and efficiency of the live imaging analysis of caspase-3 activation with SCAT3 to other assays of $NaAsO_2$-induced caspase-3 activation, we first assayed caspase-3 cleavage following exposure of PC12 cells to $NaAsO_2$ by Western blotting. The immunoreactive signals of cleaved caspase-3 protein (≈17 kDa), an active form of caspase-3, and uncleaved caspase-3 protein (≈32 kDa), were detected (Fig. 5). Exposure of PC12 cells to $NaAsO_2$ for 360 min did not significantly affect the amount of cleaved caspase-3 relative to the total amount of cleaved and uncleaved caspase-3 (Fig. 5A). In contrast, exposure to $NaAsO_2$ for 1200 min increased the level of cleaved caspase-3 and correspondingly decreased the level of uncleaved caspase-3 in a dose-dependent manner (Fig. 5B). The level of cleaved caspase-3 was significantly ($p < 0.0001$) increased by 1200-min exposure to 10 μM $NaAsO_2$.

3.4. Effects of $NaAsO_2$ on the activity of caspase-3

We next examined the enzymatic activity of caspase-3 by exposure of PC12 cells to $NaAsO_2$. Caspase-3 activity of PC12 cells was significantly increased by exposure to 10 μM $NaAsO_2$ for 360 and 1200 min ($p < 0.05$ and $p < 0.001$, respectively), while lower doses of $NaAsO_2$ (1 and 5 μM) did not have any significant effects on caspase-3 activity (Fig. 6A and B). Exposure to 10 μM $NaAsO_2$ for 1200 min induced the highest increase in caspase-3 activity of PC12 cells, and this increased activity was completely blocked by the caspase inhibitor Z-VAD-FMK (Fig. 6B).

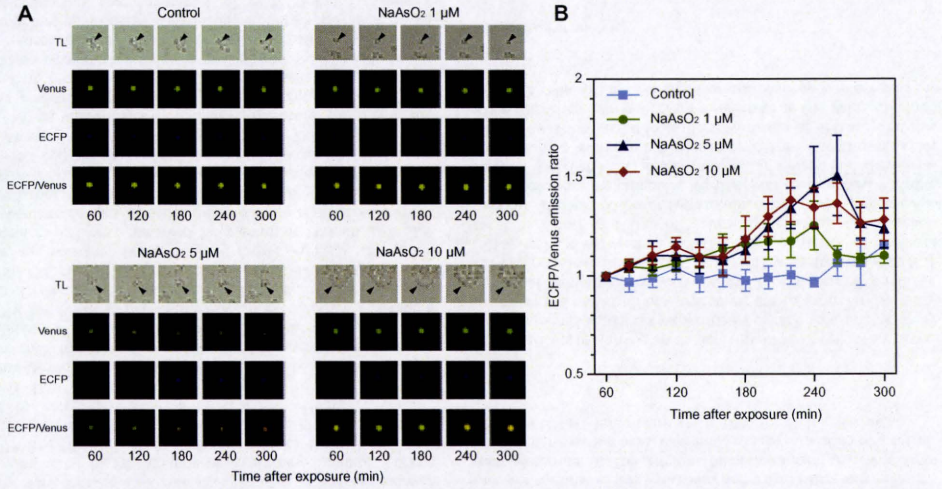

Fig. 3. Dose–response effects of $NaAsO_2$ on SCAT3-expressing PC12 cells under serum-supplemented culture conditions. A: Time-lapse images of SCAT3-expressing PC12 cells captured with transmitted light (TL), emissions of ECFP (*cyan blue*) and Venus (*yellow green*), and merged images of Venus and ECFP after conversion of fluorescent colors into pseudo colors (ECFP: *cyan blue* to *red*; Venus: *yellow green* to *green*). Arrowheads indicate SCAT3-expressing cells. B: Temporal changes in the ECFP/Venus emission ratio of SCAT3-expressing PC12 cells. The ratio at each time point was calibrated with the ratio at 60 min after arsenite exposure, which was set at 1. Values are the means ± SEM of five independent experiments. (For interpretation of the references to color in this figure legend, the reader is referred to the web version of this article.)

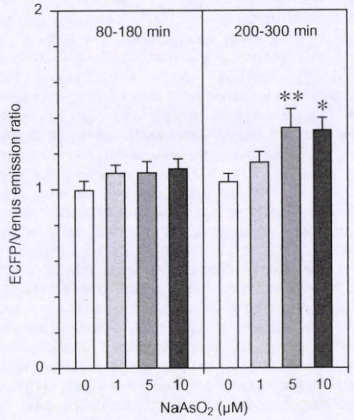

Fig. 4. Dose response effects of $NaAsO_2$ on the mean of the ECFP/Venus emission ratio of SCAT3-expressing PC12 cells under serum-supplemented culture conditions. The mean of the ECFP/Venus emission ratio was calculated during 80–180 min, or 200–300 min, after exposure to $NaAsO_2$ was initiated. Values are the means ± SEM of five independent experiments. **, $p < 0.01$ and *, $p < 0.05$ vs. control group (0 μM of $NaAsO_2$), respectively.

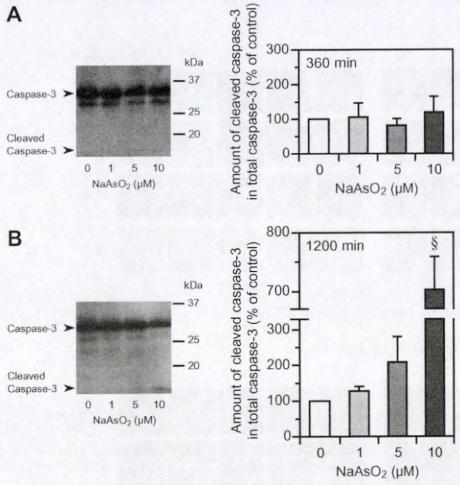

Fig. 5. Effect of $NaAsO_2$ on cleavage of the caspase-3 protein in PC12 cells following 360-min (A) or 1200-min (B) exposure to the indicated concentrations of $NaAsO_2$. The protein levels of capase-3 were assayed using Western blotting analysis. Immunoreactive caspase-3 bands are shown at left. Values are the means ± SEM of five independent experiments for the 360-min exposure and of four independent experiments for the 1200-min exposure.

3.5. Effects of $NaAsO_2$ on DNA fragmentation

We next assessed the sensitivity of other assays of the cytotoxic effects of $NaAsO_2$ that determine $NaAsO_2$ effects on downstream effects of caspase activation. We first assayed the effect of $NaAsO_2$ on apoptosis by analysis of DNA fragmentation using an ELISA kit. The amount of nucleosomes generated from DNA fragmentation in PC12 cells was significantly ($p < 0.0001$) increased 1200 min after administration of 10 μM $NaAsO_2$ (Fig. 7). However, the amount of apoptotic nucleosomes in cells exposed to 1 or 5 μM $NaAsO_2$ was not significantly different from that of the control group.

3.6. Effects of $NaAsO_2$ on cell viability

We finally assayed the effect of $NaAsO_2$ on the viability of PC12 cells. No significant effect of $NaAsO_2$ on PC12 cell viability was observed one day after $NaAsO_2$ exposure was initiated (Fig. 8). However, cell viability was decreased on day 2 after $NaAsO_2$ exposure in a dose-dependent manner. Cell viability was significantly decreased by $NaAsO_2$ at doses of 5 or 10 μM ($p < 0.001$ or $p < 0.0001$, respectively), compared to that of the control group.

4. Discussion

Live imaging analysis of SCAT3-transfected cells using FRET technology is useful for monitoring the activity of caspase-3 (Takemoto et al., 2003; Kanuka et al., 2005; Kuranaga et al., 2006; Takemoto et al., 2007). The emission ratio of ECFP to Venus is elevated when the activation of caspase-3 is caused by death stimuli. We carried out live imaging of SCAT3-expressing PC12 cells and determined the temporal patterns of the emission ratio of ECFP to Venus as one step towards a proposed new method for cyto- and/or neuro-toxicity evaluation of environmental chemicals.

First, to determine the appropriate conditions for live imaging, we investigated the effects of culture conditions with or without serum-supplementation on the ECFP/Venus emission ratio during exposure to $NaAsO_2$. We observed an elevation in the ECFP/Venus emission ratio during 200–300 min after initiation of exposure to $NaAsO_2$ in the presence or absence of serum. However, under serum-free culture conditions, a significant difference in the ECFP/Venus emission ratio was not detected, because this ratio gradually increased in SCAT3-expressing PC12 cells even without exposure to $NaAsO_2$. The increase in this ratio without serum-supplementation or $NaAsO_2$ exposure may be due to the fact that serum deprivation induces cell death by apoptosis in PC12 cells (Greene, 1978; Morimoto et al., 2000; Shibano et al., 2002). The results of our current study indicate that the conditions of SCAT3-expressing cell culture are an important factor in evaluation of the cytotoxicity of chemicals. Thus, we found that culture of the cells in serum-supplemented medium is a prerequisite for the precise evaluation of the toxicity of chemicals by live imaging of SCAT3-expressing PC12 cells.

We next determined the dose–response relationship between $NaAsO_2$ and the ECFP/Venus emission ratio of SCAT3-expressing PC12 cells, which were cultured in medium supplemented with serum. The emission ratio of ECFP/Venus did not change until 180 min after exposure to $NaAsO_2$ at any dose, but afterwards this ratio increased with time. The mean of the ECFP/Venus emission ratio during 200–300 min after $NaAsO_2$ exposure was initiated was significantly increased by $NaAsO_2$ at a dose of 5 or 10 μM, but not at a dose of 1 μM. Accordingly, doses of 1 and 5 μM of

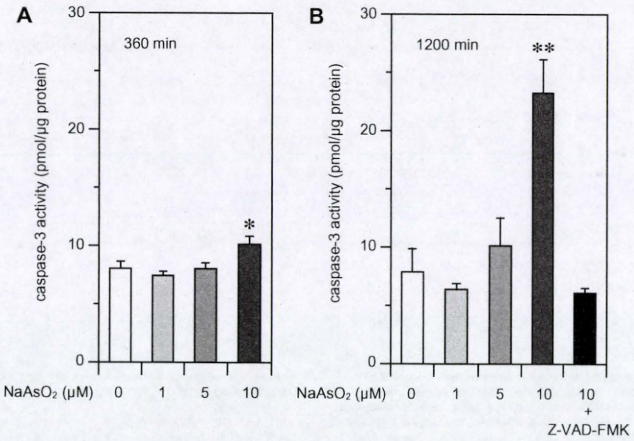

Fig. 6. Effects of $NaAsO_2$ on caspase-3 activity of PC12 cells. Cells were exposed to the indicated concentrations of $NaAsO_2$ for 360 min (A) or 1200 min (B). Caspase-3 activity of cell lysates was expressed as the amount of pNA (pmol) generated per protein (μg) extracted from the cells. Values are the means ± SEM of four or five independent experiments. **, $p < 0.001$ and *, $p < 0.05$ vs. control group (0 μM of $NaAsO_2$), respectively.

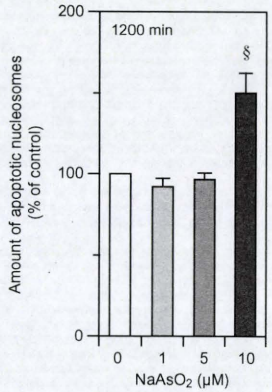

Fig. 7. Effects of $NaAsO_2$ on DNA fragmentation in PC12 cells. The level of apoptotic nucleosomes in PC12 cells following 1200-min exposure to the indicated concentrations of $NaAsO_2$ was assayed using an ELISA. The amount of nucleosomes generated from DNA fragmentation is expressed relative to that of control cells (0 μM of $NaAsO_2$) whose value was set at 100%. Values are the means ± SEM of four independent experiments. §, $p < 0.0001$ vs. control group (0 μM of $NaAsO_2$).

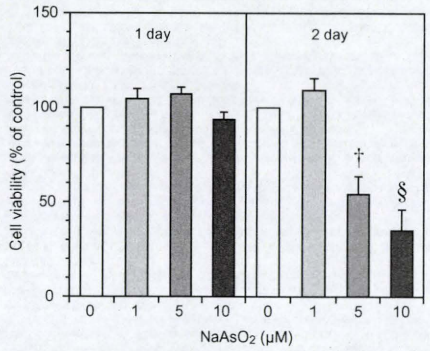

Fig. 8. Effects of $NaAsO_2$ on the viability of PC12 cells. PC12 cells were exposed to the indicated concentrations of $NaAsO_2$ for 1 or 2 days. The viability of PC12 cells was expressed relative to the viability of cells without $NaAsO_2$ exposure, whose value was set at 100%. Values are the means ± SEM of six independent experiments. † and §, $p < 0.001$ and $p < 0.0001$ vs. control group (0 μM of $NaAsO_2$).

$NaAsO_2$ may be defined as the no-observed-adverse-effect level (NOAEL) and lowest-observed-adverse-effect level (LOAEL), respectively, in which the adverse effect is defined as death of PC12 cells by apoptosis. Our findings suggest that live imaging analysis using SCAT3 is a suitable method for determination of the toxicity of chemicals.

SCAT3 is composed of a caspase-3 cleavage peptide sequence linking two fluorescent proteins (Takemoto et al., 2003). Increases in the emission ratio of ECFP to Venus in SCAT3-expressing PC12 cells therefore indicate that activation of caspase-3 occurs during $NaAsO_2$-induced death of PC12 cells. In fact, our current study showed that $NaAsO_2$ increases the protein level and enzymatic activity of the cleaved form of caspase-3 and facilitates DNA-fragmentation. Moreover, the increased activity of caspase-3 induced in PC12 cells by 10 μM of $NaAsO_2$ was completely suppressed by an inhibitor of caspases. Based on our combined results, we can conclude that $NaAsO_2$ induces apoptotic death of PC12 cells via activation of caspase-3.

Analysis of caspase-3 activation by western blotting of caspase-3 cleavage, by assay of caspase-3 activity, and also by live imaging of SCAT3-expressing cells, suggests that $NaAsO_2$ activates caspase-3, followed by induction of apoptotic cell death. However, western blotting analysis required a longer exposure time and a higher dose

of $NaAsO_2$ to detect significant effects. A significant increase in the protein level of active caspase-3 was observed when PC12 cells were exposed to 10 μM of $NaAsO_2$ for 1200 min, but not when the cells were exposed to 10 μM of $NaAsO_2$ for 360 min, or when the cells were exposed to lower doses of $NaAsO_2$ for 1200 min. Similar results have been reported using human neuroblastoma SH-SY5Y cells, in which the level of active caspase-3 was significantly increased by exposure to $NaAsO_2$ (50 μM) for 1440 min, but not for 360 min (Watcharasit et al., 2008). In the present study, when we assayed caspase-3 activation using a caspase-3 activity assay, we observed a slight, but significant, increase in the caspase-3 activity of PC12 cells when the cells were exposed to 10 μM of $NaAsO_2$ for 360 min. However, such an increase did not occur following exposure to 5 μM of $NaAsO_2$. Another study that assayed caspase-3 activation using a caspase-3 activity assay showed that a significant increase in the activity of caspase-3 in PC12 cells is induced by exposure to 8 μM of arsenic trioxide for 1440 min (Piga et al., 2007). In contrast to the above methods of assay of caspase activation, live imaging analysis of SCAT3-expressing PC12 cells could rapidly detect significant effects of exposure to $NaAsO_2$ not only at 10 μM, but also at 5 μM. Thus, significant increases in the ECFP/Venus emission ratio occurred within 300 min after exposure to $NaAsO_2$ at doses of both 5 and 10 μM. Based on the combined data, we propose that live imaging analysis using SCAT3-expressing cells is a more sensitive and more efficient method for detection of cell death via caspase-3 activation than other methods. The only drawback that needs to be addressed is that it is difficult to precisely compare the temporal effects of $NaAsO_2$ on SCAT3-expressing PC12 cells of live imaging with the cumulative effects of exposure of PC12 cells to $NaAsO_2$ determined by other methods.

The use of the SCAT3-FRET technique enabled monitoring of the activity of caspase-3 at a single cell level as shown in Figs. 1 and 3, which would not be possible to do using Western blotting or caspase-3 activity assays. Furthermore, immunoreactive bands of active caspase-3 that were detected by Western blotting analysis were generally very weak. The only significant effect on caspase-3 activation that could be detected by Western blotting was when cells were exposed to 10 μM $NaAsO_2$ for 1200 min. These results indicate that the sensitivity of Western blotting analysis for detection of caspase-3 activation by $NaAsO_2$ is lower than that of live imaging analysis. Therefore, it may be necessary to obtain protein samples from a considerable number of cells for toxicity evaluation using Western blotting methods.

The SCAT3-FRET assay could be applied to a high throughput toxicity assay using a fluorescent microplate reader, although such an assay may decrease, or eliminate, the possibility of detection of the toxicity of chemicals at a single cell level. Live imaging analysis would not be more labor intensive than other methods since most fluorescent time-lapse microscopes, such as that used in the current study, can automatically image living cells. Thus, an improvement in the efficiency and accuracy of detection of chemical cytotoxic effects may be accomplished, at least in part, by live imaging analyses.

In the present study, we showed that exposure of cells to $NaAsO_2$ for 1200 min significantly increased the amount of nucleosomes generated by DNA fragmentation in PC12 cells at a dose of 10 μM $NaAsO_2$ but not at smaller doses. Moreover, the results of the cell viability assay suggest that the cytotoxic effects of $NaAsO_2$ on PC12 cell viability could only be detected 2 days after exposure to $NaAsO_2$. Another study which assayed the effect of $NaAsO_2$ exposure on cell viability using the MTT assay reported that exposure to $NaAsO_2$ for 1440 min inhibited the viability of PC12 cells in a dose-dependent manner, and that its IC_{50} value was approximately 22 μM when assayed over the range of 0.1–100 μM (van Vliet et al., 2007). Other studies that used staining with the DNA dye Hoechst 33258 (bis-benzimide) as a measure of apoptosis, showed that 15–20% of the PC12 cells that were exposed to 15 μM of $NaAsO_2$ for 1440 min were killed by apoptosis but less than 5% of the cells were killed after an exposure of 480 min (Cai et al., 2006; Cai and Xia, 2008). It is known that caspase family members disassemble the nuclear lamina, which provides mechanical support to the cell nucleus and plays an essential role in chromatin organization. Disruption of the membrane is followed by degradation of the nuclear envelope (Kihlmark et al., 2001). It was reported that an uncleavable mutation of lamin causes a significant delay in the onset of chromatin condensation and DNA fragmentation in cells killed by apoptosis (Rao et al., 1996). These data indicate that activation of caspase-3 occurs prior to chromatin condensation and DNA fragmentation. Therefore, an apoptotic assay based on DNA fragmentation and cell viability would require a long time to determine whether or not exposure to $NaAsO_2$ has an adverse effect on cells.

Most of the chemicals discharged into the environment remain to be evaluated regarding their toxicity towards human life. Furthermore, to work out a hazard assessment for a myriad of environmental chemicals is a demanding task. Although the analysis of animal toxicology is a useful approach for assessment of chemical hazards, it takes a long time to evaluate the toxicity of a chemical in this way. We believe that live imaging analyses of cultured cells, which will enable screening of the toxicity of chemicals within a short time and with high accuracy, will greatly facilitate hazard assessment of environmental chemicals.

Acknowledgments

This work was supported in part by the Environment Technology Development Fund from the Ministry of the Environment Japan (KS-02) to S. Tsukahara and by a Health and Labour Sciences Research Grant to M. Kakeyama. We thank Dr. M. Miura (University of Tokyo, Tokyo, Japan) for providing the pcDNA-SCAT3 vector.

Appendix A. Supplementary data

Supplementary data associated with this article can be found, in the online version, at doi:10.1016/j.tiv.2010.07.022.

References

Araragi, S., Kondoh, M., Kawase, M., Saito, S., Higashimoto, M., Sato, M., 2003. Mercuric chloride induces apoptosis via a mitochondrial-dependent pathway in human leukemia cells. Toxicology 184, 1–9.
Azad, N., Iyer, A.K., Manosroi, A., Wang, L., Rojanasakul, Y., 2008. Superoxide-mediated proteasomal degradation of Bcl-2 determines cell susceptibility to Cr(VI)-induced apoptosis. Carcinogenesis 29, 1538–1545.
Bustamante, J., Dock, L., Vahter, M., Fowler, B., Orrenius, S., 1997. The semiconductor elements arsenic and indium induce apoptosis in rat thymocytes. Toxicology 118, 129–136.
Cai, B., Xia, Z., 2008. p38 MAP kinase mediates arsenite-induced apoptosis through FOXO3a activation and induction of Bim transcription. Apoptosis 13, 803–810.
Cai, B., Chang, S.H., Becker, E.B., Bonni, A., Xia, Z., 2006. p38 MAP kinase mediates apoptosis through phosphorylation of BimEL at Ser-65. J. Biol. Chem. 281, 25215–25222.
Carlisle, D.L., Pritchard, D.E., Singh, J., Patierno, S.R., 2000. Chromium(VI) induces p53-dependent apoptosis in diploid human lung and mouse dermal fibroblasts. Mol. Carcinog. 28, 111–118.
Chattopadhyay, S., Bhaumik, S., Nag Chaudhury, A., Das Gupta, S., 2002. Arsenic induced changes in growth development and apoptosis in neonatal and adult brain cells in vivo and in tissue culture. Toxicol. Lett. 128, 73–84.
Choi, M.K., Kim, B.H., Chung, Y.Y., Han, M.S., 2002. Cadmium-induced apoptosis in h9c2, a7r5, and c6-glial cell. Bull. Environ. Contam. Toxicol. 69, 335–341.
Close, A.H., Guo, T.L., Shenker, B.J., 1999. Activated human T lymphocytes exhibit reduced susceptibility to methylmercury chloride-induced apoptosis. Toxicol. Sci. 49, 68–77.
Columbano, A., Ledda-Columbano, G.M., Coni, P.P., Faa, G., Liguori, C., Santa Cruz, G., Pani, P., 1985. Occurrence of cell death (apoptosis) during the involution of liver hyperplasia. Lab. Invest. 52, 670–675.
Dong, S., Shen, H.M., Ong, C.N., 2001. Cadmium-induced apoptosis and phenotypic changes in mouse thymocytes. Mol. Cell Biochem. 222, 11–20.

Dong, S., Liang, D., An, N., Jia, L., Shan, Y., Chen, C., Sun, K., Niu, F., Li, H., Fu, S., 2009. The role of MAPK and FAS death receptor pathways in testicular germ cell apoptosis induced by lead. Acta Biochim. Biophys. Sin. (Shanghai) 41, 800–807.
Gambelunghe, A., Piccinini, R., Abbritti, G., Ambrogi, M., Ugolini, B., Marchetti, C., Migliorati, G., Balducci, C., Muzi, G., 2006. Chromium VI-induced apoptosis in a human bronchial epithelial cell line (BEAS-2B) and a lymphoblastic leukemia cell line (MOLT-4). J. Occup. Environ. Med. 48, 319–325.
Gennari, A., Cortese, E., Boveri, M., Casado, J., Prieto, P., 2003. Sensitive endpoints for evaluating cadmium-induced acute toxicity in LLC-PK1 cells. Toxicology 183, 211–220.
Greene, L.A., 1978. Nerve growth factor prevents the death and stimulates the neuronal differentiation of clonal PC12 pheochromocytoma cells in serum-free medium. J. Cell Biol. 78, 747–755.
Habeebu, S.S., Liu, J., Klaassen, C.D., 1998. Cadmium-induced apoptosis in mouse liver. Toxicol. Appl. Pharmacol. 149, 203–209.
Hill, R., Leidal, A.M., Madureira, P.A., Gillis, L.D., Waisman, D.M., Chiu, A., Lee, P.W., 2008. Chromium-mediated apoptosis: involvement of DNA-dependent protein kinase (DNA-PK) and differential induction of p53 target genes. DNA Repair (Amst.) 7, 1484–1499.
Homma-Takeda, S., Kugenuma, Y., Iwamuro, T., Kumagai, Y., Shimojo, N., 2001. Impairment of spermatogenesis in rats by methylmercury: involvement of stage- and cell-specific germ cell apoptosism. Toxicology 169, 25–35.
Hossain, K., Akhand, A.A., Kato, M., Du, J., Takeda, K., Wu, J., Takeuchi, K., Liu, W., Suzuki, H., Nakashima, I., 2000. Arsenite induces apoptosis of murine T lymphocytes through membrane raft-linked signaling for activation of c-Jun amino-terminal kinase. J. Immunol. 165, 4290–4297.
Iwama, K., Nakajo, S., Aiuchi, T., Nakaya, K., 2001. Apoptosis induced by arsenic trioxide in leukemia U937 cells is dependent on activation of p38, inactivation of ERK and the Ca^{2+}dependent production of superoxide. Int. J. Cancer 92, 518–526.
Jiang, X.H., Wong, B.C., Yuen, S.T., Jiang, S.H., Cho, C.H., Lai, K.C., Lin, M.C., Kung, H.F., Lam, S.K., 2001. Arsenic trioxide induces apoptosis in human gastric cancer cells through up-regulation of p53 and activation of caspase-3. Int. J. Cancer 91, 173–179.
Kanuka, H., Kuranaga, E., Takemoto, K., Hiratou, T., Okano, H., Miura, M., 2005. Drosophila caspase transduces Shaggy/GSK-3beta kinase activity in neural precursor development. EMBO J. 24, 3793–3806.
Kihlmark, M., Imreh, G., Hallberg, E., 2001. Sequential degradation of proteins from the nuclear envelope during apoptosis. J. Cell Sci. 114, 3643–3653.
Kuranaga, E., Kanuka, H., Tonoki, A., Takemoto, K., Tomioka, T., Kobayashi, M., Hayashi, S., Miura, M., 2006. Drosophila IKK-related kinase regulates nonapoptotic function of caspases via degradation of IAPs. Cell 126, 583–596.
Luo, K.Q., Yu, V.C., Pu, Y., Chang, D.C., 2001. Application of the fluorescence resonance energy transfer method for studying the dynamics of caspase-3 activation during UV-induced apoptosis in living HeLa cells. Biochem. Biophys. Res. Commun. 283, 1054–1060.
Morimoto, Y., Nishihira, J., Kemmotsu, O., Shibano, T., Gando, S., Shikama, H., 2000. Pentobarbital inhibits apoptosis in neuronal cells. Crit. Care Med. 28, 1899–1904.
Nagai, T., Ibata, K., Park, E.S., Kubota, M., Mikoshiba, K., Miyawaki, A., 2002. A variant of yellow fluorescent protein with fast and efficient maturation for cell-biological applications. Nat. Biotechnol. 20, 87–90.
Namgung, U., Xia, Z., 2001. Arsenic induces apoptosis in rat cerebellar neurons via activation of JNK3 and p38 MAP kinases. Toxicol. Appl. Pharmacol. 174, 130–138.
Pachauri, V., Saxena, G., Mehta, A., Mishra, D., Flora, S.J., 2009. Combinational chelation therapy abrogates lead-induced neurodegeneration in rats. Toxicol. Appl. Pharmacol. 240, 255–264.
Piga, R., Saito, Y., Yoshida, Y., Niki, E., 2007. Cytotoxic effects of various stressors on PC12 cells: involvement of oxidative stress and effect of antioxidants. Neurotoxicology 28, 67–75.
Rana, S.V., 2008. Metals and apoptosis: recent developments. J. Trace Elem. Med. Biol. 22, 262–284.
Rao, L., Perez, D., White, E., 1996. Lamin proteolysis facilitates nuclear events during apoptosis. J. Cell Biol. 135, 1441–1455.
Rehm, M., Dussmann, H., Janicke, R.U., Tavare, J.M., Kogel, D., Prehn, J.H., 2002. Single-cell fluorescence resonance energy transfer analysis demonstrates that caspase activation during apoptosis is a rapid process. Role of caspase-3. J. Biol. Chem. 277, 24506–24514.
Rudolf, E., Cervinka, M., 2006. The role of intracellular zinc in chromium(VI)-induced oxidative stress, DNA damage and apoptosis. Chem. Biol. Interact. 162, 212–227.
Russo, P., Catassi, A., Cesario, A., Imperatori, A., Rotolo, N., Fini, M., Granone, P., Dominioni, L., 2005. Molecular mechanisms of hexavalent chromium-induced apoptosis in human bronchoalveolar cells. Am. J. Respir. Cell Mol. Biol. 33, 589–600.
Shabani, A., Rabbani, A., 2000. Lead nitrate induced apoptosis in alveolar macrophages from rat lung. Toxicology 149, 109–114.
Shenker, B.J., Guo, T.L., Shapiro, I.O.I.M., 1999. Induction of apoptosis in human T-cells by methyl mercury: temporal relationship between mitochondrial dysfunction and loss of reductive reserve. Toxicol. Appl. Pharmacol. 157, 23–35.
Shibano, T., Morimoto, Y., Kemmotsu, O., Shikama, H., Hisano, K., Hua, Y., 2002. Effects of mild and moderate hypothermia on apoptosis in neuronal PC12 cells. Br. J. Anaesth. 89, 301–305.
Takemoto, K., Nagai, T., Miyawaki, A., Miura, M., 2003. Spatio-temporal activation of caspase revealed by indicator that is insensitive to environmental effects. J. Cell Biol. 160, 235–243.
Takemoto, K., Kuranaga, E., Tonoki, A., Nagai, T., Miyawaki, A., Miura, M., 2007. Local initiation of caspase activation in Drosophila salivary gland programmed cell death in vivo. Proc. Natl. Acad. Sci. USA 104, 13367–13372.
Toimela, T., Tahti, H., 2004. Mitochondrial viability and apoptosis induced by aluminum, mercuric mercury and methylmercury in cell lines of neural origin. Arch. Toxicol. 78, 565–574.
Tse, W.P., Cheng, C.H., Che, C.T., Lin, Z.X., 2008. Arsenic trioxide, arsenic pentoxide, and arsenic iodide inhibit human keratinocyte proliferation through the induction of apoptosis. J. Pharmacol. Exp. Ther. 326, 388–394.
Tse, W.P., Cheng, C.H., Che, C.T., Zhao, M., Fan, R.Q., Lin, Z.X., 2009. Realgar-mediated growth inhibition on HaCaT human keratinocytes is associated with induction of apoptosis. Int. J. Mol. Med. 24, 189–196.
Tyas, L., Brophy, V.A., Pope, A., Rivett, A.J., Tavare, J.M., 2000. Rapid caspase-3 activation during apoptosis revealed using fluorescence-resonance energy transfer. EMBO Rep. 1, 266–270.
van Vliet, E., Eskes, C., Stingele, S., Gartlon, J., Price, A., Farina, M., Ponti, J., Hartung, T., Sabbioni, E., Coecke, S., 2007. Development of a mechanistically-based genetically engineered PC12 cell system to detect p53-mediated cytotoxicity. Toxicol. In Vitro 21, 698–705.
Wang, S., Leonard, S.S., Ye, J., Ding, M., Shi, X., 2000. The role of hydroxyl radical as a messenger in Cr(VI)-induced p53 activation. Am. J. Physiol. Cell Physiol. 279, C868–C875.
Watcharasit, P., Thiantanawat, A., Satayavivad, J., 2008. GSK3 promotes arsenite-induced apoptosis via facilitation of mitochondria disruption. J. Appl. Toxicol. 28, 466–474.
Wong, H.K., Fricker, M., Wyttenbach, A., Villunger, A., Michalak, E.M., Strasser, A., Tolkovsky, A.M., 2005. Mutually exclusive subsets of BH3-only proteins are activated by the p53 and c-Jun N-terminal kinase/c-Jun signaling pathways during cortical neuron apoptosis induced by arsenite. Mol. Cell Biol. 25, 8732–8747.

Original Paper

Neuro
endocrinology

Neuroendocrinology
DOI: 10.1159/000327541

Received: August 24, 2010
Accepted after revision: March 15, 2011
Published online: April 22, 2011

Effects of Aromatase or Estrogen Receptor Gene Deletion on Masculinization of the Principal Nucleus of the Bed Nucleus of the Stria Terminalis of Mice

Shinji Tsukahara[a] Mumeko C. Tsuda[b] Ryohei Kurihara[a] Yukinori Kato[a]
Yoshiko Kuroda[a] Mariko Nakata[b] Kai Xiao[b] Kazuyo Nagata[b] Katsumi Toda[c]
Sonoko Ogawa[b]

[a]Division of Life Science, Graduate School of Science and Engineering, Saitama University, Saitama City, [b]Laboratory of Behavioral Neuroendocrinology, Graduate School of Comprehensive Human Sciences, University of Tsukuba, Tsukuba, and [c]Department of Biochemistry, School of Medicine, Kochi University, Nankoku, Japan

Key Words
Aromatase · Estrogen receptor · Bed nucleus of the stria terminalis · Masculinization · Sexual dimorphism · Sexually dimorphic nucleus · Sexual differentiation

Abstract
The principal nucleus of the bed nucleus of the stria terminalis (BNSTp) is a sexually dimorphic nucleus, and the male BNSTp is larger and has more neurons than the female BNSTp. To assess the roles of neuroestrogen synthesized from testicular androgen by brain aromatase in masculinization of the BNSTp, we performed morphometrical analyses of the adult BNSTp in aromatase knockout (ArKO), estrogen receptor-α knockout (αERKO), and estrogen receptor-β knockout (βERKO) mice and their respective wild-type littermates. In wild-type littermates, the BNSTp of males had a larger volume and greater numbers of neuronal and glial cells than did that of females. The volume and neuron number of the BNSTp in ArKO and αERKO males and glial cell number of the BNSTp in αERKO males were significantly smaller than those of wild-type male littermates, and they were not significantly different from those in female mice with either gene knockout. In contrast, there was no significant morphological difference in the BNSTp between βERKO and wild-type mice. Next, we examined the BNSTp of ArKO males subcutaneously injected with estradiol benzoate (EB) on postnatal days 1, 2, and 3 (1.5 μg/day). EB-treated ArKO males had a significantly greater number of BNSTp neurons than did oil-treated ArKO males. The number of BNSTp neurons in EB-treated ArKO males was comparable to that in wild-type males. These findings suggested that masculinization of the BNSTp in mice involves the actions of neuroestrogen that was synthesized by aromatase and that this estrogen mostly binds to ERα during the postnatal period.

Introduction

Sexual differentiation of the brain in mammalian species, including rodents and primates, is affected by testicular androgen during development, and it results in the formation of sexually dimorphic nuclei within the central nervous system [1, 2]. The bed nucleus of the stria terminalis (BNST) of the limbic system includes a sub-

KARGER

Fax +41 61 306 12 34
E-Mail karger@karger.ch
www.karger.com

0028–3835/11/0000–0000$38.00/0

Accessible online at:
www.karger.com/nen

Shinji Tsukahara
Graduate School of Science and Engineering, Saitama University
255 Shimo-Okubo, Sakura-ku
Saitama City, Saitama 338-8570 (Japan)
Tel. +81 48 858 3420, E-Mail stsuka@mail.saitama-u.ac.jp